UNIVERSITEIT VAN PRETORIA
UNIVERSITY OF PRETORIA
YUNIBESITHI YA PRETORIA

ENVIRONMENTAL FACTORS AFFECTING THIN CONCRETE PAVEMENTS

PHILIP LLEWELLYN HOWARD

A dissertation submitted in partial fulfilment of the requirements for the degree of

MASTER OF ENGINEERING (STRUCTURAL ENGINEERING)

In the

FACULTY OF ENGINEERING, BUILT ENVIRONMENT AND INFORMATION TECHNOLOGY

UNIVERSITY OF PRETORIA

December 2021

DISSERTATION SUMMARY

ENVIRONMENTAL FACTORS AFFECTING THIN CONCRETE PAVEMENTS

P.L. HOWARD

Supervisor: Professor E.P. Kearsley

Department: Civil Engineering

University: University of Pretoria

Degree: Master of Engineering (Structural engineering)

An ultra-thin continuously reinforced concrete pavement (UTCRCP) has a thickness of less than 75 mm while thin concrete pavements has a thickness of less than 150 mm thickness. Both pavements are reinforced with steel reinforcement and/or steel fibres to strengthen the concrete in tension. These pavement layers placed over an existing asphalt surface to strengthen the pavement structure. The performance of these concrete pavements are dependent on the response of the concrete pavement to both environmental and traffic loading.

Significant research has already been done on the effects of traffic loading on the performance of UTCRCP and limited research on the effect of environmental loading on thin concrete pavements (pavements with a thickness less than 150 mm thickness). Significant research on the effect of environmental loading on pavements of ordinary thickness (± 300 mm thickness) has already been conducted and due to the limited research done on the effect of environmental loading conditions on the behaviour of UTCRCP, this research studied the environmental factors effecting the performance of ordinary concrete pavements. This was done to determine the properties of concrete pavements that are of a main concern when considering their response to environmental loading. Literature points to the material properties and environmental conditions as being the predominant source of defects seen in pavements, which are further accentuated by traffic loading, leading to the premature failure of the concrete pavement.

This study looked at the behaviour of thin continuously reinforced concrete pavement sections of 50, 75 and 100 mm thickness of two different concrete strengths in response to the ambient environmental conditions, to determine the effect of pavement thickness and material properties on the response of the

pavements to environmental loading. These pavement sections were cast as being unrestrained to determine the strains that are experienced by the pavement and linked to the potential internal moment and internal stress development and curvature that would occur within a continuous concrete pavement. Concrete pavements were cast, by using concrete with and without supplementary cementitious material (SCM). The material properties of the concrete were measured to link the behaviour of the pavement section back to the material properties of the concrete.

It was found that the environmental factor affecting the behaviour of the thin concrete pavements the most was precipitation, with the worst effect being seen in the concrete pavements not containing any SCM. The thermal effect on the behaviour of the thin pavements was minor with a ± 100 με fluctuation in the strain readings being measured due to the heating and cooling of the concrete pavements. The worst effects of environmental loading were seen within the 75 mm thick concrete pavements, marking this a critical pavement thickness while the 50 mm thick pavements, on the other hand, performed the best with the lowest change in length, curvature and internal stresses and moment development within the concrete.

The material properties were found to play a significant role in the behaviour of the concrete pavements. The addition of SCM to concrete produced concrete that was less water absorbent than concrete without SCM. Concrete containing SCM held on to moisture a lot stronger than concrete without SCM. This resulted in less shrinkage and less swelling of concrete containing SCM due to less moisture movement. It was found that by adding SCM to concrete, the pavement was not as sensitive to the environmental conditions the pavements were exposed to with less curvature and internal stresses and moment development within the concrete pavements.

DECLARATION

I, the undersigned hereby declare that:

- I understand what plagiarism is and I am aware of the University's policy in this regard;
- The work contained in this thesis is my own original work;
- I did not refer to work of current or previous students, lecture notes, handbooks or any other study material without proper referencing;
- Where other people's work has been used this has been properly acknowledged and referenced;
- I have not allowed anyone to copy any part of my thesis;
- I have not previously in its entirety or in part submitted this thesis at any university for a degree.

DISCLAIMER:

The work presented in this report is that of the student alone. Students were encouraged to take ownership of their projects and to develop and execute their experiments with limited guidance and assistance. The content of the research does not necessarily represent the views of the supervisor or any staff member of the University of Pretoria, Department of Civil Engineering. The supervisor did not read or edit the final report and is not responsible for any technical inaccuracies, statements or errors. The conclusions and recommendations given in the report are also not necessarily that of the supervisor, sponsors or companies involved in the research.

Signature of student: *PHoward*

Name of student: **Philip Llewellyn Howard**

Student number: **16040679**

Date: **30/08/2021**

ACKNOWLEDGEMENTS

I wish to express my sincere gratitude and appreciation to my supervisor *Professor E.P. Kearsley* for her continuous support and guidance through the duration of this research study, for believing in my abilities and for creating the opportunity to peruse my postgraduate studies. I would like to thank and covey my gratitude to all those who helped and contributed to making this dissertation a success and would like to recognise the following persons in particular:

- My Lord and Saviour, *Jesus Christ*, for providing me with the wisdom, knowledge, discernment, understanding, revelation, ability and strength to carry out and complete this study.

- *Mr. Johan Scholtz* and *Mr. Jaco Botha* for their technical and practical assistance during the course of this study.

- *Mr. Hendrik Louw*, *Mrs. Madeleine van Wyk* and *Mrs. Megan Weyers* for their assistance and support during the course of this study.

- To my parents, *Mr. Basil G. Howard* and *Mrs. Leonie Howard* for their continuous support, affirmation and prayer that carried me through this study.

- To *Dr. Karen Renaud*, *Mrs. Felicia J. Nel*, *Mrs. Abigail L. Howard* and *Mr. Daniel J. Fourie* for proofreading this report and their continuous love and support.

TABLE OF CONTENTS

LIST OF TABLES

LIST OF FIGURES

LIST OF SYMBOLS

β	Absorptivity coefficient
α	Thermal diffusivity ($W/m°C$)
ρ	Density (kg/m^3)
ε	Strain (m/m)
°C	Degrees Celsius
°F	Degrees Fahrenheit
D	Slab thickness (m)
μ	Microns ($\times 10^{-6}$)
φ_c	Thermal expansion of concrete (με/°C)
ΔT_{eq}	Equivalent linear temperature difference (°C/cm)
κ	Curvature (1/m)
k	Thermal conductivity ($W/m°C$)
x	Depth into the material (m)
Q_H	Internal heat generated per unit time and volume (W/m^3)
c	Specific heat capacity ($J/kg°C$)
t	Time (s).
T	Temperature (°C)
q_c	Convection heat flux (W/m^2)
h_c	Heat transfer coefficient ($W/m^2°C$)
T_c	Surface temperature (°C)
T_a	Ambient air temperature (°C)
w	Wind velocity (m/s)
q_s	Solar absorption heat flux (W/m^2)
q_{solar}	Solar radiation (W/m^2)
q_r	Surface emission heat flux (W/m^2)

θ	Emissivity coefficient = 0.88
δ	Stefan-Boltzmann radiation constant = $5.67 \times 10^{-8}\ W/m^{2\circ}C^4$
T_∞	Ambient air temperature (°C)
η	Porosity
m_s	Mass of the saturated sample to the nearest 0.01g (g)
m_d	Mass of the dry sample to the nearest 0.01g (g)
A	Area of the sample (mm^2)
d	Thickness of the sample (mm)
ρ_w	Density of water ($10^{-3} g/mm^3$ or $1000 kg/m^3$)
Ø	Diameter
ε_v	Deformation of the porous body
S_w	Degree of saturation of the pores (ratio)
K_b	Drained bulk modulus of porous body (Pa)
K_s	Bulk modulus of solid skeleton (Pa)
p_c	Capillary pressure (Pa)
R	Universal gas constant (8.314 J/mK)
T_k	Temperature (kelvin)
RH	Relative humidity (%)
M	Molar mass of the water (0.01802 kg/mol)
z	Section modulus (mm^3)

LIST OF ABBREVIATIONS

w/c	water/cement ratio
w/b	water/binder ratio
UTCRCP	Ultra-thin continuously reinforced concrete pavement
LVDT	Linear variable differential transducer
VW	Vibrating wire
VSLAM	Visual simultaneous localization and mapping
FDM	Finite difference method
RD	Relative density
HS	Higher strength
NS	Normal strength
E-value	Static modulus of elasticity
IST	Initial setting time
FST	Final setting time
UPV	Ultrasonic Pulse Velocity
MPa	Mega pascal
GGBS	Ground granulated blast furnace slag
BSM	Bitumen stabilised material

SIGN CONVENTION

Positive	=	Compression
		Expansion
		Curling (upwards curvature)
Negative	=	Tension
		Contraction
		Warping (downwards curvature)

1 INTRODUCTION

1.1 BACKGROUND

Ultra-thin continuously reinforced concrete pavement (UTCRCP) is defined as a concrete pavement layer built with a thickness less than 75 mm (Groenewald & Van Wijk, 2010) while thin concrete pavements have a thickness of less than 150 mm thickness. Both pavements are reinforced with steel reinforcement and/or steel fibres to strengthen the concrete in tension. Therefore, research conducted on thin concrete covers both ultra-thin and thin concrete pavements. The research already done on ultra-thin pavements (continuously reinforced and unreinforced) has predominantly focussed on the design, load bearing capacity and economics of ultra-thin pavements using heavy vehicle simulator tests and test sections on both urban and national roads in South Africa. Research already done focused on looking at the behaviour of the concrete pavements when subjected to traffic loading and not at environmental effects on the ultra-thin concrete pavement (Groenewald & Van Wijk, 2010; Kilian et al., 2014; Du Plessis et al., 2007) which Bredenhann et al. (2018) highlights as the main reason for the majority of defects found in ultra-thin continuously reinforced concrete pavements (UTCRCP).

After concrete has been mixed, the cement within the concrete begins to hydrate and the concrete starts to develop strength, moving from a plastic liquid to a solid state. The hydration of the concrete leads to heat being generated, which results in the thermal expansion of the concrete and then the subsequent thermal contraction of the concrete when cooling. This movement can result in stresses developing within the freshly cast concrete that could potentially exceed the early age strength of the concrete. Additionally, during the process of the hydration of the cement paste, the moisture within the pores of the concrete is used for the hydration process to take place and, as a result, the moisture content within the concrete steadily reduces and shrinkage of the concrete begins to take place. This type of shrinkage is known as autogenous shrinkage (Brooks & Neville, 2010; Ćećez et al., 2012). The moisture content within the concrete is further reduced due to the loss of moisture to the surrounding environment known as drying shrinkage (Bissonnette et al., 1999). Autogenous shrinkage is a shrinkage that takes place uniformly throughout the concrete while drying shrinkage is predominant at the surface of the concrete exposed when to the ambient environment (Brooks & Neville, 2010; Ćećez et al., 2012).

Curling is defined as the curvature of the concrete pavement that results from a temperature gradient within the concrete slab when the top and bottom surfaces are at two different temperatures due to the influence of the surrounding environment (Van Dam, 2015; Hansen & Mohamed, 1997). As a result of drying shrinkage within the pavement, the total length of the

concrete section reduces and warping of the concrete slab takes place, which is referred to as the curvature of the slab that is induced by a moisture gradient within the concrete due to the drying and wetting cycles of the concrete pavements' surface as a result of seasonal environmental effects (Van Dam, 2015; Hansen & Mohamed., 1997). The environmental effects on the concrete pavement are not the only factors effecting the curvature of the concrete pavement, Asbahan & Vandenbossche (2011) list three factors that affect slab curvature: 1) Temperature and moisture conditions at time of pavement construction, 2) the concrete material properties (thermal expansion, dry shrinkage, creep and elastic modulus) and 3) resistance to slab deformation (self-weight, friction and resistant movement joints). The temperature gradient within the concrete at the time that the concrete sets (when concrete moves from being a plastic material to being a solid), known as the built-in temperature gradient, greatly affects the curling of the concrete pavement and this is due to the response of the slab to a change in environmental conditions, being dependent on the magnitude and direction of the built-in temperature gradient (Asbahan & Vandenbossche, 2011).

There has been significant research already done on the warping and curling behaviour of ordinary concrete pavements of approximately 300 mm thick, with the pavements being either restrained or unrestrained (Asbahan & Vandenbossche, 2011; Phillips et al., 2006; Janssen et al. 2014). This research indicates that it is important to recognise the shape/curvature of the pavement at the time of traffic loading in order to fully understand the development of stresses within the concrete pavement. This is due to the pavement losing contact with the supporting structure, resulting in areas where concentrated loads can form, causing failure of the pavement (Asbahan & Vandenbossche, 2011).

Therefore, not only the length change and internal stress development, but also the warping and curling of thin concrete pavements need to be researched to have a full understanding of the environmental effects affecting the behaviour of thin concrete pavements.

1.2 OBJECTIVES OF THE STUDY

The main objectives of the study were:

- To determine the built-in temperature gradient in pavements of different thicknesses.
- To evaluate the effect of environmental condition on the length change, internal stresses, internal moment and curvature of thin concrete pavements for different pavement thicknesses.

- To determine how the variation in the daily and seasonal environmental conditions effect pavements of different thicknesses in terms of length change, internal stresses, internal moment and curvature.
- A secondary objective was to determine the effect of the concrete's material properties on the response (temperature gradient, length change, internal stresses, internal moment and curvature) of thin concrete pavements to environmental effects.

1.3 SCOPE OF THE STUDY

The study is limited in the following ways:

- Only two difference concrete strengths (normal strength of 40 MPa and higher strength of 55 MPa) were considered.
- The thicknesses of the thin pavements cast for the two different concrete strengths were 50, 75 and 100 mm thick to evaluate the effect of pavement thickness on the magnitude of shrinkage, internal stress development, curling and warping.
- The total early-age deformation of the pavements was not separated into plastic, autogenous and dry shrinkage but only considered as the total early age deformation of the concrete.
- The effects of daily and seasonal variation in environmental conditions on the pavement were measured for a period of 125 days. The effect of 3 seasons was recorded, but time constraints and the Covid-19 pandemics regulations made it impossible to record data during summer.
- The material properties of the concrete (compressive strength, split tensile strength, modulus of rupture, static modulus of elasticity, setting times, heat of hydration and shrinkage) were measured at different dates of 2, 7, 14, 28, 90 and 180 days with the samples being cured alongside the pavements to provide an accurate representation of the properties of the concrete pavement so that the curling and warping behaviour could be related to the material properties as they develop over time.
- All the thin concrete pavements were reinforced with Ø5.6 mm bars placed at the neutral axis of the pavement section so the pavement segments are representative of a continuously reinforced concrete pavement. The effect of steel reinforcement on the pavements behaviour in response to environmental loading fell outside of the scope of this study.

1.4 METHODOLOGY

There is a need to cast concrete pavements of different thicknesses and monitor the temperature and moisture content within the concrete from the time of casting and over an extended period of time. The pavement curvature in response to a change in the environment around the thin pavements was compared. By casting pavements of 50, 75 and 100 mm thickness, the effect of pavement thickness on not only internal strain and stress development but also the curling and warping of concrete pavements could be determined and by casting concrete of two different strengths, the effect of the concrete's material properties on the internal stresses, curling and warping of the concrete pavements could be determined.

The early age and drying shrinkage of the concrete were continuously measured. Shrinkage prisms were cast with relative humidity sensors placed at the centre and near the surface of the shrinkage prisms to relate the decrease in moisture content within the concrete to the drying shrinkage of the concrete. Early age shrinkage was measured in a temperature and humidity-controlled room. The early age and drying shrinkage were used to determine the deformation of the concrete due to plastic, autogenous and drying shrinkage seen in the concrete pavement.

1.5 ORGANISATION OF THE REPORT

The report consists of the following chapters and appendices:

- Chapter 1 serves as introduction to the report.
- Chapter 2 investigates and records the findings from literature.
- Chapter 3 describes the experimental procedures that were used through the course of the study.
- Chapter 4 reports on the mechanical properties of the concretes used in this study.
- Chapter 5 reports the results and conclusions from the tests and experiments on the behaviour of ultra-thin concrete pavements.
- Chapter 6 contains the conclusions and recommendations of the study.
- Chapter 7 contains the list of references.
- Appendices A through F contains data used in the study.

2 LITERATURE REVIEW

2.1 BACKGROUND TO ULTRA-THIN CONTINUOUSLY REINFORCED CONCRETE CAVEMENTS (UTCRCP)

Ultra-thin continuously reinforced concrete pavements (UTCRCP) are concrete pavements with a thickness of less than 75 mm (Groenewald & Van Wijk, 2010). UTCRCP were introduced in South Africa in 2007 in response to 70% of the road networks in South Africa being older than the intended 20-year design life of the pavements (Bredenhann et al., 2018). As a result of severe budgetary constraints and the need to structurally strengthen the existing pavements, UTCRCP were implemented to meet the requirements of the new innovative pavement repair strategy which needed to meet the following requirements (Bredenhann et al., 2018; Du Plessis et al., 2007):

- Being applied to an existing road surface with a minimum amount of preparation work to the existing road surface and structure.
- Construction of the new road surface must take place using equipment available in South Africa.
- New road surface should be open to traffic within 48 hours.
- The structural life expectancy of the road should be more than 30 years with a minimum amount of maintenance required during this period.
- That the road surface should be safe under all conditions.
- The new pavement must be cost effective.

Currently in South Africa there are two main types of UTCRCP in use, namely (Groenewald & Van Wijk, 2010):

- A high strength heavily steel reinforced concrete pavement, which is used mainly for the national roads which see high volumes of traffic.
- Normal strength concrete with nominal reinforcing steel, which is most often used for urban roads that see low to medium volumes of traffic.

The first pavement type has received the most attention by researchers due to the need for the national roads network in South Africa requiring an immediate upgrade and a refinement in the design process of these pavements to ensure they meet the requirement of the innovative pavement repair strategy (Bredenhann et al., 2017; Bredenhann et al., 2018; Du Plessis et al., 2007; Du Plessis et al., 2014; Ebels et al., 2010; Kearsley et al., 2014; Steyn et al., 2005).

Research has also been conducted on multiple normal strength URCRCP sections to also determine their effectiveness in being used as an overlay for pavements in urban areas subjected to low to medium volumes of traffic (2000 vehicles per day) (Groenewald & Van Wijk, 2010).

Steyn, et al. (2005) studied the performance of thin concrete pavements with different thicknesses that were placed on different support structures subjected to 400 000 equivalent 80 kN axle loads and a panel of 30 experienced road engineers evaluated the performance of each pavement and support structure combination. These researchers found that (Steyn et al., 2005):

- The UTCRCP is an effective method for carrying heavy vehicle loads if the concrete is supported adequately.
- When studying pavement thickness of 50 mm, 75 mm, 100 mm and 140 mm, the 75 mm pavement was found to be a critical pavement thickness which performed the worst in all the tests conducted and that pavements thicker and thinner than this 75mm pavement thickness were not as sensitive to the supporting material stiffness.
- The compressive and tensile stresses experienced in the pavements from the vehicle loading were lower than the compressive and tensile strength of the material used.

Based on the research done by Bredenhann et al. (2018), the most common defects that have been observed on UTCRCP are:

- buckling of the UTCRCP layer,
- blow-ups,
- transverse cracking,
- day joints opening and steel breaking,
- punch outs,
- debonding of UTCRCP from the asphalt layer,
- horizontal movement of pavement after blow ups occur,
- spalling of concrete at day joint and transverse cracks, and
- vertical deformation of UTCRCP.

Bredenhann et al. (2018) found that the predominate cause of the defects listed above were due to the daily and seasonal variations in the environmental conditions that the concrete pavements were exposed to. Bredenhann et al. (2018) studied and confirmed through finite element modelling (FEM) that the movement of the concrete pavement in response to a change in the

environmental conditions surrounding the pavement were the main cause for debonding, blow-ups and cracking of the concrete pavement which lead to water being able to enter through cracks and to reach the supporting material, weakening the supporting structure and allowing pumping of the supporting layers to take place, this allows for to vertical deformation of the pavement and punch outs to take place.

The pavement structure for a UTCRCP consists of an ultra-thin reinforced concrete pavement placed on a 30 mm finely graded asphalt concrete (AC) interlayer, to provide a level surface for the construction of the concrete pavement and to ensure uniform thickness of the concrete pavement. This is placed on a 170 mm thick bitumen stabilised material (BSM) upper subbase layer and a 300 mm cement treated lower subbase layer placed over a selected gravel layer (Bredenhann et al., 2018). It was found that debonding between the different layers of the supporting structure of a UTCRCP and the asphalt pavement itself, due to the repeated movement of the concrete pavement in response to changes in the environmental condition surrounding the concrete pavement resulted in the majority of the failures of a UTCRCP due to the concrete pavement no longer being uniformly supported through its length and as a result having localised areas for concentrated loads leading to the failure of the concrete pavement (Bredenhann et al., 2017; Bredenhann et al., 2018). Bredenhann et al. (2018) drilled 33 cores from a UTCRCP and summarised the results found from these cores in Figure 2.1 of how often debonding occurred in the UTCRCP and in which layers debonding most commonly occurred in. Bredenhann et al. (2018) found that most of the defects that occurred in UTCRCPs were due to thermal stresses that develop within the concrete pavement due to daily and seasonal temperature cycles and that the ingress of moisture into the concrete pavement and its supporting structure resulted in a further worsening of the debonding defects of the pavement with the supporting layers resulting in the premature failure of the concrete pavement.

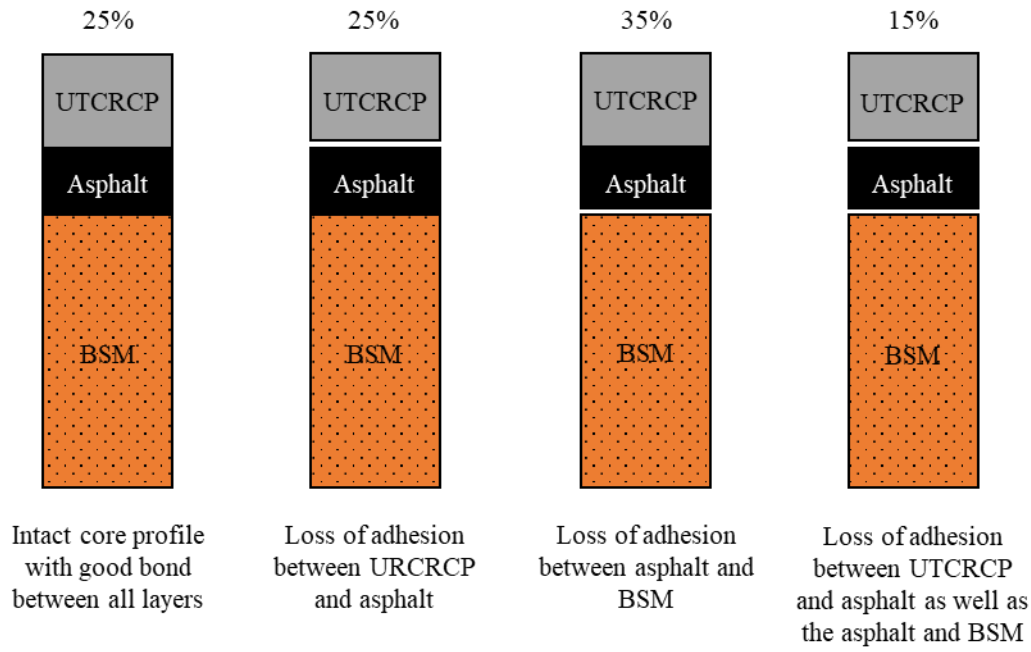

Figure 2.1: Results from 33 cores drilled from a UTCRCP (adapted from Bredenhann et al., 2018)

The deformation of a concrete pavement is not only due to the traffic loading experienced by the concrete pavement and the supporting substructure but also occurs due to the thermal stresses that develop within a concrete pavement due to a daily and seasonal changes in the ambient environment conditions and due to moisture entering and leaving the concrete pavement and its supporting substructure (Bredenhann et al., 2018).

The effects of environmental loading of a concrete pavement have been found to be the predominant cause of distress in a concrete pavement with traffic loading further accentuating this distress resulting in the premature failure of the structure before the end of its designed service life (Asbahan & Vandenbossche, 2011; Bredenhann et al., 2018; Fwa ,1987). The two predominant causes of distress of a concrete pavement are due to temperature and moisture within a concrete pavement, specifically the gradient caused by the temperature and moisture distribution. The temperature gradient within the concrete pavement results in thermal stresses developing within the concrete, while the moisture gradient results in differential shrinkage of the pavement, with the dominant effect being at the surface of the pavement. These gradients result in uniform contraction/expansion of the pavement and curvature of the pavement. The uniform contraction/expansion results in a uniformly distributed stress within the pavement if restrained while the curvature results in a bending moment within the pavement developing, this results in the uplift of the pavement from the supporting substructure and this is resisted by

the self-weight of the concrete, restraints and friction, which results in stresses developing within the concrete pavement (Janssen, 1987; Kadam & Mohod, 2016). These stresses that develop within the concrete pavement often result in the formation of minor cracks within of the concrete pavement which are worsened by the effects of traffic loading.

When concrete is cast, the cement within the concrete begins to hydrate and this chemical reaction is an exothermic reaction that generates a significant amount of heat. When a concrete pavement is cast, the heat that is generated is only capable of escaping through the surface and base of the pavement thus leading to a temperature gradient forming. The temperature gradient within the concrete at the time that the concrete sets is known as the built-in temperature gradient. This built-in temperature gradient affects the curling and warping of the concrete pavement due to the response of the slab to a change in environmental conditions, being dependent on the magnitude and direction of the built-in temperature gradient (Asbahan & Vandenbossche, 2011). The amount and rate at which heat is generated within the plastic concrete is also an important characteristic to consider due to this affecting the setting time of the concrete and the thermal expansion that takes place in the plastic concrete, which is followed by a thermal contraction of the hardened concrete. The thermal contraction of the hardened concrete could result in stresses developing within the concrete and cracks forming due to the concrete not yet having sufficient strength to resists the thermal stresses.

2.2 EARLY AGE TEMPERATURE EFFECTS CAUSED BY HYDRATION

When cement hydrates, there is heat that is generated due to the exothermic chemical reaction which takes place between the water and the cement and this chemical reaction between the water and cement occurs most rapidly within the first 24 hours in the life of the concrete (Pérez, 2013; Lim et al., 2016; Wang et al., 2007). The heat generated within the fresh plastic concrete can be quite large and the concrete experiences thermal expansion as a result of the heat generated. Once the concrete sets, the rate of the chemical reaction between the water and cement decreases and as a result, the rate of heat generated also decreases and the concrete begins to cool with the heat being lost to the surrounding environment. With the hardened concrete cooling, thermal contraction of the concrete takes place which leads to thermal stresses developing within the concrete due to the hardened concrete resisting the thermal contraction taking place (Pérez, 2013; Lim et al., 2016; Wang et al., 2007).

Figure 2.2 depicts the different temperature rises that are seen within concrete with varying cement contents and additional supplementary cementitious materials (SCM). From this figure, it is seen that there are different heat evolutions that occur within concrete based on the cement and SCM contents in concrete. Figure 2.3 depicts the temperature distribution in a concrete pavement and its support structure at different points in time and when different events took place in the life of the pavement. From Figure 2.3, the magnitude and direction of a typical built-in temperature gradient within a pavement due to the heat of hydration of the cement within the concrete can be seen. Figure 2.3 also depicts the temperature distribution when the joint of the pavement begins to crack due to thermal contraction of the hardened concrete. Both Figure 2.2 and Figure 2.3 depict the importance of the heat generated in concrete.

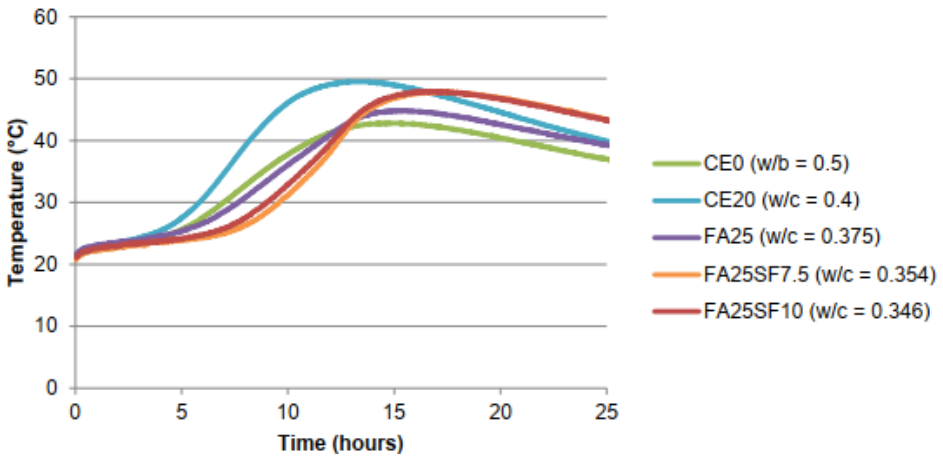

**CE = Cement; FA = Fly ash and SF = Silica fume*

**The numbers represent the % of the cement content added to the cementitious material in the mix.*

Figure 2.2: Temperature rise of concrete with SCM (Smith, 2015)

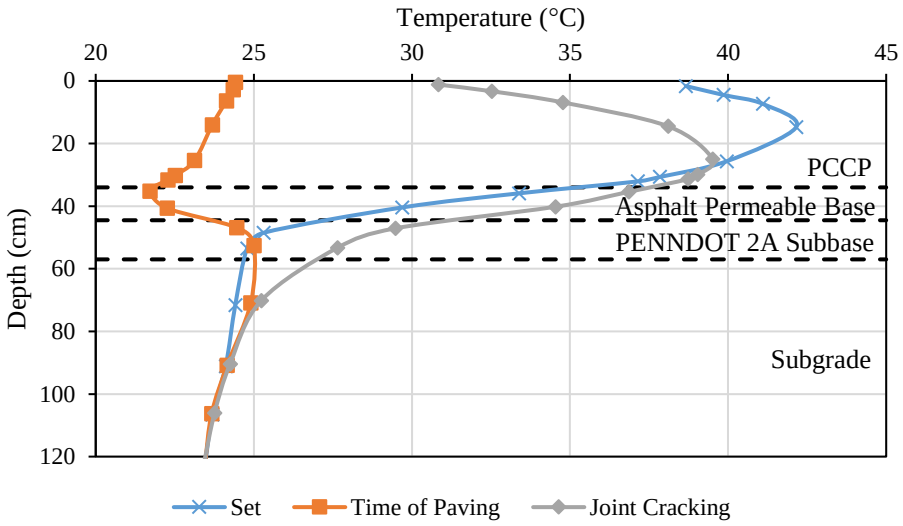

Figure 2.3: Temperature distribution in a pavement and support structure (adapted from Phillips et al., 2006)

2.3 SETTING TIME

The setting time of concrete is a complex parameter to determine, with many methods already being developed to determine this property of the concrete. Selecting the correct method for the determination of the setting time of the concrete is important due to the different methods having their own limitations and applications for intended use. The setting time of the concrete is an important parameter of concrete because it gives an indication of the point where the concrete is no longer a plastic fluid but begins to transition into becoming a solid and stresses can begin to develop within the concrete. The setting time is broken up into two components: initial setting time (IST) and final setting time (FST). The IST is defined as the point where the concrete has stiffened to such an extent that plasticity and workability of the concrete is lost and further consolidation of the concrete can no longer be achieved without damaging the concrete (Pérez, 2013). The FST is the point where the concrete begins to stiffen and stresses can begin to develop within the concrete. This is the point where the concrete becomes a solid material (Pérez, 2013). The setting time of the concrete is an important parameter to define in concrete pavements due to the built-in temperature and moisture gradients that exist within the concrete when the concrete reaches FST. These built-in gradients within the concrete influence the magnitude of the movement experienced by the pavement due to a change in the temperature and moisture gradients within the concrete in response to a daily and seasonal fluctuation in the environmental conditions surrounding the concrete which affects the internal stresses development, internal moment development and curvature on the concrete pavement.

The current methods that have been developed to determine the setting time of concrete are (Lim et al., 2016):

- Penetration based setting time.
- Longitudinal (P-wave) ultrasonic wave propagation.
- Semi-adiabatic calorimetry testing.

Penetration Based Setting Time

The ASTM C403 (2016) is a well-established method for the determination of the setting time of concrete which uses penetration resistance to determine the IST and FST by measuring the time taken for the concrete to reach a penetration resistance of 3.5 MPa and 27.6 MPa respectively for the IST and FST of the concrete (Pérez, 2013; Lim et al., 2016; Wang et al., 2007). This method of determining the setting times of the concrete has quite a few drawbacks, namely (Pérez, 2013; Lim et al., 2016; Wang et al., 2007):

- The test can only be performed on concrete mortar (concrete with aggregate less than 4.75 mm) therefore requiring the sieving of concrete with aggregate greater than 4.75 mm through a 4.75 mm sieve to perform the test on the concrete mortar only, which is not a fair representation of the concrete and requires the concrete to be workable for sieving. This could also lead to other complications such as sampling size required and energy required to sieve the concrete which need to remain constant.
- This method is quite labour intensive, requiring continuous testing at evenly spaced time intervals to determine the setting times of the concrete.
- The setting times are determined based on arbitrarily defined penetration resistance values.
- This test method is very sensitive to the environmental conditions that the concrete being tested is exposed to.

Longitudinal (P-wave) Ultrasonic Wave Propagation

This method makes use of ultrasonic pulse velocity (UPV) methods where either the wave transmission method or wave reflection method can be used (Lim et al., 2016). The wave transmission method measures the velocity, energy and frequency of the primary waves (P-waves) traveling through the material while the wave reflection method monitors the loss in the reflection of a shear wave (S-wave) at an interface between a steel plate and a cementitious material over time (Lim et al., 2016). The ultrasonic wave velocity curves of the concrete are measured over time and these velocity curves can be used to see how the elastic modulus and

poisons ratio begin to develop in the concrete as it hardens (Pérez, 2013). The P-waves are the waves with the highest velocity and have been found in previous research to be less sensitive than S-waves to the contact formed between the sample and the transducer. The P-waves have also been found to be more accurate in the determination of the velocity through a sample of concrete due to a high signal-to-noise ratio (Lim et al., 2016). The manner in which the setting times of concrete are determined using UPV methods can be seen in Figure 2.4.

Research has been done to corelate the setting times determined by UPV methods and penetration testing such as the ASTM C403 (2016). Researchers found that there is not a good correlation between the setting times determined by UPV and that of penetration testing (Pérez, 2013; Lim et al., 2016; Wang et al., 2007), with Lim et al. (2016) stating that the UPV test method gives a poor indication of the setting time in concrete and that the method is more useful for the tracking of the physical changes that take place in the concrete over time. This is due to the UPV being a function of the dynamic modulus of the concrete which changes as the hydration products within the concrete grow.

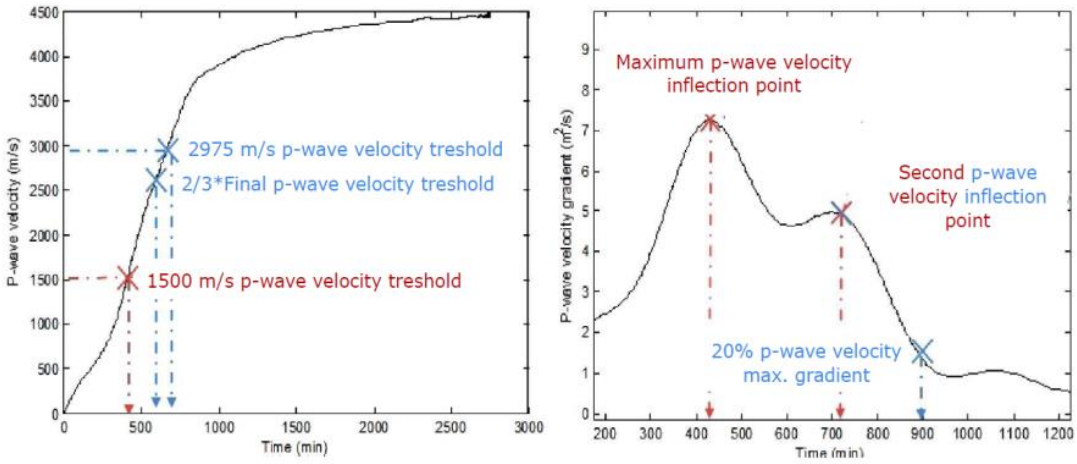

Figure 2.4: The setting time of concrete determined using UPV testing (red = IST and blue = FST) (Pérez, 2013)

Semi-adiabatic Calorimetry

As the semi-adiabatic calorimetry test looks at the heat gained and lost to the environment due to the chemical reaction of the hydration of the cement within concrete, the semi-adiabatic calorimetry method has been found to be a good measure to assess the setting time, stiffening and maturity of the concrete based on the temperature versus time curves that are generated by conducting a semi-adiabatic calorimetry test on a sample of concrete (Lim et al., 2016).

There are two methods that have been developed to determine the setting times of concrete based on the temperature verses time graphs that are generated (Wang et al., 2007):

- The derivatives method, which quantifies the initial and final setting time by determining the first and second derivative of temperature versus time. The peak of the second derivative of the temperature versus time function is defined as the IST of the concrete and the peak of the first derivative of the temperature versus time function defined as the FST of the concrete (Wang et al., 2007; Pérez, 2013). The breakdown of the definition of the derivatives method is shown in Figure 2.5.
- The fractional method defines the IST and FST of the concrete as the times corresponding to the maximum temperature rise of the concrete and defines the IST of the concrete as the time corresponding 20% of the maximum temperature rise and the FST as 50% of the maximum temperature rise (Wang et al., 2007; Lim et al., 2016). The breakdown of the definition of the fractional method is shown in Figure 2.6.

Wang et al. (2007) found that the fractional method is more robust and easier to use than the derivatives method, with the fractional method having a very good correlation between the setting time determined by the fractional method and penetration resistance testing in accordance with ASTM C403 (2016) of mortar as shown in Figure 2.7.

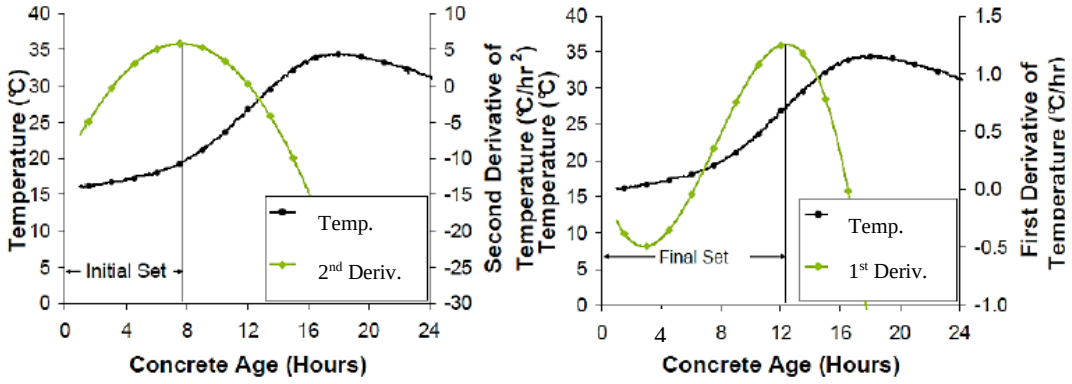

Figure 2.5: Setting times of concrete using the derivatives method (Pérez, 2013)

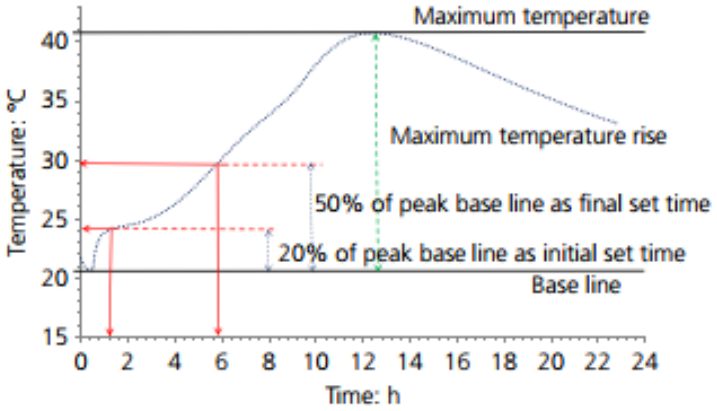

Figure 2.6: The fractional method used to determine the setting time of concrete (Lim et al., 2016)

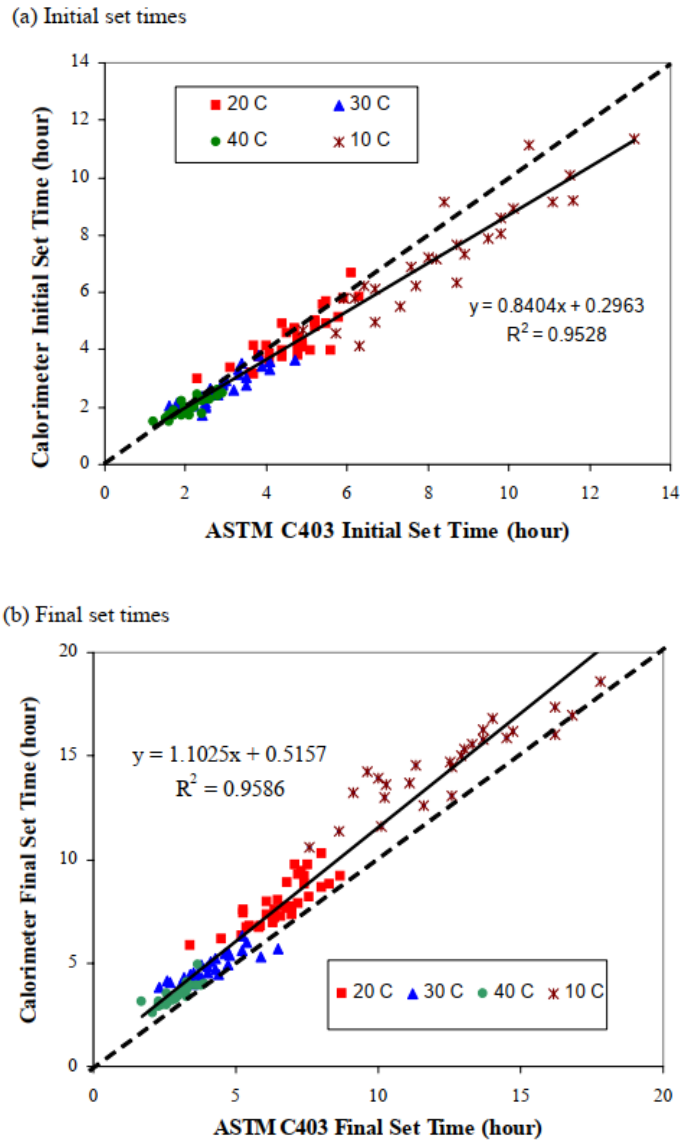

Figure 2.7: Correlation of (a) IST and (b) FST determined by the fractional method and ASTM C403 (2016) (Wang et al., 2007)

2.4 SHRINKAGE OF CONCRETE

Shrinkage within concrete represents a time dependent reduction in the volume of concrete due to the loss of moisture and due to carbonation of the concrete (Brooks & Neville, 2010; Ćećez et al., 2012; Domone & Soutsos, 2017). Shrinkage of concrete is affected by many factors which include ambient temperature and relative humidity, type and quantity of cement, water/cement (w/c) ratio, grain size and composition of the aggregate, concrete strength, workability, curing, and age of the concrete (Brooks & Neville, 2010; Ćećez et al., 2012). Figure 2.8 gives a detailed summary of factors that affect the volumetric deformation of concrete. From this figure, it can be seen that the deformation of concrete is a complicated issue, and its magnitude is influenced by many factors.

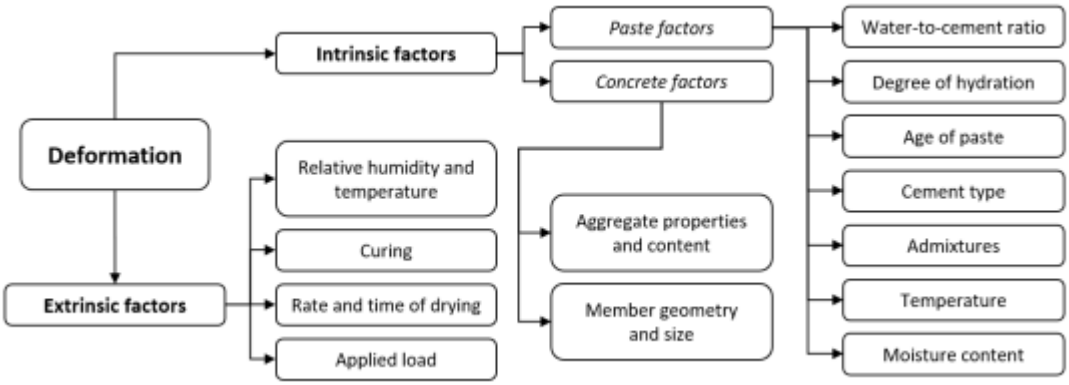

Figure 2.8: Factors effecting the deformation of concrete (Visser, 2019)

Figure 2.9 shows the generalize effect of w/c ratio and cement content on the shrinkage of concrete. Figure 2.10 demonstrates the effect of ambient relative humidity on the shrinkage of concrete while Figure 2.11 shows the effect that volume to surface ratio has on the ultimate shrinkage of concrete. From these figures it is seen that a drier ambient environment results in a larger amount of shrinkage taking place within the concrete. This is due to moisture being sucked out of the concrete into the dryer environment. It is also seen that increasing the volume of concrete that is being cast in a given area results in a reduction in the shrinkage of the concrete due to the increase in thickness resulting in an increase in time required to dry the core of the concrete. The shrinkage of concrete in pavements where movement is restrained can result in the formation of cracks if the shrinkage strain exceeds the strain required to induce a tensile stress equivalent to the tensile strength of the concrete. The concretes material properties also plays a role in the stresses that develop due to the elastic modulus (E-value) and creep of the concrete, where a concrete with a lower E-value would experience less stresses for the same strain as that of a concrete with a higher E-value due to the relationship that exists between the

properties of $E = \frac{\sigma}{\varepsilon}$ and the stresses that are also alleviated within the concrete due to creep which is the time dependent strain deformation of the concrete (Domone & Soutsos, 2017).

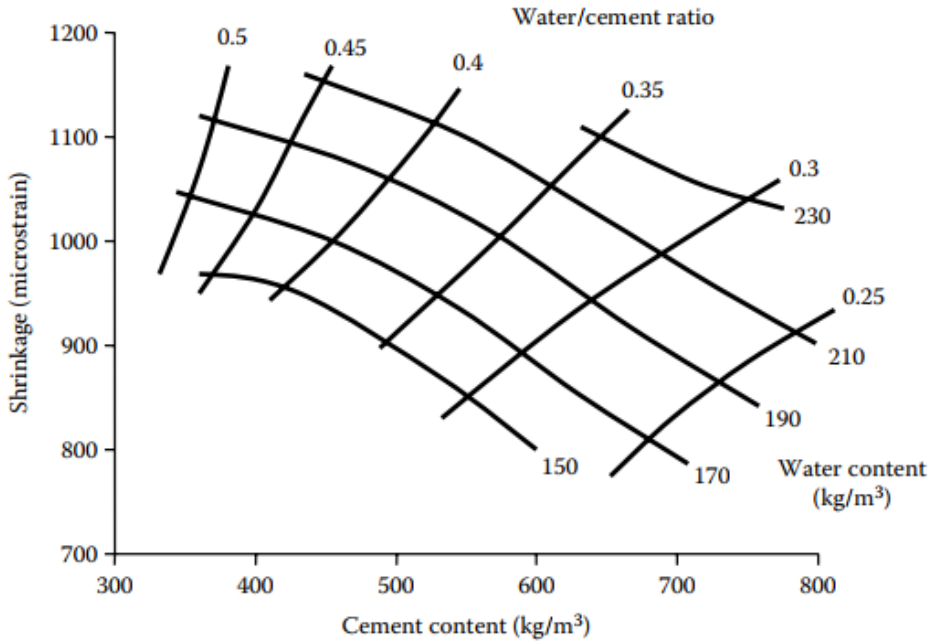

Figure 2.9: Effect of mix composition on shrinkage (Domone & Soutsos, 2017)

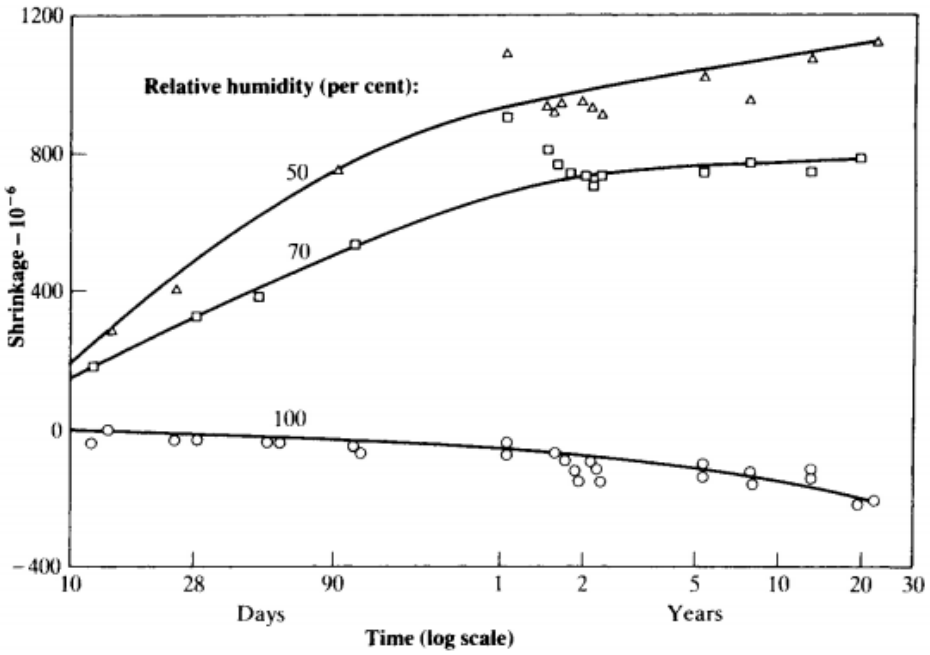

Figure 2.10: Effect of relative humidity on shrinkage (Brooks & Neville, 2010)

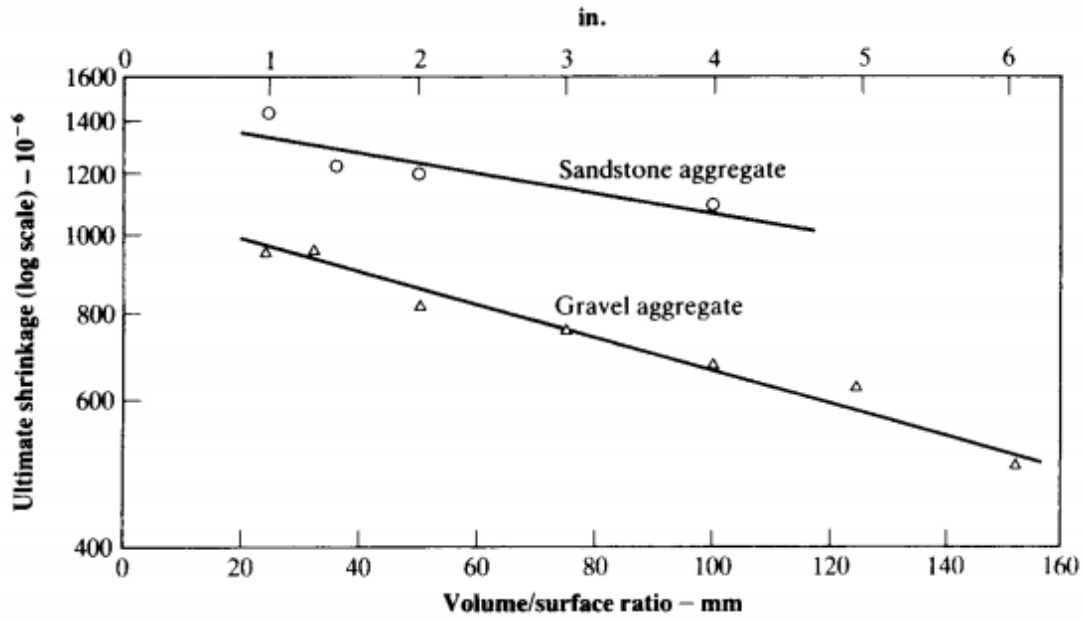

Figure 2.11: Relationship between ultimate shrinkage and volume/surface ratio (Brooks & Neville, 2010)

There are four main types of shrinkage (Brooks & Neville, 2010; Ćećez et al., 2012):

- Plastic shrinkage
- Autogenous shrinkage
- Drying shrinkage
- And carbonation shrinkage

2.4.1 Plastic shrinkage

Plastic shrinkage occurs at an early stage within the life of the concrete before the concrete begins to set. Plastic shrinkage develops on the surface of fresh concrete due to the evaporation of water on the surface of the concrete or due to suctions from dryer concrete below the surface of the concrete cast (Brooks & Neville, 2010; Ćećez et al., 2012). Plastic shrinkage results in cracking of the concrete surface due to the concrete not yet having any strength to resist the tensile force developed in the concretes surface. The main factor affecting plastic shrinkage of concrete is the rate of moisture evaporation on the surface of the concrete and is therefore dependent on wind speed, temperature of the concrete, ambient air temperature and relative humidity (Brooks & Neville, 2010; Ćećez et al., 2012; Domone & Soutsos, 2017). In order to reduce the amount of plastic shrinkage within concrete, the concrete needs to be protected

against the surrounding environment that would cause evaporation of water on the surface of the concrete to take place and afford sufficient time for the concrete to cure and gain strength.

2.4.2 Autogenous shrinkage

With no additional external moisture entering the concrete, autogenous shrinkage (also known as chemical shrinkage) occurs as a result of the reduction in moisture content within the concrete, as water is used for the hydration of cement within the pores of the concrete (Ali & Urgessa, 2014; Brooks & Neville, 2010; Ćećez et al., 2012). Autogenous shrinkage persists within concrete so long as the hydration of cement takes place. Lura & Wyrzykowski (2016) found that the hydration of cement ceases when the internal relative humidity within concrete falls below 80%. Autogenous shrinkage represents only about 50 to 300 με of the shrinkage within normal strength concrete while higher autogenous shrinkage can be expected in high strength concrete with a cement content of 450 to 550 kg/m^3, w/c ratio of 0.20 to 0.25 and concrete containing supplementary cementitious material such as fly ash, ground granulated blast furnace slag (GGBS) and silica fume. Autogenous shrinkage is dependent on the w/c ratio of the concrete where a decrease in the w/c ratio results in an increase in autogenous shrinkage (Brooks & Neville, 2010; Ćećez et al., 2012; Domone & Soutsos, 2017). This form of shrinkage is the most prevalent when the hydration reactions within the concrete occur most rapidly, with the greatest effects occurring within the first few hours and days after casting of the concrete (Brooks & Neville, 2010; Ćećez et al., 2012; Domone & Soutsos, 2017). There is no method that can eliminate this form of shrinkage within concrete but can only be compensated for during the determination of the mix design of the concrete by considering the cement content and w/c ratio of the concrete (Visser, 2019).

2.4.3 Drying shrinkage

Drying shrinkage is the shrinkage that occurs due to a loss of moisture within the concrete to the surrounding environment (Brooks & Neville, 2010; Ćećez et al., 2012). Moisture exists within concrete as water vapour, capillary water, absorbed water, interlayer water and chemically combined water where the loss in capillary, absorbed and interlayer water are largely responsible for drying shrinkage within concrete due to the capillary tensile forces that are formed within the pores of the concrete when moisture within these pores begins to diffuse out of the concrete, this force increases as moisture is lost within these pores and for a concrete with a smaller pore size (Domone & Soutsos, 2017). Water that is lost within concrete can only escape through the surface of the concrete and as a result the inner core of a specimen acts as a restrain against movement, furthermore the amount of shrinkage that takes place is dependent on the specimen size and proportions with this effect being depicted in Figure 2.11 (Brooks & Neville, 2010; Ćećez et al., 2012; Domone & Soutsos, 2017). The longer the path that moisture

must travel to diffuse out of the concrete to the surrounding environment, the less shrinkage will take place due to the pore size reduction within the concrete restricting moisture transportation in and out of the concrete and the longer it will take for shrinkage of the concrete to take place as shown in Figure 2.12. Other factors that affect drying shrinkage are porosity, amount of free water in the concrete, paste content, cement fineness and ambient temperature and relative humidity (Ćećez et al., 2012).

The drying shrinkage that takes place within concrete is not fully recoverable and can be split into 2 components, being reversible and irreversible shrinkage, which can be seen in Figure 2.13. The maximum amount of shrinkage that takes place within concrete takes place within the first drying cycle and a substantial portion of this shrinkage is irreversible upon rewetting of the concrete due to this shrinkage being caused by factors such as self-desiccation of the concrete and changes in the microstructure and chemical composition of the concrete (Brooks & Neville, 2010; Bullard et al., 2017; Ćećez et al., 2012; Domone & Soutsos, 2017).

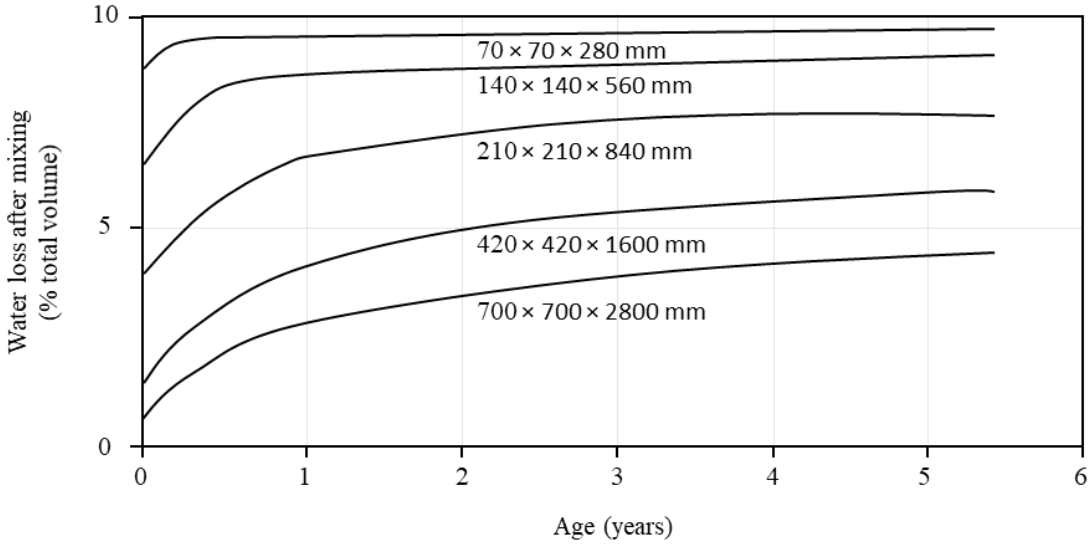

Figure 2.12: Effect of specimen size on the rate of water loss (adapted from Neville, 2011)

The shrinkage which takes place within the cement paste is restrained by the aggregate within the concrete thereby reducing the total amount of shrinkage measured (Brooks & Neville, 2010; Domone & Soutsos, 2017). Figure 2.14 shows just how significant the effect of aggregate content is on shrinkage of concrete and how increasing the aggregate content within concrete, can reduce the overall shrinkage of the concrete.

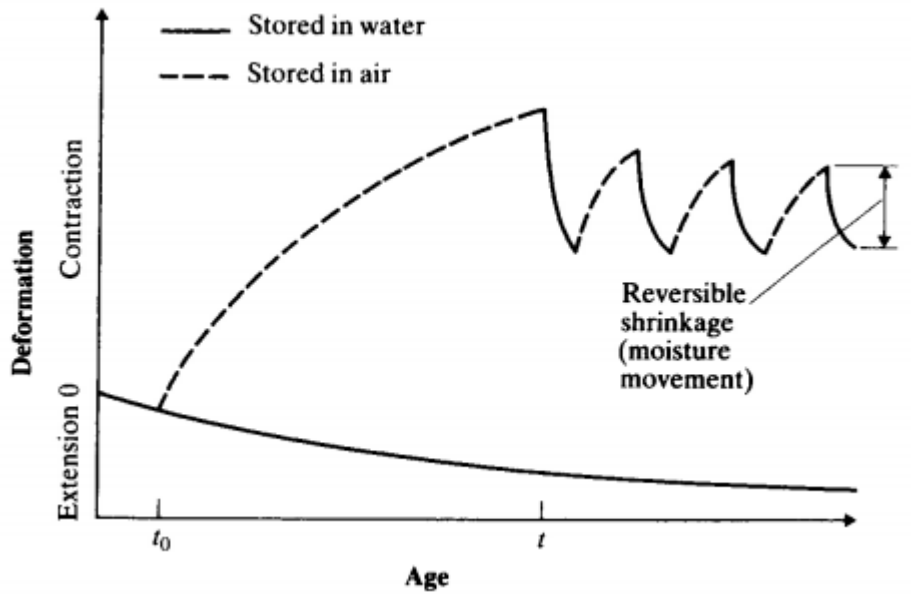

Figure 2.13: Moisture movement within concrete (Brooks & Neville, 2010)

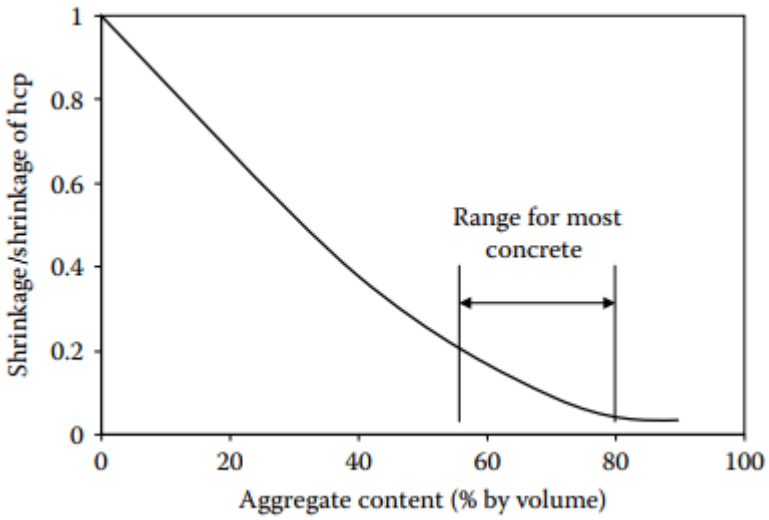

Figure 2.14: The effect of aggregate content on shrinkage (Domone & Soutsos, 2017)

2.4.4 Carbonation shrinkage

Carbonation shrinkage is a long-term shrinkage that occurs due to the intrusion of carbon dioxide from the environment into the concrete which alters the chemical composition of the concrete (Brooks & Neville, 2010; Ćećez et al., 2012; Domone & Soutsos, 2017). Unlike the other forms of shrinkage, carbonation shrinkage does not result from a loss in moisture content within the concrete but due to a change in chemistry within the concrete. When carbon dioxide meets water, it forms carbonic acid which reacts with the calcium hydroxide of the concrete to form calcium carbonate. Other components of the concrete are also degraded but the overall degradation of the concrete is known as carbonation shrinkage (Brooks & Neville, 2010; Ćećez et al., 2012; Domone & Soutsos, 2017). The amount of carbonation shrinkage is dependent on the permeability of the concrete, w/c ratio, carbon dioxide content of the air and ambient temperature and relative humidity (Brooks & Neville, 2010; Ćećez et al., 2012; Domone & Soutsos, 2017). Figure 2.15 demonstrates just how significant carbonation shrinkage is when considering the total shrinkage realised within concrete when exposed to a carbon dioxide rich environment at various ambient relative humidity levels. This type of shrinkage falls outside the scope of this study.

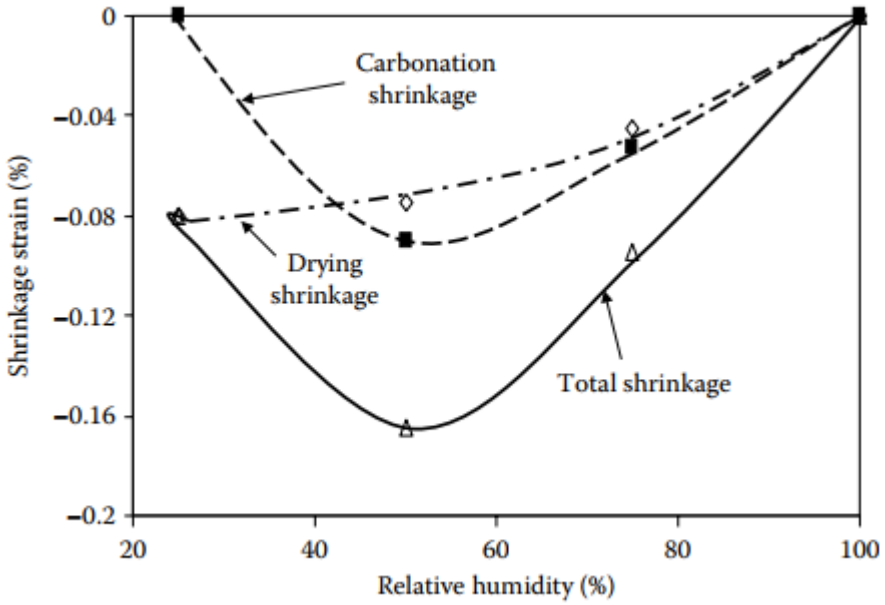

Figure 2.15: Ambient relative humidity versus shrinkage (Domone & Soutsos, 2017)

2.4.5 Shrinkage related to internal relative humidity.

It is generally agreed that there are multiple mechanisms involved in the drying of concrete, but all the mechanisms are dependent on the moisture content within the pores of the concrete (Bella et al., 2017). This is due to the strong van der Waals attractive forces that exist between individual water molecules that induce a capillary pressure on the solid skeleton of the concrete (Bella at al., 2017). The moisture content within concrete is commonly quantified by determining the internal relative humidity of the concrete (Azenha et al, 2011; Zahng et al., 2010) and the Kelvin-Laplace equation (Equation 2.1) is the equation commonly used to determine the change in pressure exerted by the moisture within the pores of the concrete due to a change in the internal relative humidity.

$$p_c = \frac{\rho_w R T_k \ln(RH)}{M} \qquad \text{(Equation 2.1)}$$

Where:

p_c = Capillary pressure (Pa)
ρ_w = Density of the water ($1000 kg/m^3$)
R = Universal gas constant ($8.314\ J/mK$)
T_k = Temperature (kelvin)
RH = Relative humidity (%)
M = Molar mass of the water ($0.01802\ kg/mol$)

Bishop (1959) developed Equation 2.2 which relates the deformation of a porous body to the change in the capillary pressure, bulk moduli and the degree of saturation of the solid material (Bella et al., 2017). Bella et al. (2017) found that Equation 2.2 predicts the shrinkage within concrete with good agreement with the values determined through measuring the drying shrinkage of the concrete as shown in Figure 2.16.

$$\varepsilon_v = -S_w p_c \left(\frac{1}{K_b} - \frac{1}{K_s}\right) \qquad \text{(Equation 2.2)}$$

Where:

ε_v = Deformation of the porous body
S_w = Degree of saturation of the pores (ratio)
K_b = Drained bulk modulus of porous body (Pa)
K_s = Bulk modulus of solid skeleton (Pa)

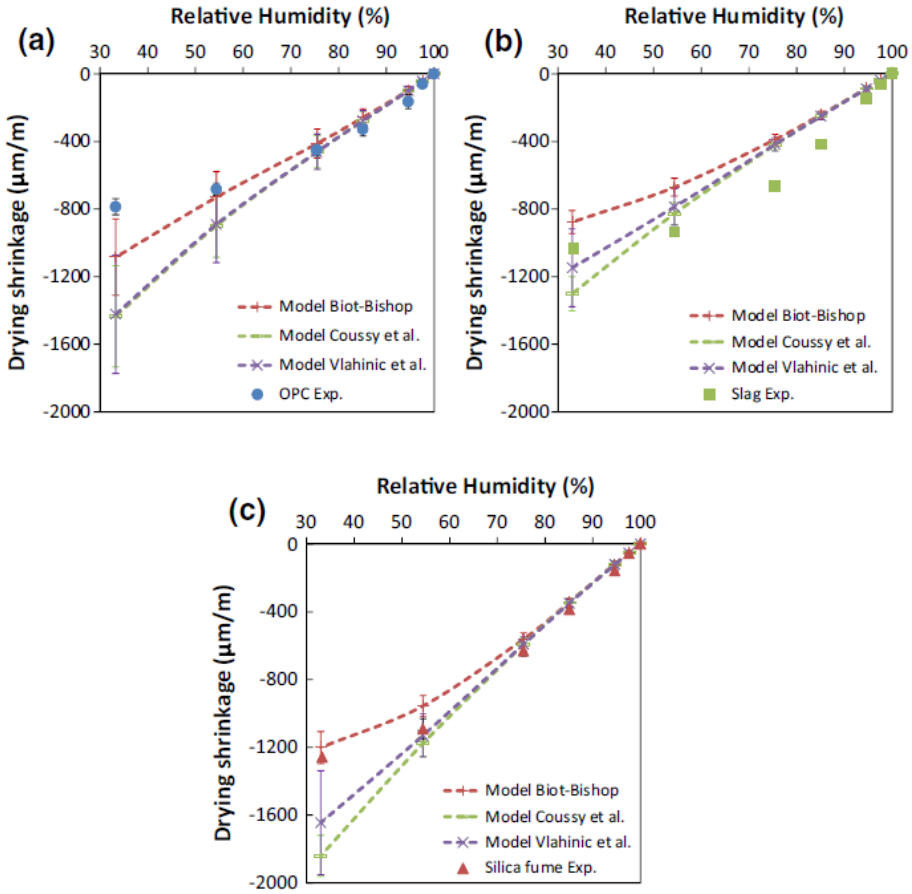

Figure 2.16: Corelation of measured and predicted shrinkage for (a) ordinary portland cement (OPC), (b) concrete containing slag and (c) concrete containing silica fume (Bella et al., 2017)

Figure 2.17 depicts the relationship between the internal relative humidity and the shrinkage of the concrete. It is seen that the shrinkage realised by the concrete is not directly proportional to the decrease in the moisture content of the concrete. This is due to the moisture gradient that exists within concrete. The varying internal relative humidity measure at different depths within a concrete sample can be seen in Figure 2.18. This figure shows that the surface of the concrete dries at a much faster rate than the interior of a concrete sample thereby generating a moisture gradient within the concrete which, when using Equation 2.2, results in a shrinkage gradient within the concrete causing the concrete with lower shrinkage to restrain the zones of the concrete with higher shrinkage, resulting in internal stresses developing within the concrete.

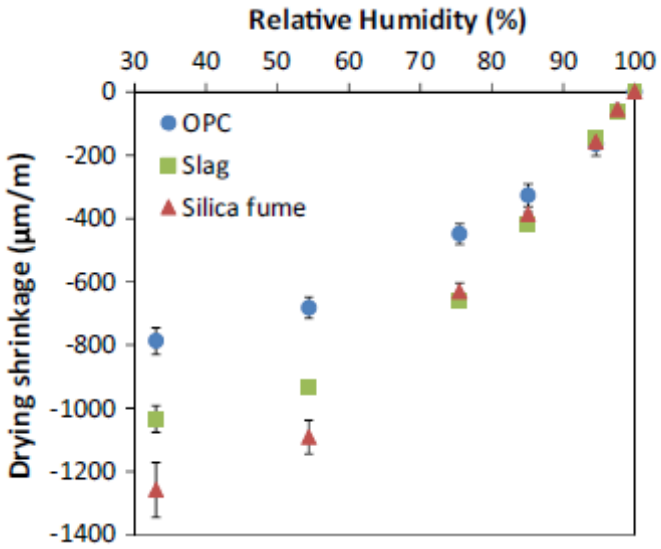

Figure 2.17:Internal relative humidity versus drying shrinkage (Bella et al., 2017)

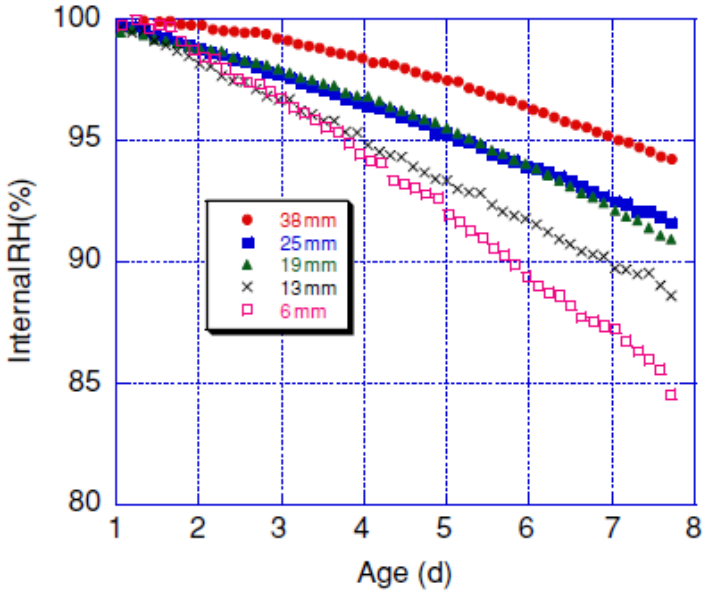

Figure 2.18: Internal relative humidity over time at different measurement depths within concrete (Grasley et al., 2006)

2.5 INTERNAL STRESSES IN CONCRETE PAVEMENTS

The stresses that occur within a concrete pavement are not only due to wheel loading but also due to environmental loading (Armaghani et al., 1987; Armaghani & Richardson., 1987; Dempsey et al., 1987; Flanagon & Hudson, 1987; Janssen, 1987). The deterioration or damage that occurs in concrete pavements are predominantly due to the environmental effects, material problems and applied loads (Flanagon & Hudson, 1987). When speaking about environmental loading, this refers to the effects that the ambient environment has on the concrete pavement. Ordinary concrete pavements rarely have a uniform temperature throughout their thickness, and it is even less likely to have a uniform moisture content throughout the concrete slab depth (Armaghani et al., 1987; Armaghani & Richardson., 1987; Dempsey et al., 1987; Flanagon & Hudson, 1987; Jeong & Zollinger, 2005; Janssen, 1987). This non-uniform distribution of moisture and temperature within the concrete is known as a moisture gradient and temperature gradient. When considering environmental loading on a concrete pavement, the moisture and temperature gradients that develop within the concrete pavement have the largest effect on the development of stresses within the concrete pavement (Armaghani & Richardson., 1987). This is due to these two properties controlling the curvature of the pavement and as a result the internal stresses that are develop within the concrete pavement (Armaghani et al., 1987; Armaghani & Richardson., 1987; Dempsey et al., 1987; Flanagon & Hudson, 1987; Janssen, 1987). The response of a typical concrete pavement to an internal temperature and moisture gradient can be seen in Figure 2.19 when the pavement is placed directly on supporting granular material or when debonding occurs. It should be noted that stresses do not develop within an unrestrained concrete pavement but rather in a pavement that is restrained against the movement as depicted in Figure 2.19. This in combination with traffic loading results in significant stresses developing within the concrete pavement.

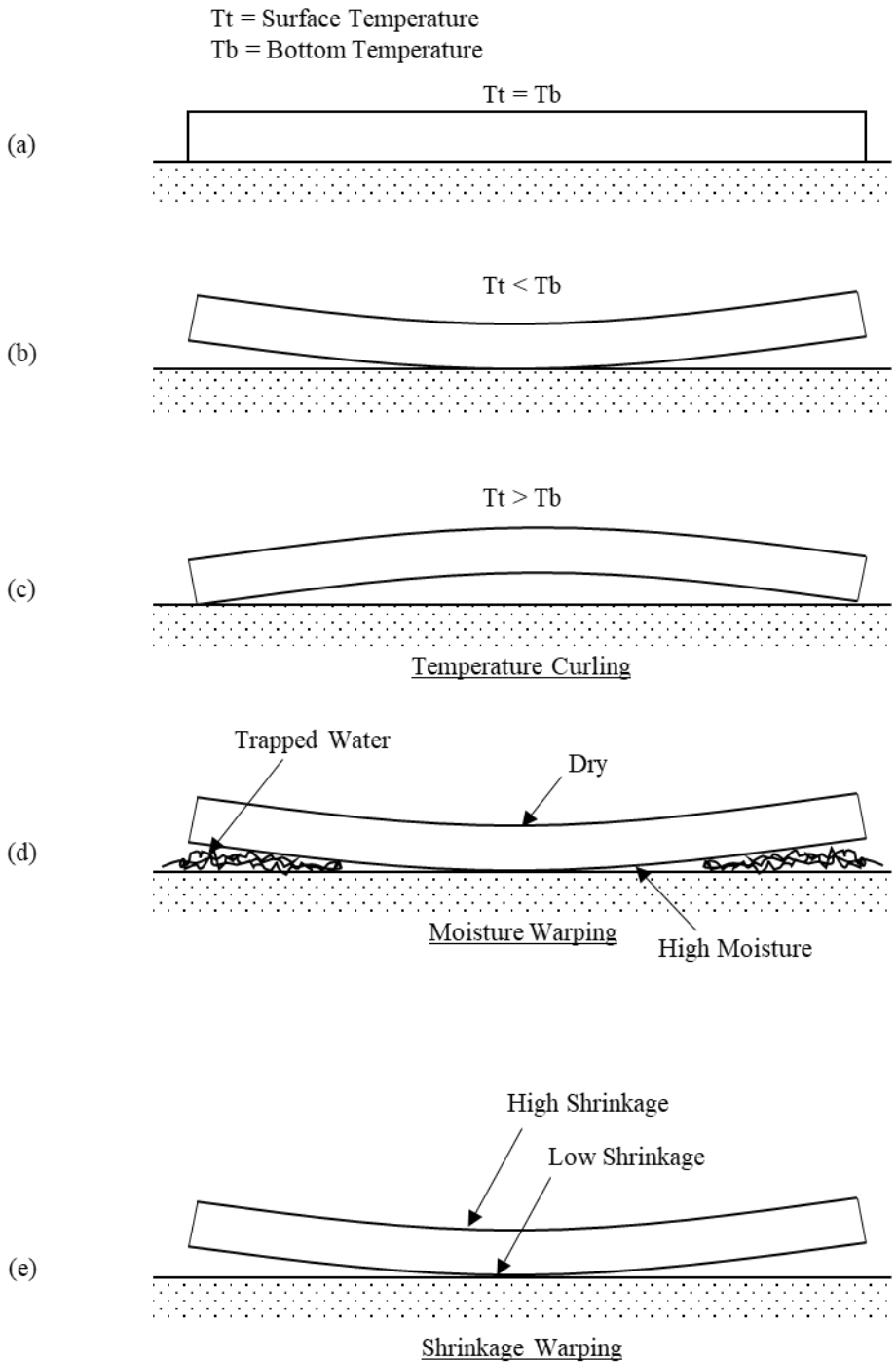

Figure 2.19: The curling and warping of concrete pavement slabs (adapted from Armaghani et al., 1987)

2.5.1 Temperature gradients

During the day, the concrete surface is exposed to the ambient environment and the surface of the concrete begins to heat up at a faster rate than the rest of the concrete due to solar radiation and increase in air temperature in contact with the surface of the concrete. This heat is then diffused down into the concrete at a rate dependent on the thermal properties of the concrete. This leads to a temperature gradient that develops within the concrete due to the uneven distribution of heat within the concrete pavement. The reverse case is also true when the ambient temperature surrounding the concrete is lower than that inside the concrete, then heat that was stored within the concrete throughout the day diffuses out of the concrete through the surface of the concrete to the surrounding environment resulting in another temperature gradient but in the opposite direction to that seen during the daytime.

Figure 2.20 and Figure 2.21 show the magnitude and direction of these temperature gradients and how they change through the course of the day in response to a change in the ambient environmental conditions. From these figures, the most extreme temperature distributions within the concrete pavement can be seen to occur just after sun rise (between 4:00 a.m. and 8:00 a.m.) and just before the sun sets (between 4:00 p.m. and 8:00 p.m.). This makes sense due to the coldest time of day occurring just before the sun rises and the hottest time of the day occurring a few hours after 12:00 a.m. in the day due to solar radiation still heating up the surface of the concrete and the surrounding environment until the point that the sun sets.

Armaghani et al. (1987) studied the temperature distribution through a 230 mm (9-inch) thick concrete slab in Florida, United States for 230 days and found that the largest positive temperature gradients within the concrete were experienced between 12:00 a.m. to 3:00 p.m. in the afternoon and the largest negative temperature gradients were experienced between 5:00 a.m. to 7:00 a.m. in the morning. It was also discovered that the pavement experienced a more or less uniform temperature distribution namely at around 9:00 a.m. and 7:00 p.m. in a daily cycle (Armaghani et al., 1987). These correspond to the points when the pavement is heating up and cooling down.

From Figure 2.21 is can be seen that the greatest changes in the temperature distribution within the concrete pavement occurs within the top 100 mm of the pavements thickness, for this reason the maximum thickness of thin pavements investigated in this study will be of 100 mm thickness.

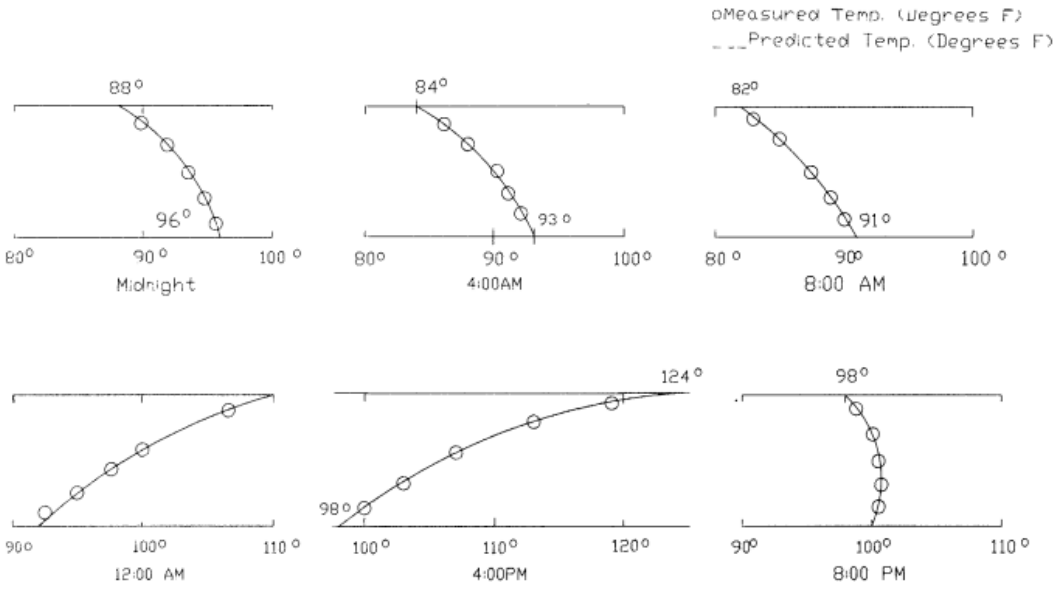

Figure 2.20: Temperature gradient in a 230 mm thick pavement (Armaghani & Richardson, 1987)

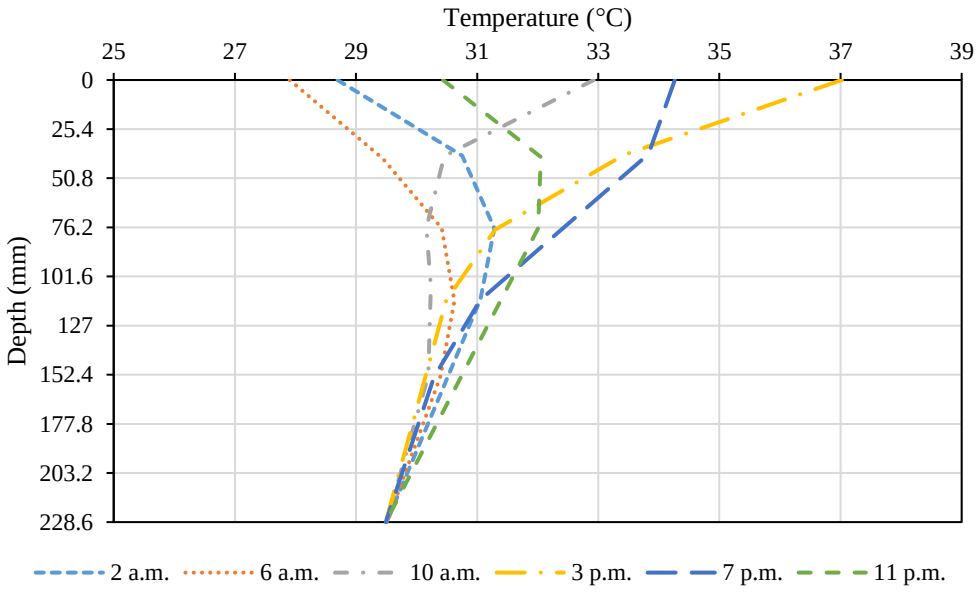

Figure 2.21: Temperature distribution over 24 hours (adapted from Hill et al., 1987)

Figure 2.22 depict how heat propagates/diffuses into and out of a 230 mm (9-inch) thick concrete pavement over a period of 24-hours. The general trend is that the surface that is in contact with the changing environment will see the greatest and most rapid changes in

temperature with the effects being propagated/diffused further into the material. These temperature differentials that develop within the concrete over time can be seen in Figure 2.23. Armaghani et al. (1987) found that in a 230 mm (9-inch) thick concrete pavement that there is approximately a 2 to 4 hour delay between the time when the top surface begins to see a change in temperature and the bottom surface begins to see a proportional change in temperature. This is due to the thermal conductivity properties of the concrete and is also the reason why there is a rapid increase and decrease in the temperature differential seen during the daytime hours typically between 6:00 a.m. and 18:00 p.m.

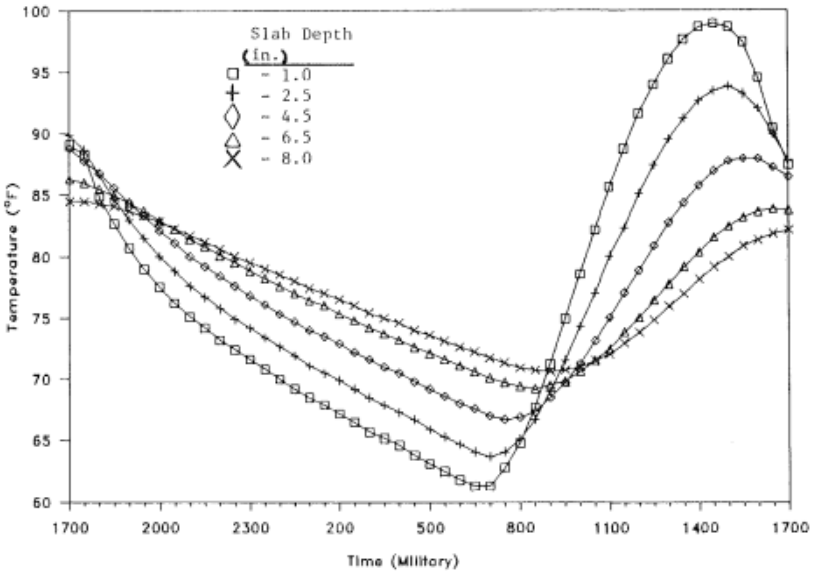

Figure 2.22: Temperature variation with depth (Armaghani et al., 1987)

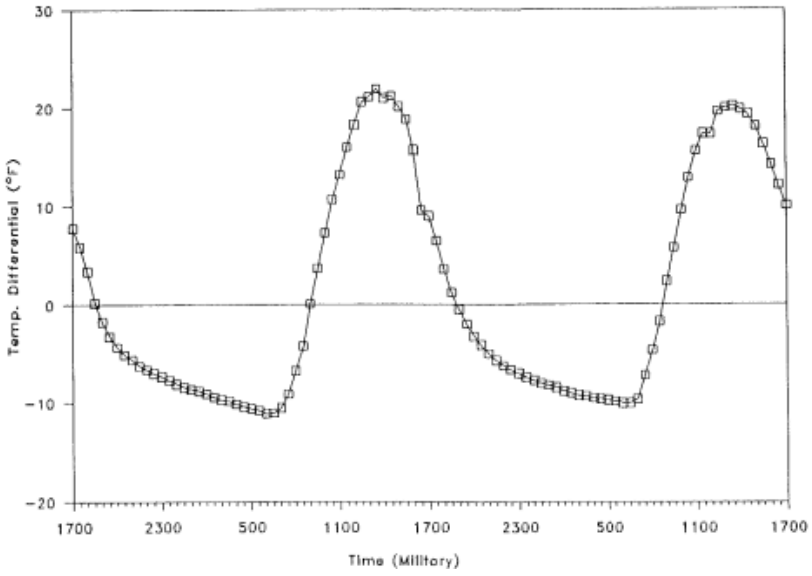

Figure 2.23: Temperature differential over time (Armaghani et al., 1987)

2.5.2 Moisture gradients

Similar to a temperature gradient within the concrete pavement, there exists an uneven moisture distribution within the concrete with the worst effect being seen at the surface of the concrete (Janssen, 1987; Gao et al., 2016). Shrinkage occurs within the concrete as moisture is removed from the hardened cement paste and due to the hydration of the hardened cement paste (Ali & Urgessa, 2014; Janssen, 1987; Gao et al., 2016). This shrinkage takes place at different rates and in different forms within a concrete pavement. Figure 2.24 shows the typical moisture gradient that exist with a concrete slab both at an early age and after 28 days. This figure also shows the effect that this moisture gradient has on the shrinkage and movement of the concrete pavement. The behaviour in Figure 2.24 was derived from experiments done on concrete slabs with various w/c ratios as shown in Figure 2.25. This moisture distribution within the concrete pavement is further supported by the moisture measurements in a 300 mm concrete pavement shown in Figure 2.26. From these three figures it can be seen that the top and bottom surfaces of the slab are the regions that are the most affected by moisture transportation into and out of the concrete. Janssen (1987) found that the effects of surface drying, and moisture absorption only penetrates as far as 50.8 mm (2 inches) into the concrete and the remainder of the deformation of the concrete is due to self-desiccation of the hardened cement paste. This is supported by the research and experiments conducted by other researchers (Ali & Urgessa, 2014; Goa et al., 2016; Lange et al., 2006; Grasley, 2001).

Moisture movement within the concrete occurs in response to the internal relative humidity within the pores of the concrete wanting to be at an equilibrium relative humidity with the surrounding environment (Ali & Urgessa, 2014). Drying shrinkage of the concrete is most prevalent on the top surface of the concrete due to the surface experiencing the greatest amount of moisture loss from being exposed to the ambient environment. In the core of the concrete slab, self-desiccation of the concrete takes place due to the hydration of the hardened cement paste. This causes a uniform contraction of the concrete pavement while the moisture content experienced in the bottom of the concrete is dependent on the moisture content of the supporting medium below the concrete pavement. This is in response to the bottom surface of the pavement wanting to be at an equilibrium relative humidity content with that of the soil (Ali & Urgessa, 2014; Gao et al., 2016). The deformation and subsequent stress development within the concrete due to a moisture gradient will therefore predominantly be controlled by the moisture distribution in the top and bottom 50.8 mm (2 inches) of the concrete pavement (Janssen, 1987, Gao et al., 2016**)**.

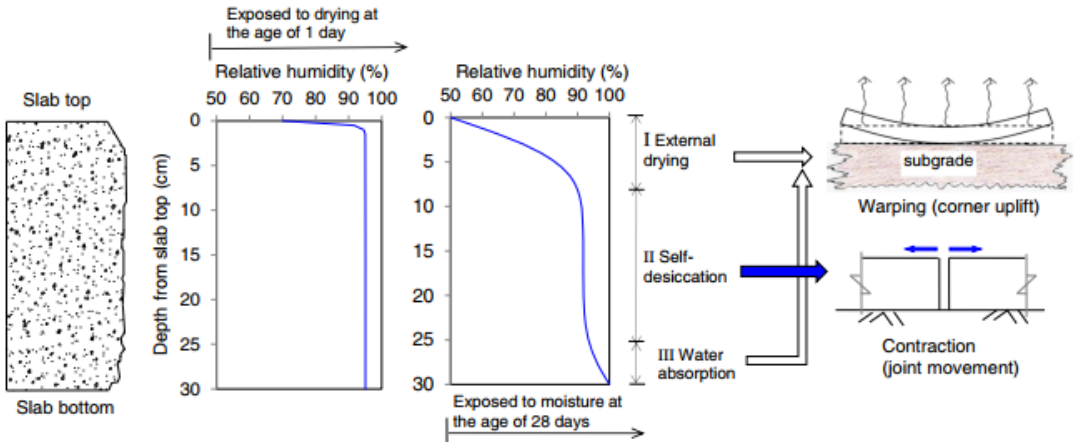

Figure 2.24: Moisture distribution and slab deformation (Gao et al., 2016)

When the concrete experiences a decrease in moisture content there is a corresponding shrinkage that takes place and if this shrinkage is prevented from taking place, tensile stresses begin to develop within the concrete (Janssen, 1987; Kadam & Mohod, 2016). The moisture gradient within the concrete pavement leads to curvature of the pavement and this curvature is resisted by the self-weight of the concrete pavement, pavement restraint and friction leading to internal stresses developing (Janssen, 1987). Fwa (1987) found that in tropical regions, pavements can experience distress due to moisture entering and leaving the permeable concrete where some pavements experienced a 20 to 40 mm swell after a tropical storm and after the moisture evaporated this caused the concrete joints to open and moisture to enter the supporting material.

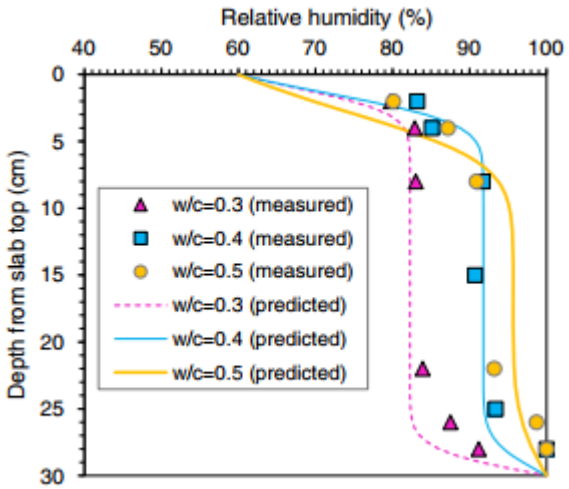

Figure 2.25: Relative humidity distribution in concrete (Gao et al., 2016)

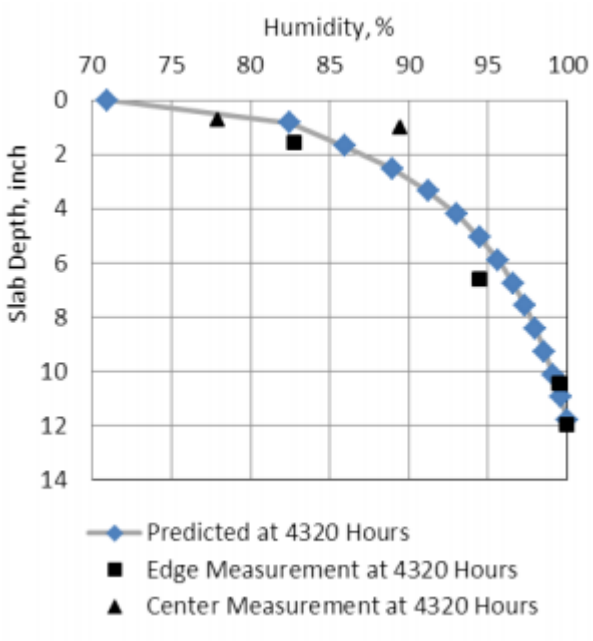

Figure 2.26: Moisture gradient through a 300 mm thick concrete pavement (Nassiri, 2011)

From the research on ordinary thick pavements (± 300 mm thickness), the most significant change in the temperature and moisture gradient of the concrete pavements is seen to be localised to a depth of 50 mm from the surface of the concrete (top or bottom surface), with the centre portion seeing minor changes in temperature and moisture content with time. For this reason the maximum thickness of the pavement consider in this study is a 100 mm thick pavement, to asses whether there is a greater variation/ distribution of temperature/ moisture in the concrete or if due to how thin the pavements are, the temperature/ moisture is distributed more evenly throughout the pavements thickness.

2.6 CURVATURE OF CONCRETE PAVEMENTS

Temperature and moisture differentials within a concrete slab result in curvature of the concrete slab. The deformation that occurs in a concrete slab due to a temperature and moisture differential is typically referred to as curling and warping in the concrete pavement (Armaghani et al., 1987; Dempsey et al., 1987; Hansen & Mohamed, 1997; Jeong & Zollinger, 2005; Nassiri, 2011; Shah, 1965). A temperature differential within the concrete slab can result in the slab being curved either upwards or downwards deepening on the temperature gradient within the pavement. If the pavements surface is warmer than the slabs base, then the pavement typically curves downwards while if the surface is cooler than the base, the pavement tends to curve upwards (Jeong & Zollinger, 2005). This behaviour of the pavement has already been

shown in Figure 2.19. The moisture gradient within a concrete pavement typically results in upwards curvature due to the pavement surface experiencing significantly more drying shrinkage than the pavement's base (Jeong & Zollinger, 2005; Gao et al., 2016).

Though multiple sources (Armaghani et al., 1987; Dempsey et al., 1987; Hansen & Mohamed, 1997; Jeong & Zollinger, 2005; Nassiri, 2011; Shah, 1965) relate curling and warping to the temperature or moisture gradient within the pavement. This report will refer to curling as the upwards curvature (positive curling) of the concrete pavement while warping refers to the downwards curvature (negative curling) of the concrete pavement. This notation and definition are depicted in Figure 2.27.

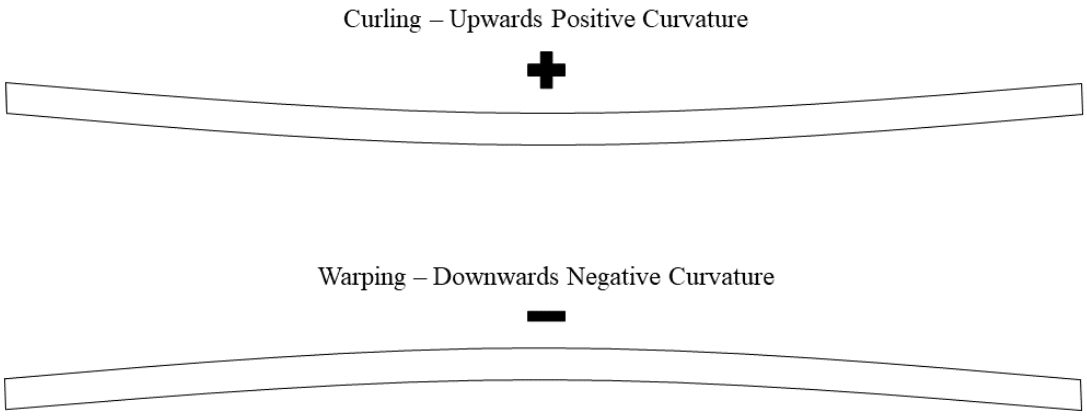

Figure 2.27: Definition of curling and warping notation

Curling and warping of a concrete pavement is an important behavioural characteristic to consider when designing a concrete pavement due to the pavement losing contact with the supporting base due to the curling and warping of the pavement. As a result of curling and warping, the concrete pavement is no longer uniformly supported throughout the pavements length by the base, this causes an increase in the reaction force under the areas where the pavement is in contact with the base material. Flanagan & Hudson (1987) found that the environmental factors (moisture and temperature gradients within the pavement) lead to distress of the concrete pavement which is worsened by the effects of traffic loading. The self-weight of the pavement, friction and restraint of the pavement limit the curling and warping movement of the concrete pavement thereby inducing stresses within the concrete slab, which can cause minor cracks to form within the concrete pavement. These cracks can grow due to the presence of traffic loading causing further distress of the concrete pavement and eventual failure of the pavement before the end of its design service life (Flanagan & Hudson, 1987).

The curling and warping of a concrete pavement are determined by the curvature of the pavement where a positive curvature indicates upwards deformation of the pavement and negative curvature corresponds to a downwards deformation of the pavement (as defined previously in Figure 2.27), where strain in the top and bottom of the slab is used to compute the slab curvature (Asbahan & Vandenbossche, 2011; Hansen & Mohamed, 1997; Phillips et al., 2006; Janssen & Snyder, 2000). Equation 2.3 was derived to express curvature based on the strain in the top and bottom of the pavement. This equation was derived using the following assumptions (Hansen & Mohamed, 1997):

1.) The slab is elastic, homogeneous, and isotropic with temperature-independent material properties.

2.) Plane sections remain plane after bending.

3.) Stresses and strains in the vertical direction are zero.

4.) The deflection of the slab is small compared with the slab dimensions.

5.) Temperature or shrinkage strains vary in the vertical direction only.

$$\kappa = -\frac{\varepsilon_{top}-\varepsilon_{bottom}}{D(1+\varepsilon_{top}+\varepsilon_{bottom})} \quad \text{(Equation 2.3)}$$

Where:

κ = Slab curvature (1/m)

ε_{top} = Strain at the top of the slab at the time of interest (m/m = Ɛ)

ε_{bottom} = Strain at the bottom of the concrete (Ɛ)

D = Distance between the top and bottom of the slab where strain is calculated or strain measurements are taken (m).

Asbahan & Vandenbossche (2011) stated that the curvature of the concrete pavement can be estimated using three different approaches: 1) Curvature based on temperature and moisture measurements, 2) Curvature based on strain measurements and 3) Curvature based on surface profile measurements.

2.6.1 Curvature based on temperature and moisture measurements

The temperature and moisture gradients within a concrete pavement are typically nonlinear and vary daily and seasonally due to the environmental conditions surrounding the concrete (Asbahan & Vandenbossche, 2011; Hansen & Mohamed, 1997; Phillips et al., 2006, Janssen & Snyder, 2000). Equation 2.4 and Equation 2.5 represent how the strain within the concrete is determined based on the temperature and moisture gradient within the concrete pavement (Hansen & Mohamed, 1997 and Jeong et al. 2001).

$$\varepsilon_{Temp} = \varphi_c \Delta T_{eq} \quad \text{(Equation 2.4)}$$

$$\varepsilon_{Moisture} = -\varepsilon_{\infty} \Delta \left[1 - \left(\frac{RH}{100}\right)^3\right]_{eq} \quad \text{(Equation 2.5)}$$

Where:

ε_{Temp} = Strain in the concrete due to a temperature gradient (με)

$\varepsilon_{Moisture}$ = The strain in the concrete due to a moisture gradient (με)

φ_c = Thermal expansion coefficient of the concrete (με/°C)

ΔT_{eq} = Equivalent linear temperature difference (°C/cm)

ε_{∞} = Ultimate shrinkage strain (με)

$\Delta \left[1 - \left(\frac{RH}{100}\right)^3\right]_{eq}$ = Equivalent linear humidity difference.

Figure 2.28 depicts the curvature that occurs due to an equivalent linear temperature gradient within a concrete pavement. From this figure it is seen that there is a linear relationship between the curvature experience by the pavement and the internal linear equivalent temperature difference. Figure 2.29 depicts how the linear equivalent humidity difference changes over time for a 300 mm thick concrete pavement and Figure 2.30 shows the corresponding shrinkage that is realised within the concrete pavement. These two figures show that there is a daily and seasonal fluctuation in the drying shrinkage within the concrete due to the daily and seasonal ambient environmental conditions. The shrinkage of the pavement remains more or less constant with a slight variation of between 50 to 100 με over this 5-year period with the largest effects taking place due to a change in seasons.

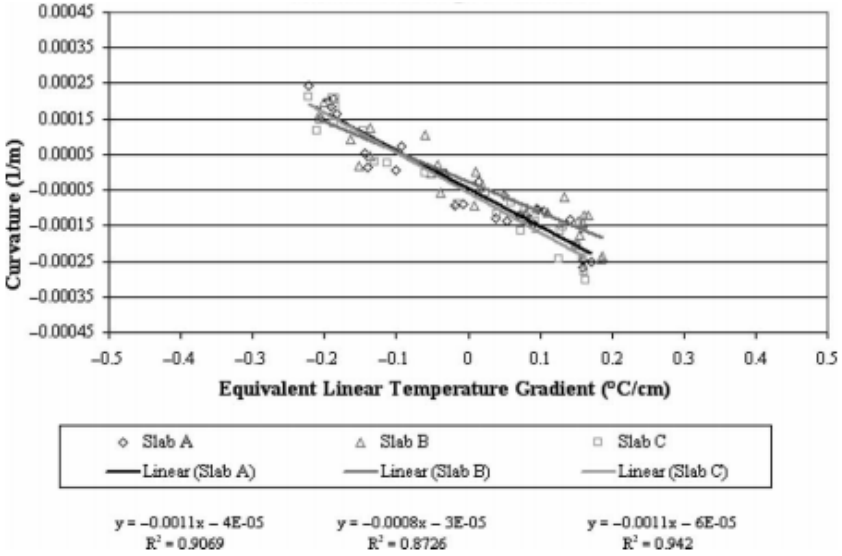

Figure 2.28: Curvature due to a temperature gradient (Phillips et al., 2006)

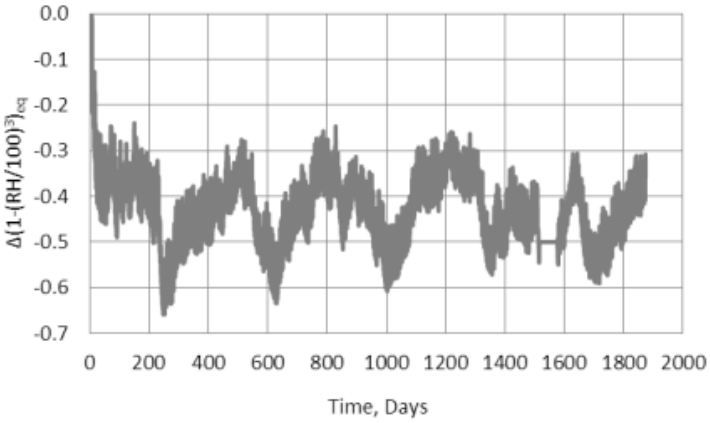

Figure 2.29: The equivalent linear humidity difference for 300 mm thick concrete (Nassiri, 2011)

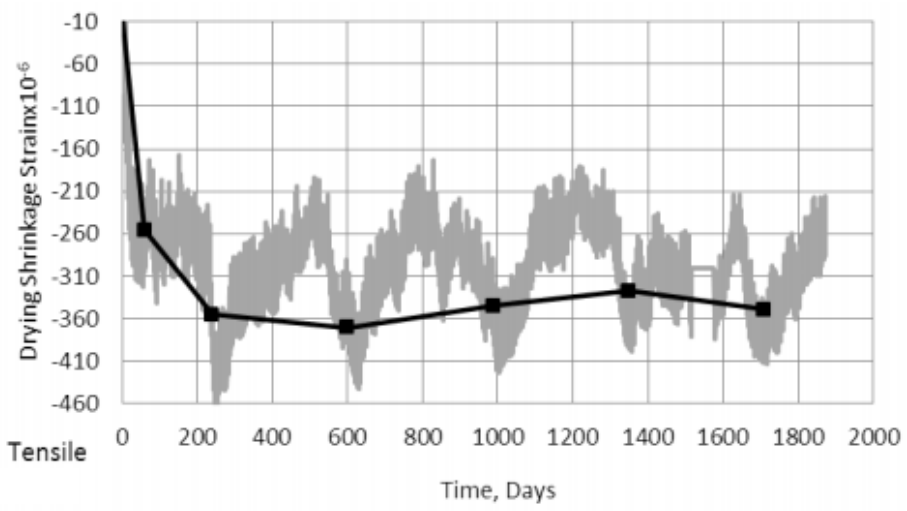

Figure 2.30: The predicted drying shrinkage realised (Nassiri, 2011)

2.6.2 Curvature based on strain measurements

Another method used to determine the shape of the slab is by measuring the actual strain that is induced within the concrete. These strain gauges measure the total strain within the concrete pavement that is caused by temperature changes, moisture changes and other factors that would affect the shape of the slab (creep and slab restraints) (Asbahan & Vandenbossche, 2011). Figure 2.31 depicts a change in curvature for a change in temperature gradient in a 300 mm thick concrete pavement with the curvature being determined based on strain measurements taken in the top and bottom of the concrete using a vibrating wire (VW) strain gauge. This figure shows similar results and trends to that shown in Figure 2.28 determined using Equation 2.4 and Equation 2.5. As a result of the total strain being measured, the strain due to a temperature gradient and moisture gradient within the concrete can be subtracted using Equation 2.4 and Equation 2.5 to determine the effect of other factors such as creep and slab restraining conditions on the slabs deformation (Asbahan & Vandenbossche, 2011). Figure 2.32 shows the change in curvature of a 300mm thick pavement over time for both a restrained and unrestrained pavement when temperature effects are removed from the data.

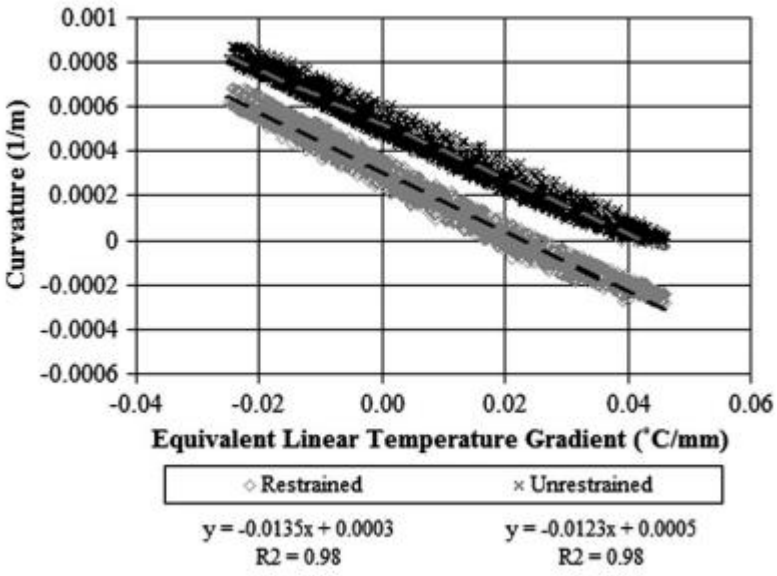

Figure 2.31: Curvature of a 300 mm thick concrete slab (Asbahan & Vandenbossche, 2011)

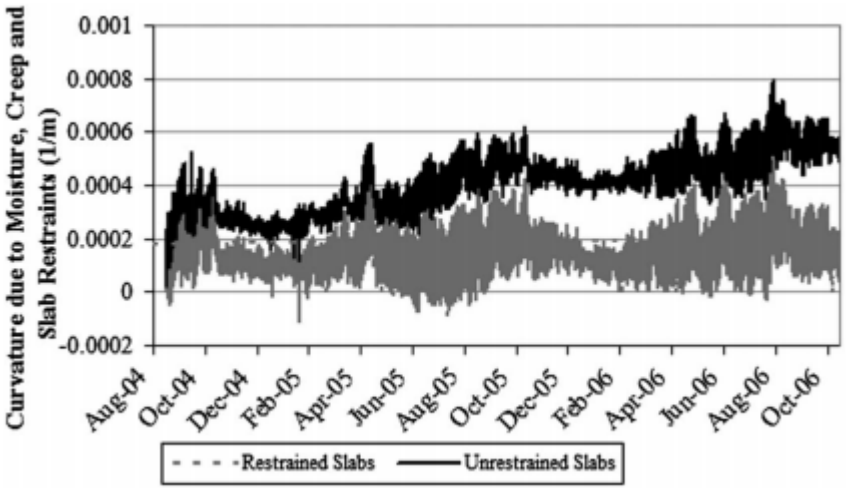

Figure 2.32: Curvature due to moisture, creep and slab restraint (Asbahan & Vandenbossche, 2011)

2.6.3 Curvature based on surface profile measurements

The final method for determining the shape of the concrete pavement is by measuring the profile of the concrete surface to determine the curvature of the concrete pavement. This method gives the true curvature of the concrete pavement due to temperature gradients, moisture gradients and other factors such as creep and slab restraints. In the past, this form of curvature was measured by using a Dipstick device that accurately determines the slope of the concrete surface over the length that the device measures and the overall curvature of the pavement can be determine by summing up the repeated measurements taken over the length of pavement measured, to determine the curvature of the pavements surface (Asbahan & Vandenbossche, 2011), or if a non-invasive method is preferred, the curvature of the surface can be measured by using Visual Simultaneous Localization and Mapping (VSLAM) whereby a surface is accurately scanned using a 3D scanner, and a digital twin is produced with sum-millimetre accuracy (less than 100 μm) where the texture and profile of the surface can be measured (Broekman et al., 2020). This method also provided continuous scanning of the pavement surface so that an entire stretch or length of a pavement may be measured.

Figure 2.33 depicts the curvature that was measured over time for a 300 mm thick concrete pavement using the Dipstick device while Figure 2.34 shown the change in surface profile over time based on surface profile measurements. Both figures show the change in curvature over time of the concrete pavement while Figure 2.34 gives a better indication of the magnitude that the pavement displaces over time based on ambient environmental conditions.

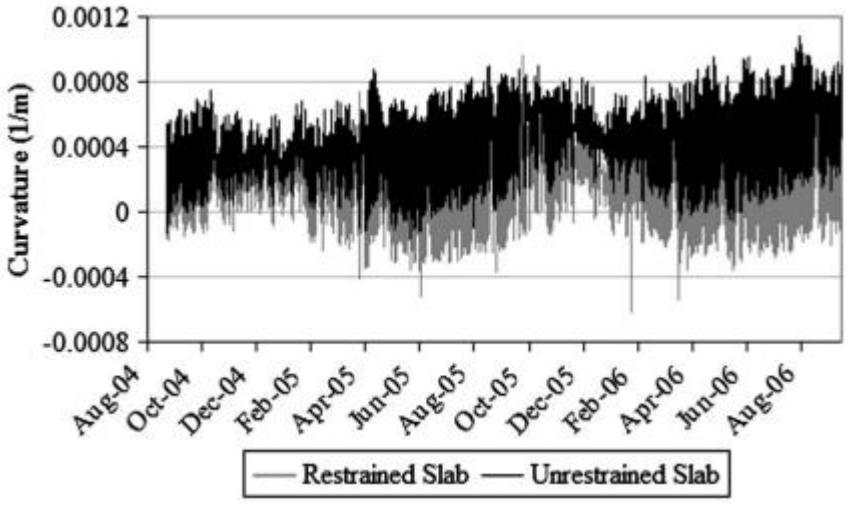

Figure 2.33: Curvature of a 300 mm thick pavement from surface profile measurements (Asbahan & Vandenbossche, 2011)

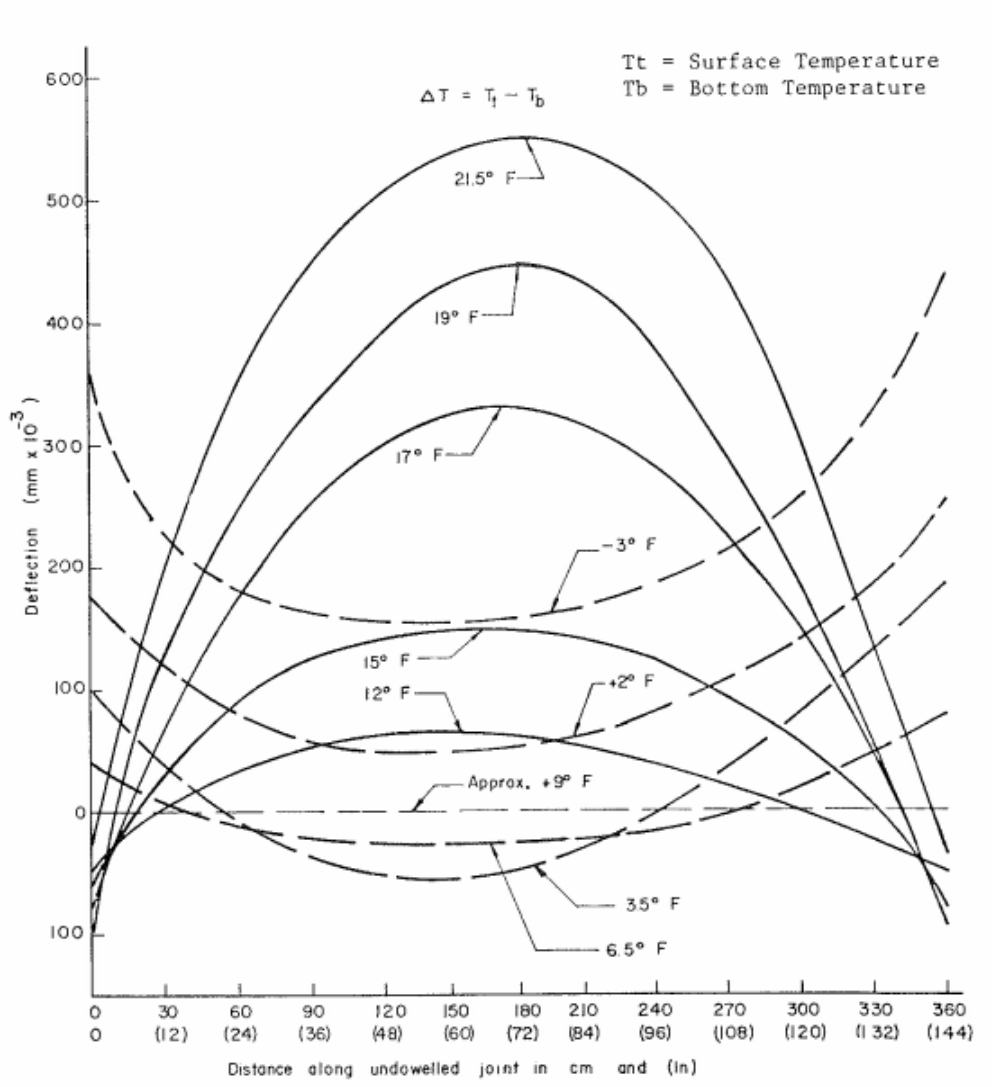

Figure 2.34: Deflection profile for differential temperatures (Armaghani et al., 1987)

2.7 MODELLING OF HEAT TRANSFER

There are a number of methods for the modelling of heat transfer through a variety of materials with various boundary conditions, shapes, and sizes (Emerson, 1973; Çengel & Ghajar, 2015; Nassiri, 2011). Equation 2.6 is the partial differential equation that governs one-dimensional transient heat transfer (Emerson, 1973; Çengel & Ghajar, 2015; Nassiri, 2011), which can be used to predict the temperature distribution through the thickness of a concrete pavement and its supporting structure.

$$k\frac{d^2T}{dx^2} + Q_H = \rho c\frac{dT}{dt} \qquad \text{(Equation 2.6)}$$

Where:

k = thermal conductivity ($W/m°C$)

T = temperature (°C)

x = depth into the material (m)

Q_H =the internal heat generated per unit time and volume (W/m^3)

ρ = the density of the material (kg/m^3)

c = the specific heat capacity of the material ($J/kg°C$)

t = the time (s).

Equation 2.6 summarises the properties of the concrete that effect the transfer of heat through the thickness of a concrete pavement over time. As a result, the factors that play a significant role in the transfer of heat through the concrete pavement are the thermal properties (density, specific heat capacity, thermal conductivity, and thermal diffusivity), the internal heat generated (heat of hydration) and the boundary conditions. Figure 2.35 illustrates the boundary conditions surrounding concrete pavements, internal heat generated and the transfer of heat between the surrounding environment, concrete pavement, and the pavement support structure.

Due to the concrete pavement being significantly wider and longer when compared to its depth, the heat transferred through the concrete pavement is commonly seen as a one-dimensional problem (Nassiri, 2011). Equation 2.6 can be solved by using methods such as the finite difference method (FDM) which provides an accurate prediction of the temperature distribution and heat transfer through the concrete pavement (Emerson, 1973; Çengel & Ghajar, 2015; Nassiri, 2011) for a given set of input parameters. In order for the desired level of accuracy to be achieved, the boundary conditions, internal heat generated and thermal properties of the concrete need to be correctly defined as the model is highly dependent on the parameters selected (Nassiri, 2011).

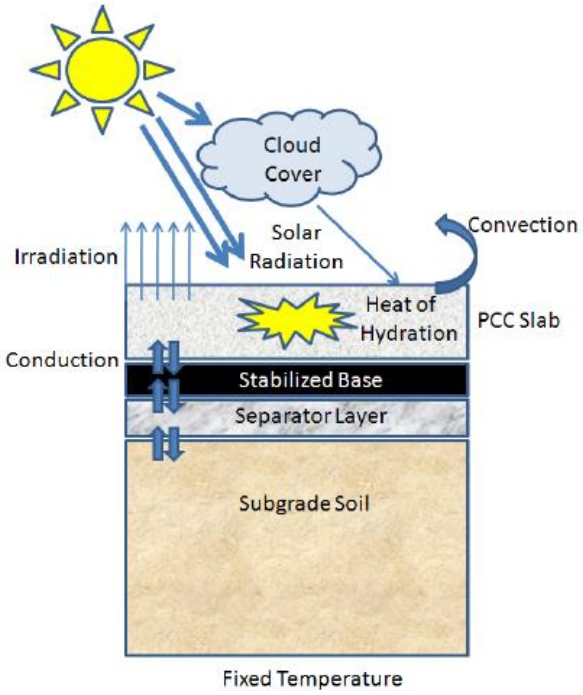

Figure 2.35: Heat transfer between the pavement and surrounding environment (Nassiri, 2011)

The stability of the FDM can be further improved by the use of Equation 2.7 to determine the appropriate time intervals (Δt) and depth intervals (Δx) to be used in the model for a given set of thermal properties of the concrete (Çengel & Ghajar, 2015; Nassiri, 2011).

$$\Delta t = \frac{\Delta x^2}{4\frac{k}{\rho c}} \qquad \text{(Equation 2.7)}$$

2.8 THERMAL PROPERTIES OF CONCRETE AND BOUNDARY CONDITIONS

When considering how heat is transferred through a body of concrete, the most important properties of the concrete are the density (ρ), specific heat capacity (c), thermal conductivity (k) and thermal diffusivity ($\propto$) (Asadi et al., 2018). The thermal properties of the concrete are interconnected with the relationship being expressed in Equation 2.8:

$$\propto = \frac{k}{\rho c} \qquad \text{(Equation 2.8)}$$

Specific heat capacity is a property of the concrete that gives a measure of the materials ability to undergo a temperature change and the amount of energy that is required to cause this temperature change (Akpolat et al, 2015; Nassiri, 2011). Thermal conductivity gives an

indication of a materials ability to conduct heat and thermal diffusivity gives an indication of the rate at which heat is diffused into and out of a material (Akpolat et al, 2015; Nassiri, 2011).

These thermal properties in combination with the boundary conditions determine the amount and rate at which heat is transferred into and out of a concrete pavement. Table 2.1 contains a summary of the typical boundary conditions that a concrete pavement faces and the corresponding equations that model these boundary condition for the transfer of heat from the surrounding environment into the concrete pavement. From this table, it is seen that the conditions surrounding the concrete pavement influence the heat transferred through the concrete pavement, but the heat transferred is dependent on the properties and composition of the concrete as shown in Equation 2.6. The equations in Table 2.1 merely quantify the energy available to be transferred through the pavement and is restricted to the surface of the pavement. This energy, in the form of heat, gets transferred/defused further into the concrete based on Equation 2.6 at a rate which is dependent on the concretes thermal properties.

Concrete is a heterogeneous porous solid (Domone & Soutsos, 2017) with the concrete consisting out of three phases namely a solid (cement, coarse aggregate, and fine aggregate), a liquid (water and/or admixture) and a gaseous (air) phase (Benhamou et al., 2017). All three phases affect the thermal properties of the concrete, and the thermal properties of the concrete are highly dependent on the porosity and moisture content of the concrete as well as the type of materials used in the concrete and their relative proportions to one another (Nassiri, 2011). Changing the minerology, void ratio/porosity and/or the moisture content of the concrete will result in a change in the thermal properties of the concrete. It has already been shown in Figure 2.36 that by changing the thermal properties of the concrete, the amount and rate at which heat is transferred into and through the concrete is also altered and as a result the behaviour of the pavement will also be altered.

Table 2.2 contains a summary of the typical values for the thermal properties of some of the most commonly used materials in concrete pavements as well as the values that are typically expected for ordinary weight concrete. Table 2.3 and Table 2.4 contain the thermal properties for material used for the supporting structure of a concrete pavement (Nassiri, 2011). Due to the thermal properties of concrete being dependent on the materials used to form the concrete and these materials relative proportions to one another, Equation 2.9 can be used to determine the thermal properties of the concrete based on the concrete’s mix design (Lei et al., 2011; Nassiri, 2011).

$$\vartheta = \vartheta_c V_c + \vartheta_w V_w + \vartheta_{ca} V_{ca} + \vartheta_{fa} V_{fa} + \vartheta_{am} V_{am} \quad \text{(Equation 2.9)}$$

Where:

ϑ = the thermal property of the concrete that needs to be determined with the material properties being found in Table 2.2.

V_c, V_w, V_{ca}, V_{fa} and V_{am} = the respective volumetric fractions of cement, water, coarse aggregate, fine aggregate, and admixture in the concrete.

ϑ_c, ϑ_w, ϑ_{ca}, ϑ_{fa} and ϑ_{am} = Thermal property of the constituent material such as cement, water, coarse aggregate, fine aggregate and admixture in the concrete.

Table 2.1: Typical boundary conditions for one-dimensional heat transfer (adapted from Nassiri, 2011)

Heat Transfer Mechanism	Corresponding model	Defining Parameters	Reference	Equation
Convection	$q_c = h_c(T_c - T_a)$	q_c = Convection heat flux (W/m^2) h_c = Heat transfer coefficient ($W/m^2°C$) T_c = Surface temperature (°C) T_a = Ambient air temperature (°C)	Nassiri, 2011	(2.10)
	$h_c = 20 + 14w$ for $w \leq 5\ m/s$ $h_c = 25.6^{0.78w}$ for $w > 5\ m/s$	w = Wind velocity (m/s)	Nassiri, 2011	(2.11)
Solar Absorption	$q_s = \beta q_{solar}$	q_s = Solar absorption heat flux (W/m^2) β = Absorptivity coefficient = 0.65 q_{solar} = Solar radiation (W/m^2)	Nassiri, 2011; Keste & Patil, 2019	(2.12)
Irradiation	$q_r = \theta\delta(T_c^4 - T_a^4)$	q_r = Surface emission heat flux (W/m^2) θ = Emissivity coefficient =0.88 δ = Stefan-Boltzmann radiation constant = $5.67 \times 10^{-8}\ W/m^2°C^4$	Nassiri, 2011	(2.13)

Table 2.2: Typical thermal properties of materials used in concrete

Material	Thermal conductivity (W/m°C)	Specific Heat Capacity (J/kg°C)	Density (kg/m^3)	Reference
Quartzite	3.1 - 4.1	700 - 770	2350 - 2440	Andolfsson, 2013; Nassiri, 2011; Neville, 2011; Robertson, 1988
Dolerite	2.05 - 2.59	910	2500	Andolfsson, 2013; Nassiri, 2011
Limestone	2.2 - 3.2	910	2450 - 2440	Kodide & Shin, 2012; Nassiri, 2011
Sandstone	2.66 - 6.38	770	2130 - 2400	Andolfsson, 2013; Nassiri, 2011
Granite	2.46 - 3.44	780	2420	Andolfsson, 2013; Nassiri, 2011
Basalt	1.9 - 3.0	900	2520 - 2350	Andolfsson, 2013; Nassiri, 2011
Fly Ash	0.14 - 0.19	720 - 730	2100 - 2690	Asadi et al., 2018; Krishnaiah & Singh, 2006
Silica Fume	0.09 - 0.13	860 - 880	2100	Krishnaiah & Singh, 2006
Ground granulated blast furnace slag (GGBFS)	0.15 - 0.13	620 - 640	2840	Krishnaiah & Singh, 2006
Steel	62	515	7900	Çengel & Ghajar, 2015
Water	0.521 - 0.606	4187	1000	Asadi et al., 2018; Lei et al., 2011; Kodide & Shin, 2012; Nassiri, 2011
Cement	1.5	740 - 760	3130 - 3250	Asadi et al., 2018; Kodide & Shin, 2012
Normal Weight Concrete	1.4 – 4.1	750 - 1050	2050 - 2500	Asadi et al., 2018; Larsson & Svensson, 2013; Neville, 2011

Table 2.3: Thermal properties for supporting base material (adapted from Nassiri, 2011)

Material	Thermal conductivity (W/m°C)	Specific Heat Capacity (J/kg°C)	Density (kg/m^3)
Dry Gravel	0.52	838	1703
Wet Gravel	2.42	1047	1898
Asphalt	1.38	1047	2302
Stabilized Base	3.32	1005	2339
Cohesive Subgrade	1.59	1214	2066
Asphalt Concrete	1.21	921	2371

Table 2.4: Thermal properties of base materials based on different soil type classifications (adapted from Nassiri, 2011)

Material Classification	Thermal conductivity (W/m°C)	Specific Heat Capacity (J/kg°C)	Density (kg/m^3)
A-1	0.52	712	1188
A-2	0.47	712	950
A-3	0.59	838	1045
A-4	0.59	712	856
A-5	0.26	712	808
A-6	0.35	712	856
A-7	0.17	712	760

2.9 SUMMARY

From the contents of this literature review, it can be seen that temperature and moisture within and surrounding a concrete pavement has a significant effect on the service life of an UTCRCP and as a result the effect of temperature and moisture on a thin concrete pavement needs to be quantified. The effects of temperature and moisture on the behaviour of thin concrete pavements are dependent on the concrete's material properties, pavement size, curing conditions and ambient environmental conditions.

From this literature review it is seen that the shrinkage of the concrete pavement is a behavioural characteristic that changes less frequently than the temperature gradient within the concrete pavement with the shrinkage of the concrete being predominate at the surface of the concrete pavement. This shrinkage results in the pavement not only changing length but also curling with slight reversal upon rewetting of the concrete surface due to the base of the pavement remaining at a state of almost full saturation. Moisture can also enter the supporting structure through openings and/or cracks of the pavement which causes pumping and as a result, areas where the pavement is no longer supported by the base forms.

The daily and seasonal change in ambient environmental conditions results in a change in the magnitude, size and direction of a temperature gradient within the concrete pavement which causes the pavements curvature to alternate between being curled or warped on a daily basis. This behaviour could result in fatigue of the pavement and debonding of the concrete pavement from the supporting structure allowing more mobility of the concrete pavement which loses

contact with the supporting structure, resulting in concentrated loads that lead to the premature failure of the concrete pavement.

Based on the literature review, there is a need to determine the effect of pavement thickness and mix composition on the movement, shrinkage, internal stress development, internal moment development, curling and warping of thin pavements as a result of environmental conditions.

3 EXPERIMENTAL PROGRAM

3.1 INTRODUCTION

To investigate the effect of moisture, temperature and ambient environmental conditions on the behaviour of UTCRCPs, the experiments summarized in Table 3.1 were conducted on thin concrete pavements of two different strength and three different thicknesses to relate the behaviour of the pavements back the material properties of the concrete.

Table 3.1: Summary of all the experiments conducted in this study

Property	Test Method	Time Frame
Raw Material	Relative density	Before developing mix design
Workability	Slump test	Immediately after casting
Setting Time	Semi-adiabatic calorimetry Thermocouple embedded in 100 mm and 150 mm cubes	For 7 days from immediately after casting
Heat of Hydration	Semi-adiabatic calorimetry Thermocouple embedded in 100 mm and 150 mm cubes Thermocouples in pavements	For 7 days from immediately after casting
Deformation	Early age shrinkage Drying shrinkage Thermal expansion coefficient	7 Days minimum 28 Days minimum After 28 days
Mechanical	Compressive strength Splitting tensile strength Modulus of rupture Static modulus of elasticity	2, 7, 14, 28, 90 & 180 Days
Moisture movement	Porosity Sorptivity Drying out curves	14 & 28 Days
Pavements Movement	Surface mounted strain gauges Temperature gradient Moisture gradient Surface profile Ambient environmental conditions	4 Months continuous monitoring

Thin pavement sections of 50, 75 and 100 mm thickness were cast to determine the effect of pavement thickness on the behaviour of the concrete pavement. The material properties were determined before casting to develop an accurate mix design. The workability of the concrete was determined during casting to indicate the ease of placement of the concrete. The heat of hydration and temperature rise within in the concrete was measured to determine the heat evolution within the pavements and to determine the setting time of the concrete by making use of the fractional method (Pérez, 2013).

The setting time was used to quantify the built-in moisture and temperature gradient within the concrete. The thermal expansion coefficient of the concrete was determined to indicate the deformation expected within the concrete in response to a change in the ambient environmental conditions and temperature of the concrete pavement. The early age and drying shrinkage of the concrete was measured to give an indication of the deformation that could occur due to a decrease in moisture within the concrete. The decrease in moisture content was measured using relative humidity sensors placed within the drying shrinkage samples to relate the drying shrinkage to a decrease in moisture content of the concrete.

The mechanical properties were measured to fully define the mechanical performance of the concrete. The strain measured in the pavement sections could be compared to the strain required to cause tensile cracks to form. The indirect tensile strength and modulus of elasticity of the concrete were measured to use in calculating the cracking strain. The moisture movement properties were determined to define the internal structure that exists within the concrete pavements.

3.2 MATERIALS AND PROPERTIES

The materials that were used for the concrete pavements in this study were cement, quartzite aggregate, fly ash and silica fume. The cement that was used in this study was a CEM I 52.5R with a relative density of 3.14. Ferro-quartzite was selected as the rock type use in this study for the fine and coarse aggregate due to this type of aggregate being a commonly used aggregate in South Africa. For the coarse aggregate, a 9.5 mm stone was used with a relative density of 2.65 while the fine aggregate portion was made up of a 0 - 4.75 mm ferro-quartzite sand with a relative density of 2.65 and 26.5% of the material passing the 600 μm sieve. The fly ash used in this study was an unclassified fly ash with a relative density of 2.2 and the silica fume used in this study was a densified silica fume which has a relative density of 2.2.

3.3 MIX DESIGN

Two mix designs were developed and used. The mix designs were developed with the objective of achieving the same workability of 35 mm while making use of the same w/c ratio of 0.66 as shown in Table 3.2, to achieve concrete with different strengths. This was done so that the two concretes could be more comparable when looking at the behaviour of the concrete pavements. The two mix designs used in this study were developed through trial and error and it was found that by adding 35% fly ash and 15% silica fume by mass of the cement content and replacing the fine aggregate in the concrete with these fine materials resulted in an approximately 15 MPa increase in the compressive strength of the concrete after 28 days. The sand in this portion in the higher strength mix was replaced by a combination of fly ash and silica fume to replace the fine sand material with the fine SCM material. The mix designs used in this study are found in Table 3.2.

Table 3.2: Mix design used in study

Designated Mix Name	**Normal strength (NS)**	**Higher strength (HS)**	**RD**
28 Day Strength	40.6 MPa	54.1 MPa	
Material	**Quantity (kg/m^3)**	**Quantity (kg/m^3)**	
CEM I 52.5R Cement	350.00	350.00	3.14
Water	230.00	230.00	1.00
Sand (0-4.75mm)	872.60	661.80	2.65
Stone (9.5mm)	872.60	872.60	2.65
Fly ash	0.00	122.50	2.20
Silica Fume	0.00	52.50	2.20
w/c ratio	0.66	0.66	
w/b ratio	0.66	0.44	

3.4 SAMPLES CAST FOR TESTING

Table 3.3 gives a summary of the concrete specimens that were cast for the various tests conducted in this study along with the duration and times that these tests were conducted.

Table 3.3: Specimens cast for each concrete mix

Property	Test Done	Sample Used	Date of testing
Concrete heat evolution	Heat of hydration	Calorimetry cylinder 100 mm & 150 mm cubes	First 48 hours after casting
	Setting time		
Mechanical	Compressive strength	3 × 100 mm Cubes	@ 2, 7, 14, 28, 90, 180 days
	Splitting tensile strength	2 × 200 mm × Ø100 mm Cylinders	
	Modulus of rupture	2 × 100 mm × 100 mm × 500 mm Beams	
	Static modulus of elasticity	3 × 200 mm × Ø100 mm Cylinders	
Moisture movement	Sorptivity	2 × 150 mm Cubes	@ 14 & 28 days
	Porosity		
	Drying curves		
Deformation	Early age shrinkage	1 × 300 mm × Ø100 mm Cylinders	First 48 hours after casting
	Drying shrinkage	3 × 50 mm × 50 mm × 300 mm Prisms and 1 × 100 mm × 100 mm × 300 mm Prism	For a minimum of 28 days
	Thermal expansion	2 × 300 mm × Ø75 mm Cylinders	After 28 days
Curling and Warping	Thin pavement sections	1 × 50 mm × 150 mm × 2000 mm 1 × 75 mm × 150 mm × 2000 mm 1 × 100 mm × 150 mm × 2000 mm	Continuous monitoring for up to 4 months

3.5 MIXING, CASTING AND CURING

Prior to the casting of the concrete, all the materials were weighed off and pre-conditioned in a temperature-controlled room at 20°C. The concrete was then mixed in a 300L rotatable pan mixer. All the dry materials were added to the pan in order of course to fine material and mixed for 30 seconds prior to the addition of any water. After the water was introduced, the concrete was mixed for a further 5 minutes to ensure that all the material was combined properly.

After the 5 minutes had passed, the mixer was stopped and the workability of the mix was tested. Following the test for workability, the shrinkage specimens, semi-adiabatic calorimetry temperature rise samples and the thin pavement sections were cast first followed by all the necessary samples for moisture movement and mechanical testing of the concrete. All samples except the thin pavement sections were vibrated using a vibrating table until sufficient compaction was achieved, while the thin pavement sections were vibrated using a poker vibrator.

The samples and specimens of the concrete that did not require testing or measuring from the time of casting (all samples except the concrete heat evolution, temperature rise and early age shrinkage samples) were cured in a temperature-controlled room at 25°C for 24 hours and were covered to prevent any moisture loss. The thin pavement sections cast were covered using a thermal blanket to allow proper curing of the pavement sections. After 24 hours had pasted, all mechanical, moisture movement and drying shrinkage samples were demoulded and samples that needed to be cured in water were placed in a water bath at 25°C until the required testing date, while the air cured samples were placed alongside the thin pavement sections exposed to the ambient environment.

The thin pavement sections were only demoulded after 7 days to also allow the concrete sufficient time to gain strength and then were placed in a temperature and relative humidity controlled room at 25°C and 55% relative humidity for 28 days for the shrinkage of the concrete to take place and were then placed outdoors exposed to the ambient environmental conditions.

3.6 WORKABILITY OF CONCRETE

The workability of the fresh concrete was determined in accordance with SANS 5862-1:2006: Concrete tests – Consistence of freshly mixed concrete – Slump test. The workability of the concrete was measured directly after mixing of the concrete and was determined to the nearest 10 mm. This test was done to give an indication of how easily the concrete can be placed.

3.7 SEMI-ADIABATIC CALORIMETRY

The semi-adiabatic calorimetry test is a method used to measure the heat elevation and temperature rise within concrete due to the heat of hydration of concrete. The heat of hydration is the heat that is generated within a concrete mix due to the chemical reaction that takes place between cement and water (Pérez, 2013). Figure 3.1 shows the setup of the semi-adiabatic calorimetry test equipment where a sample of the concrete placed in an 800ml sealable metal cylinder with an oil filled pipe that runs through the centre of the specimen (as shown in Figure 3.1) to place a thermocouple in. This sample was then placed in a Dewar flask and sealed. The Dewar flask allows the concrete to be insulated from the surrounding environment and the heat evolution and temperature rise within the concrete was measured over time using a thermocouple. The temperature rise over time curves that were generated were then used for comparison purposes of the two mixes heat evolution and for the determination of the setting times of the concrete.

Figure 3.1: Semi-adiabatic calorimetry setup with (Left) the sealable cylinder and (Right) a Dewar flask

3.7.1 Heat of hydration

The heat of hydration of the concrete used in this study was measured due to it being shown to be an important characteristic to consider when casting concrete pavements, this was due to the heat generated within the concrete pavement that could lead to a built-in temperature gradient as a result of a non-uniform increase in the temperature within the pavement and due to temperature escaping through the surface and base of the concrete pavement (Pérez, 2013; Lim

et al., 2016; Wang et al., 2007; Nassiri, 2011; Asbahan & Vandenbossche, 2011). The temperature gradient also affects the thermal response of the concrete pavement due to the thermal expansion of the concrete pavement being a function of the temperature within the concrete at the time that concrete reaches final setting (Asbahan & Vandenbossche, 2011).

By measuring the heat of hydration of the concrete, the thermal stresses that develop within the continuously reinforced concrete pavements as a result of the thermal contraction of the hardened concrete after cooling from the heat generated in the plastic concrete can be quantified. This contraction leads to stresses developing within the hardened concrete that could lead to cracks forming in the concrete due to the low strength of the concrete during the early ages when these stresses form. Thermal stresses have already been found to be the main reason for the distress seen in UTCRCPs which is worsened by traffic loading (Bredenhann et al., 2018).

The heat of hydration of the concrete was measured using the semi-adiabatic calorimetry setup and 100 mm and 150 mm cubes with thermocouples placed in the centre of the concrete cubes. While the calorimetry setup gave an indication of the absolute temperature rise that can be seen within a body of concrete, the heat of hydration in the 100 mm and 150 mm cubes gave an indication of the size that a sample has on the temperature rise realised within the concrete, thus being more representative of the behaviour seen in thin concrete pavements. The heat of hydration was also measured in the concrete pavement sections with thermocouples placed at the surface, centre and base of each the thin pavement sections cast.

3.8 SHRINKAGE

The volumetric reduction of concrete is linked to the reduction in moisture content of the concrete as discussed in Section 2.4.

The main forms of shrinkage that takes place within a concrete pavement are plastic shrinkage, autogenous shrinkage and drying shrinkage of the concrete. The autogenous shrinkage that takes place within concrete is due to the hydration of the cement paste within concrete and occurs mainly when most of the hydration of the concrete occurs, which is within the first 7 days of the life of the concrete. The drying shrinkage of the concrete is related to the loss of moisture within the concrete and is dependent on the specimen size of the concrete, due to drying shrinkage being a surface bound effect on the concrete.

The moisture content of the concrete can be measured using relative humidity sensors to give an indication of the degree of saturation of the pores within the concrete and to relate the shrinkage within the concrete to the decrease in relative humidity within the concrete (Bella et

al., 2017; Grasley et al., 2006; Abbasnia et at., 2013; Ali and Urgessa; 2014). For this reason, relative humidity sensors were cast into drying shrinkage specimens to correlate the rate at which moisture is lost within the concrete to the drying shrinkage realised within the concrete.

3.8.1 Early age shrinkage

The early age shrinkage of the concrete comprises of all the deformation of the concrete that occurs within the early life of the concrete (within the first 7 days). The samples used to measure the early age shrinkage of the concrete comprised of a Ø100mm × 300mm cylinder cast in a mould lined with Teflon paper to create a frictionless surface. A thin metal disk was placed on the surface of the concrete to seal the specimen from moisture losses to the surrounding environment and allowed for deformation measurements to take place. The early age shrinkage was measured in a temperature and relative humidity controlled room set to 25°C and 55% relative humidity. The deformation was continuously monitored using a linear variable differential transducer (LVDT) in contact with the metal disk on the surface of the concrete from the time of casting for a minimum of 7 days. The mould surrounding the sample was then removed and the sample was allowed to dry out with the drying shrinkage of the concrete then being measured. The setup of the early age shrinkage sample are shown in Figure 3.2.

Figure 3.2: Setup for early age shrinkage measuring

3.8.2 Drying shrinkage

The drying shrinkage of the concrete was measured in a temperature and relative humidity controlled room set to 25°C and 55% relative humidity and was determined using two methods:

1.) Using three shrinkage prisms of 50 mm × 50 mm × 300 mm with metal anvils of 20 mm length and Ø6 mm embedded 15 mm into the concrete specimen. The shrinkage prisms were demoulded 24 hours after casting with the initial reading of the prism's length being taken immediately after demoulding. The prisms were then placed in a specially built stand to allow the samples to dry out from all sides. Readings of the change in length of the prisms were continuously taken until the shrinkage of the concrete levelled off. Figure 3.3 depicts the shrinkage prism samples, drying stand and drying shrinkage apparatus.

2.) The second method included one 100 mm × 100 mm × 300 mm drying shrinkage prism with metal anvils of 20 mm length and Ø6 mm embedded 15 mm into the concrete specimen. The shrinkage prism was cast with 2 SHT31 relative humidity sensors cast into the concrete to track the decrease in the moisture content within the shrinkage prism. The relative humidity sensors were placed at the centre and 10 mm from the surface of the concrete to determine the moisture gradient within the concrete. The shrinkage prism was demoulded 24 hours after casting and was placed in a shrinkage stand that allowed drying from all surfaces with an LVDT continuously measuring the change in length of the prism from the top of the concrete. This setup is shown in Figure 3.4.

The drying shrinkage of the 50 mm × 50 mm × 300 mm shrinkage prisms was used to determine the drying shrinkage of the concrete. Due to the relatively small dimensions of these prisms, it was assumed that the concrete could completely dry out and the effects of a moisture gradient were deemed to be negligible. The 100 mm × 100 mm × 300 mm shrinkage prism were used to determine the effects of a moisture gradients on the shrinkage of the concrete.

Figure 3.3: Drying shrinkage apparatus with the calibration rod

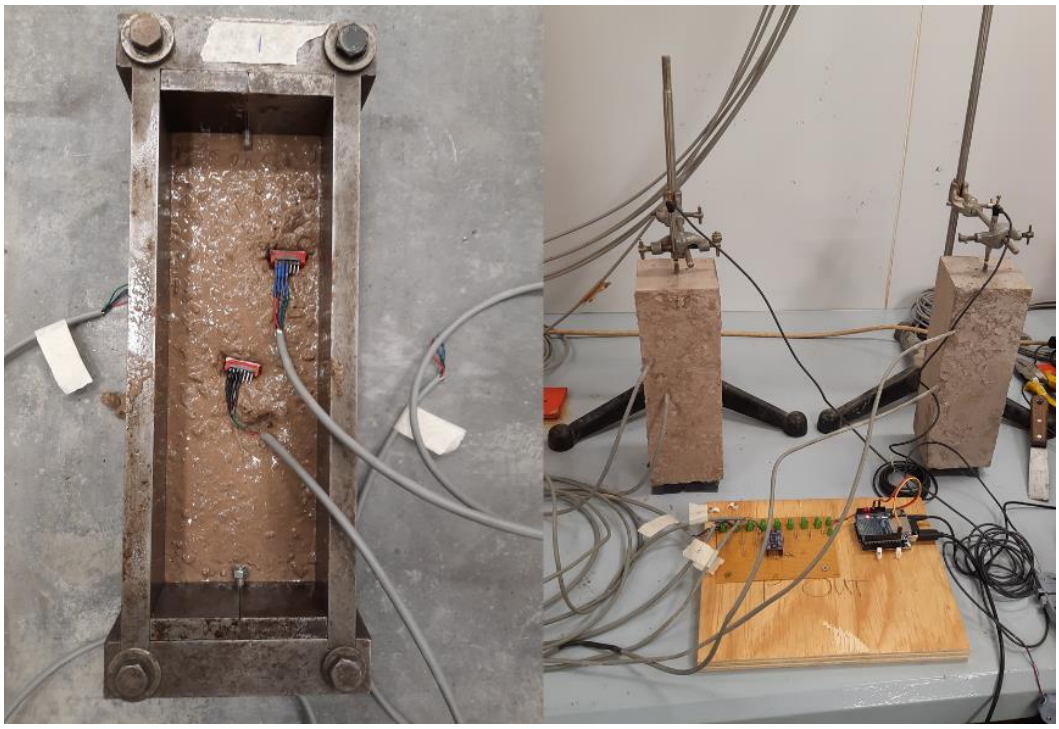

Figure 3.4: (Left) Shrinkage prism with relative humidity sensors placement and (Right) the shrinkage stands with LVDTs to measure the shrinkage of the concrete

3.9 THERMAL EXPANSION COEFFICIENT

The thermal expansion of the concrete was determined in accordance with Tex-428-A: Determining the coefficient of thermal expansion of concrete (2011). The thermal expansion setup is shown in Figure 3.5. The thermal expansion of the concrete was determined on two specimens and an average of the thermal expansion was determined to represent the thermal expansion of the concrete. The procedure included maintaining the temperature of the water bath at 10°C for an hour. The temperature of the bath was then increased to 50°C over a 2 hour period and was maintained at this temperature for an hour. The temperature of the bath was gradually decreased to 10°C over a 2 hour period using ice packets. The temperature of the bath was then maintained at 10°C for an hour. The temperature rise and fall portions of the displacement versus temperature graph were used to determine the coefficient of thermal expansion of the concrete. The test was repeated 5 times to ensure repeatability of the results.

Figure 3.5: Thermal expansion coefficient testing setup

3.10 MECHANICAL PROPERTIES

3.10.1 Compressive strength

The compressive strength of the concrete was determined according to the procedures that are outlined in SANS 50196-1:2006 Part 1: Determination of strength (2006). Each time the compressive strength of the concrete was determined it was done by crushing three 100 mm cubes to get an average strength of the concrete tested.

The 28 day characteristic compressive strength of the concrete was determined on water cured specimens while the specimens that were used to determine how the compressive strength of the concrete developed over time, tested at 2, 7, 14, 28, 90 and 180 days from the day of casting were air cured samples and stood alongside the thin pavement sections. These cubes were placed in water 24 hours prior to testing.

3.10.2 Modulus of rupture (MOR)

The modulus of rupture of the concrete was determined in accordance with the SANS 5864:2006 Concrete tests – Flexural strength of hardened concrete (2006). Each time the modulus of rupture of the concrete was determined it was done by conducting 4 point bending on two 100 × 100 × 500 mm beams to determine the flexural strength of the concrete tested.

The 28 day characteristic MOR strength of the concrete was determined on water cured specimens while the specimens that were used to determine how the MOR strength of the concrete developed over time, tested at 7, 14, 28 and 180 days from the day of casting, were air cured samples and stood alongside the thin pavements sections. These beams were placed in water 24 hours prior to testing.

3.10.3 Static modulus of elasticity

The static modulus of elasticity of the concrete (E-value) was determined in accordance with ASTM C469/C469M-14 (2014). Two concrete specimens of 100 mm diameter by 200 mm long were tested for each mixture. The instrument used for the strain measurements were fixed to the specimen before being placed in the loading press. The load was applied at a constant rate of 270 kPa/s and the load that was applied to the specimen was 40% of the ultimate failure load of the concrete and it was assumed that the cylinders compressive strength was 80% of that of the cube’s compressive strength.

The 28 day characteristic E-value of the concrete was determined on water cured specimens and the specimens that were used to determine how the elastic modulus of the concrete developed over time, tested at 7, 14, 28, and 180 days from the day of casting, were air cured

stood alongside the thin pavement sections. These cylinders were placed in water 24 hours prior to testing.

3.10.4 Splitting tensile strength

The splitting tensile strength of the concrete was determined according to SANS 6253:2006 Concrete tests – Tensile splitting strength of concrete (2006). The splitting tensile strength of the concrete gives an indication of the indirect tensile strength of the concrete and was determined by taking a 100 mm diameter cylinder (200 mm long) and cutting in half with the splitting tensile strength being determined on both halves of the cylinders.

The 28 day characteristic splitting tensile strength of the concrete was determined on water cured specimens, while specimens that were used to determine how the splitting tensile strength of the concrete developed over time, tested at 7, 14, 28 and 180 days from the day of casting, were air cured samples that stood alongside the thin pavement sections. These cylinders were placed in water 24 hours prior to testing.

3.11 MOISTURE MOVEMENT

The moisture movement properties of the concrete measured are the sorptivity, porosity and drying out curves. The sorptivity of the concrete was measured to give an indication of the rate at which water is absorbed by the concrete while the porosity gives an indication of the number of pores withing the concrete. The drying out cures gives an indication of the free water content of the concrete and how easily the water can escape the concrete and the time taken for the water to escape the concrete.

3.11.1 Sorptivity

The sorptivity was determined by coring a 70 mm ± 2 mm core from two 150 mm cubes perpendicular to the direction of casting. The outer 5 mm of the cores were then cut off the cores to create a smooth level surface after which four 30 mm disks were cut from the core. These disks were then weight in a surface dry condition and then placed in an oven at 55°C. These disks were weighed daily until the mass of the samples remained stable indicating that the sample had been fully dried out. The sorptivity of the concrete was then determined in accordance with ASTM C1585 – 20 (2020).

3.11.2 Porosity

The porosity of the concrete was determined by using Equation 3.1 where the dry mass of the sample of concrete was determined by drying out the disks prepared for sorptivity testing in Section 3.11.1 until the mass of the concrete remained stable for 48 hours. The saturated mass

of the concrete was determined by placing the concrete disks in a vacuum saturation facility under a -80 kPa pressure for 24 hours and then measuring the surface dry mass of the sample of concrete. This was done to give a measure of the porosity and pore structure of the concrete.

$$\eta = \frac{m_s - m_d}{Ad\rho_w} \quad \text{(Equation 3.1)}$$

Where;

η = porosity

m_s = mass of the saturated sample to the nearest 0.01 g (g)

m_d = mass of the dry sample to the nearest 0.01 g (g)

A = Area of the sample (mm^2)

d = thickness of the sample (mm)

ρ_w = density of water ($10^{-3} g/mm^3$)

3.11.3 Drying out curves

The drying out curves of the concrete were determined by drying out the concrete disks in a 55°C oven with the weight of the samples being measured every 24 hours until the mass of the samples remained stable. The samples were dried out to give a measure of the free water available in the concrete and the difference in the rate at which water escapes the concrete when exposed to a constant temperature. This test was conducted 14 and 28 days after casting.

3.12 THIN PAVEMENT SECTIONS

The thin pavement sections cast were all 150 mm wide by 2000 mm long so that the curvature of the concrete pavements would only be measured in one direction. The moulds used to cast the thin pavement sections are shown in Figure 3.6. These thin pavement sections were cast for each mix with a 50, 75 and 100 mm thickness, each containing two Ø5.6 mm reinforcing bars running along the length of the neutral axis of the pavement sections cast. Two relative humidity sensors were also cast into the concrete pavement sections, the sensors were placed at a quarter of the pavements thickness from the base and surface of the concrete pavement. Three thermocouples were also cast into each of the concrete pavement sections with the thermocouples placed at the surface, centre and base of the concrete pavement as shown in Figure 3.6. The relative humidity sensors were cast into the concrete pavements to measure the moisture content at the top and bottom of the concrete pavement while the thermocouples were cast into the concrete to measure the diffusion of temperature through a concrete pavement.

The strain in the top and bottom of each of the thin pavement sections were measured using a quarter bridge surface mounted strain gauge placed on the surface and base of the pavement

located at the centre of the pavements span. The surface and base of the thin pavement sections were prepared with sandpaper to create a smooth and level surface for the placement of the strain gauge as shown in Figure 3.7. After the surface was cleaned, a thin layer of HMB^{TM} X60 adhesive was used to bond the strain gauge to the concrete surface as shown in Figure 3.7. The strain, temperature and relative humidity readings of the pavement along with the ambient environmental conditions were continuously measured for up to 4 months to determine the effect of environmental conditions on the response of the concrete pavements. Figure 3.8 shows the setup of the concrete pavement sections placed outdoors exposed to the environmental conditions.

Figure 3.6: (Left) Thin pavement section moulds, (Right) relative humidity sensors and thermocouples spacing and (Centre) stand built to hold sensors

Figure 3.7: (Left) the preparation of the pavements surfaces and (Right) the HMB™ X60 adhesive bonding a strain gauge to the concrete

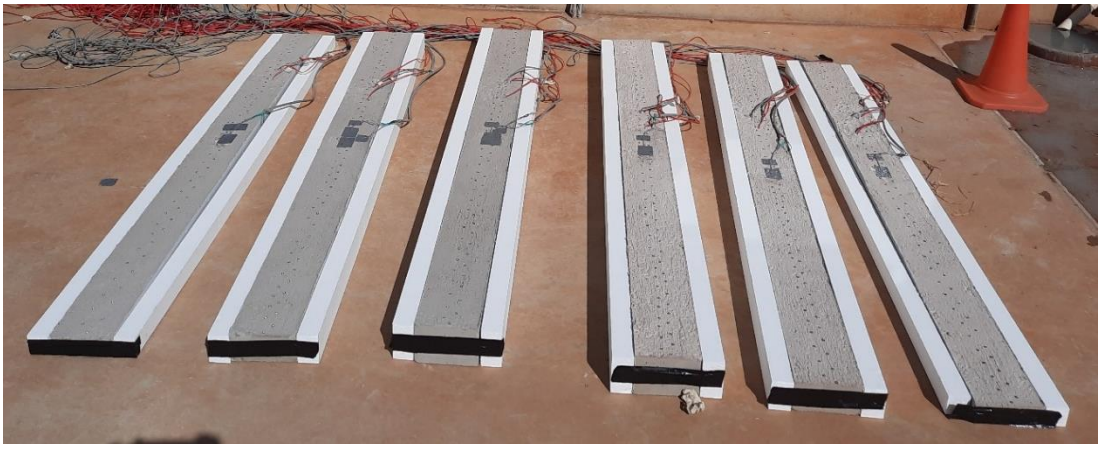

Figure 3.8: Insulated thin pavement sections exposed to environmental conditions

Prior to the demoulding of the thin pavement sections cast after 7 days of being left to cure, a micrometre was used to measure the change in length that took place within the pavements due to shrinkage and thermal contraction of the thin pavement sections cast by measuring the gap that exists between the pavement and the end block. The micrometre used is shown in Figure 3.9 along with the measurement of a 1 mm gap between the pavement and the end block.

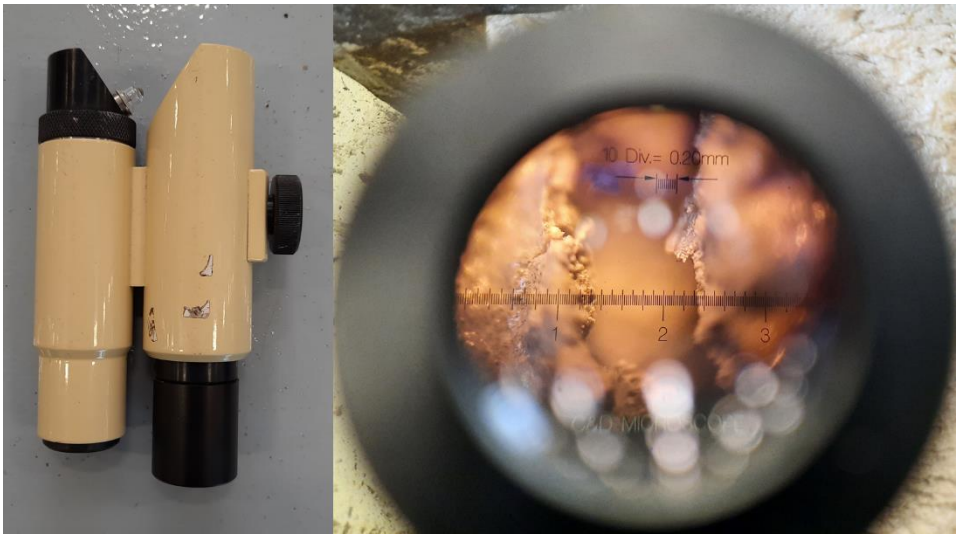

Figure 3.9: (Left) Micrometre and (right) view of a 1mm gap through micrometre

After demoulding the thin pavement section, the sides of the thin pavement sections cast were sealed using a Sikalastic ® - 560 waterproofing solution to seal the sides of the concrete from water entering and escaping from the sides of the concrete. This was done so that the pavement section could only have water entering and escaping through the surface and base of the concrete pavement to make the thin pavement sections cast more representative of a full scale pavement. The sides of the thin concrete pavement sections cast were further insulated from thermal effects by using 50 mm thick high density polystyrene strips that run the length of the pavement sections to insulate the concrete from heat entering and escaping through the sides of the concrete pavement cast. The thin concrete pavement sections were placed on a polished concrete surface so that the least amount of friction between the pavement and supporting material can be achieved so that the true change in length and movement of the thin pavement section could be measured.

4 MATERIAL PROPERTIES RESULTS AND DISCUSSION

4.1 INTRODUCTION

The material properties of concrete used in thin concrete pavements are important characteristics to consider due to the material and moisture movement properties of the concrete affecting the behaviour of the pavements. This chapter looks at how the addition of SCM used to develop concrete of higher strength affects the heat of hydration, setting time, mechanical properties, moisture movement properties, shrinkage and rate of moisture loss. The two concretes looked at in this chapter consists out of a normal strength (NS) concrete mix and a higher strength (HS) concrete mix, where the HS mix contains the SCM. The abbreviations NS and HS will be used throughout this chapter to distinguish the behaviour of the two different concretes.

4.2 HEAT OF HYDRATION AND SETTING TIME

The heat of hydration measured over the first 48 hours for the two different concrete mixtures used in this study are found in Figure 4.1 and Figure 4.2. From these figures it can be seen that the heat generated within the NS concrete mix takes place more rapidly than within the HS concrete mix, which contains 35% fly ash and 15% silica fume by mass of the cement content. Similar results were found by Visser (2019), where an addition of fly ash and silica fume to concrete was found to delay the time at which the maximum temperature rise occurred. It is also noted that the heat of hydration generated within the 100 mm and 150 mm cubes are significantly lower than that measured using the semi-adiabatic calorimetry setup but are more representative of the behaviour in the thin concrete pavements. Figure 4.1 and Figure 4.2 show that even though the 100 mm and 150 mm cubes do not experience the same heat evolution as the semi-adiabatic samples, the 100 mm and 150 mm cubes also experience a rapid increase in temperature at the same time.

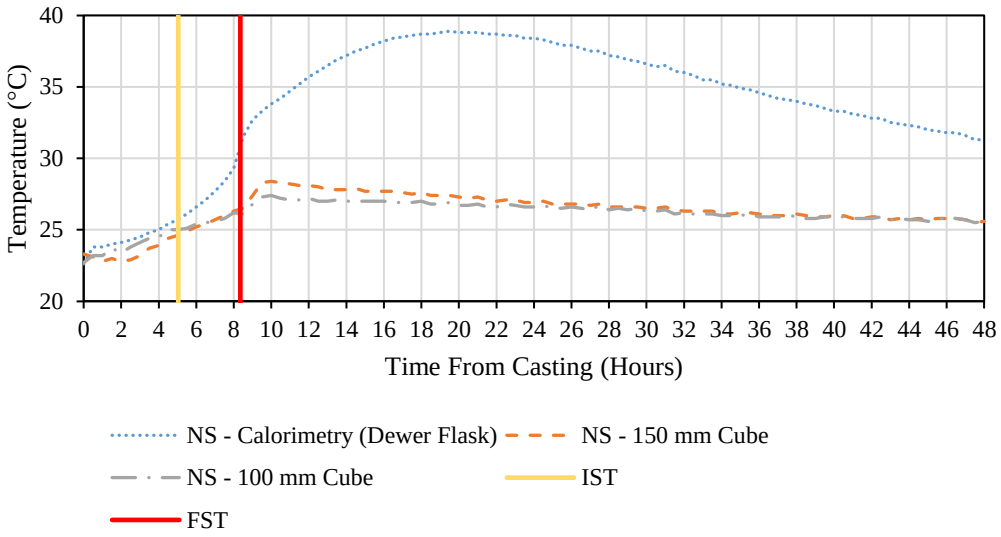

Figure 4.1: Heat of hydration curves for the NS concrete mix

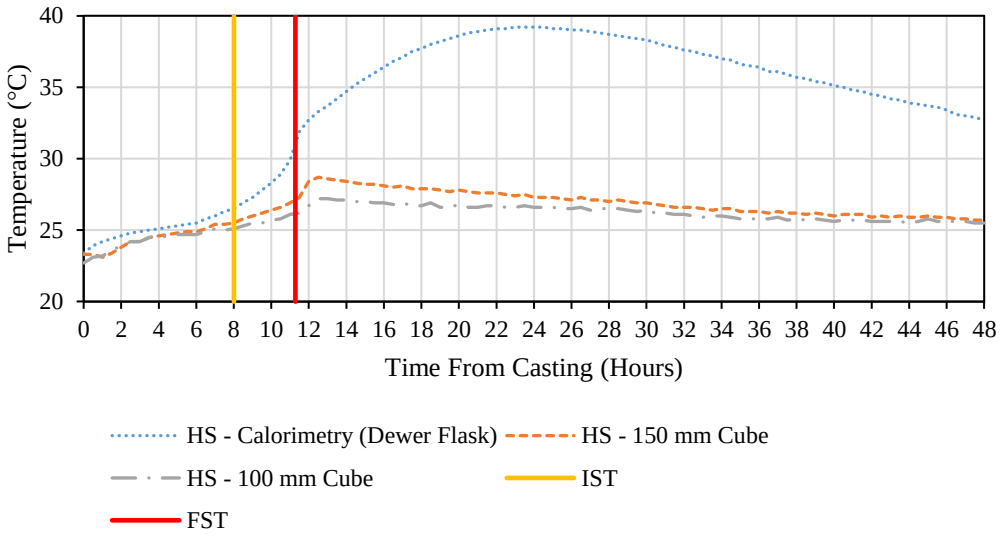

Figure 4.2: Heat of hydration of the HS concrete mix

The setting times determined using the fractional method are depicted in Figure 4.1 and Figure 4.2 with the values summarised in Table 4.1 and Table 4.2. Table 4.1 and Table 4.2 also contain the stresses that could potentially develop within the concrete due to the thermal expansion and contraction of the solid concrete. From these tables it can be seen how large the time delay in the heat of hydration development between the two concretes is. Table 4.1 and Table 4.2 shows that the concretes have very similar values for the maximum temperature reached within both of the concretes and the 20% and 50% of the peak baseline temperature determined using the fractional method. The difference seen in these two tables is when the

20% and 50% of the peak baseline temperature occurs. From these tables it is seen that the NS concrete sets more rapidly than the HS concrete, therefore by adding SCM's to concrete, both the heat of hydration development and setting time of the concrete are delayed. Table 4.1 and Table 4.2 also indicate that both concretes experience a similar stress development within the solid concrete due to the thermal expansion and contraction of the set concrete. The stresses are very low for the 100 mm and 150 mm cubes when compared with the results from the calorimetry setup indicating the greatest stress development within the concrete due to thermal movement that occurs within large casts.

Table 4.1: Setting times for the NS concrete mix

Property	NS - Calorimetry	NS – 150 mm Cube	NS – 100 mm Cube
Maximum temperature	38.90°C (19h55)	28.50°C (9h50)	27.50°C (10h00)
Baseline temperature	22.50°C	21.60°C	22.20°C
Maximum temperature rise	16.40°C	6.90°C	5.30°C
Room temperature	25.00°C	25.00°C	25.00°C
50% of peak baseline	30.70°C	25.05°C	24.85°C
20% of peak baseline	25.78°C	22.98°C	23.26°C
IST	5h00	1h30	1h00
FST	8h20	6h00	4h20
Thermal expansion temperature rise	8.20°C	3.45°C	2.65°C
Thermal expansion strain	93.64 με	39.40 με	30.26 με
Thermal expansion stress	2.51 MPa	1.06 MPa	0.81 MPa
Thermal contraction temperature drop	-5.70°C	-0.05°C	0.15°C
Thermal contraction strain	-65.09 με	-0.57 με	1.71 με
Thermal contraction stress	-1.75 MPa	-0.02 MPa	0.05 MPa

Table 4.2: Setting times determined for the HS concrete mix

Property	HS - Calorimetry	HS – 150 mm Cube	HS – 100 mm Cube
Maximum temperature	39.30°C (24h45)	28.70°C (12h30)	27.30°C (13h15)
Baseline temperature	23.30°C	23.10°C	22.70°C
Maximum temperature rise	16.00°C	5.60°C	4.60°C
Room Temperature	25.00°C	25.00°C	25.00°C
50% of peak baseline	31.30°C	25.90°C	25.00°C
20% of peak baseline	26.50°C	24.22°C	23.62°C
IST	8h00	3h05	3h30
FST	11h20	8h55	7h40
Thermal expansion temperature rise	8.00°C	2.80°C	2.30°C
Thermal expansion strain	87.12 με	30.49 με	25.05 με
Thermal expansion stress	2.30 MPa	0.80 MPa	0.66 MPa
Thermal contraction temperature drop	-6.30°C	-0.90°C	0.00°C
Thermal contraction strain	-68.61 με	-9.80 με	0.00 με
Thermal contraction stress	-1.81 MPa	-0.26 MPa	0.00 MPa

4.3 MECHANICAL PROPERTIES

The characteristic mechanical properties of the two different concretes are summarised in Table 4.3, which are determined on 28 day water cured samples. From this table, it is seen that the addition of SCM as a replacement of fine aggregate within the concrete results in an increase in the compressive, tensile and MOR strength of the concrete while keeping the E-value of the concrete constant. It was expected that the E-value would be remain, this is due to the SCM being pozzolanic in nature and contributing to the strength of the concrete while the elastic modulus of concrete is predominantly affected by the aggregate within the concrete which remained unaffected between the two concrete mixes.

Table 4.3: 28 day water cured characteristic strength values of the 2 concrete mixes

Property	NS	HS	Unit
Compressive strength	40.60	54.10	**MPa**
Splitting tensile strength	2.84	3.82	**MPa**
MOR strength	5.46	7.92	**MPa**
E-value	33.00	33.30	**GPa**

Figure 4.3 depicts the strength development of the air cured samples over time. From this figure it is seen that both of the concrete mixes have a similar rate of early age strength development with a divergence in the compressive strength between the two concretes being seen after 7 days. The 28-day compressive strength of the air cured samples are 3.59 MPa and 8.34 MPa weaker than the water cured samples for the NS and HS concrete mixes respectively. This indicates that the strength development of concrete containing SCM are more sensitive to the curing conditions that the concrete is exposed to than concrete that does not contain SCM. When looking that compressive strength of the concrete at 2 days and comparing this to the compressive stresses that possibly develops within the concrete due to thermal expansion of the pavement as shown in Table 4.1 and Table 4.2, it can be seen that a very small amount of the compressive strength capacity of the concrete is used up.

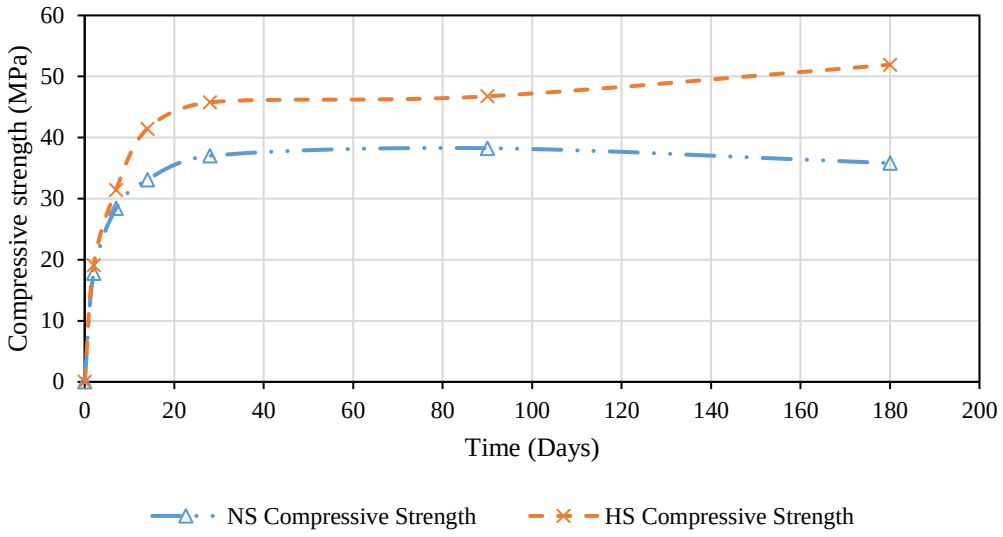

Figure 4.3: Strength development of concrete from air cured samples

Table 4.4 contains a summary of the splitting tensile strength, MOR strength and E-value determined on air cured samples and the coefficient of thermal expansion determined on water cured samples of both concretes. When comparing the mechanical properties in Table 4.3 to that of Table 4.4, it is seen that the MOR strength and the E-value are the properties most effected by the curing conditions while the splitting tensile strength of the concrete is similar to that of the 28 day water cured samples. The mechanical properties in Table 4.4 represents an average of the properties determined at 7, 14, 28 and 180 days with the actual values being summarised in Appendix D. When looking at the splitting tensile strength of the concrete in Table 4.4 and comparing this to the tensile stresses that potentially develop within the concrete due to thermal contraction shown in Table 4.1 and Table 4.2, it can be seen that a significant amount of the tensile strength capacity of the concrete is used up due to the thermal movement of the concrete even before environmental or traffic loading occurs. This could lead to minor cracks forming withing a UTCRCP.

Table 4.4: Summary of air cured samples mechanical properties and thermal expansion coefficient

Property	NS	HS	Unit
Splitting tensile strength	2.61	3.10	**MPa**
MOR Strength	3.56	4.24	**MPa**
E-value	26.82	26.40	**GPa**
Coefficient of thermal expansion	11.42	10.89	**με/°C**

4.4 MOISTURE MOVEMENT PROPERTIES

A summary of the sorptivity and porosity values determined for both concretes at 14 and 28 days are summarised in Table 4.5 for both concretes. From this table it is seen that the HS concrete has a much lower sorptivity than that of the NS mixture, indicating that the HS concrete absorbs and transmits water through the concrete at a lower rate than the NS concrete indicating that capillary suction is higher in the NS concrete than in the HS concrete. Table 4.5 indicates that the NS concrete has a lower porosity than the HS concrete. It is typically expected that the addition of SCM to concrete results in a refinement of the pore structure within the concrete due to the fine grading of the SCM added. Both concretes had the same slump of 30 mm but the relatively higher porosity of the HS mixture could have been caused by the lack of compaction of the relatively sticky HS mixture. The high sorptivity of the NS mixture could result in moisture being absorbed more easily from supporting layers, while the increased porosity of the HS mixture indicates that the concrete has a higher moisture holding capacity.

Table 4.5: Sorptivity and porosity of concrete at 14 and 28 days

Property	NS	HS	Unit
Sorptivity (14 Days)	9.50	3.90	**$mm/hr^{0.5}$**
Porosity (14 Days)	15.60	17.20	**%**
Sorptivity (28 Days)	9.35	4.90	**$mm/hr^{0.5}$**
Porosity (28 Days)	15.80	17.40	**%**

Figure 4.4 and Figure 4.5 contain the drying out curves of the moisture loss measured on the sorptivity and porosity samples. From these figures it is seen that the HS concrete mixture takes a significantly longer time to reach a stable mass and to fully dry out. For the 14 and 28 day samples, the NS concrete dried out completely within 7 days after being placed in the drying oven at 55°C, while the HS concrete took 28 days to completely dry out. This indicates that the HS concrete retained water within the pores of the concrete a lot longer than the NS concrete. Figure 4.4. and Figure 4.5 depict that both the NS and HS concretes experience the same moisture loss of ± 7% but the rate at which this moisture loss took place differed due to the difference in the pore structure within the two concretes. Another trend that is noted when comparing Figure 4.4 and Figure 4.5 is that the 28 day samples took longer to dry out than the 14 day samples indicating that a possible refinement in the pore structure of both the NS and HS concrete took place. The 28 day HS concrete sample however saw a greater increase in the time taken to dry out indicating that the addition of SCM results in a refinement of the pore structure of the concrete over time. These graphs indicate that the rate of drying can be reduced by using SCM in UTCRCP.

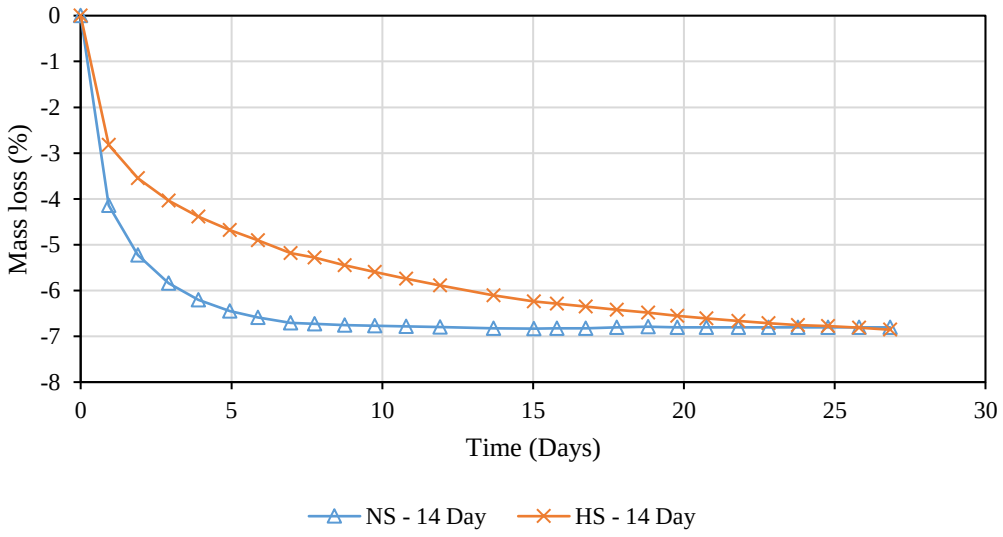

Figure 4.4: Rate of moisture loss in sorptivity samples cored from concrete after 14 days

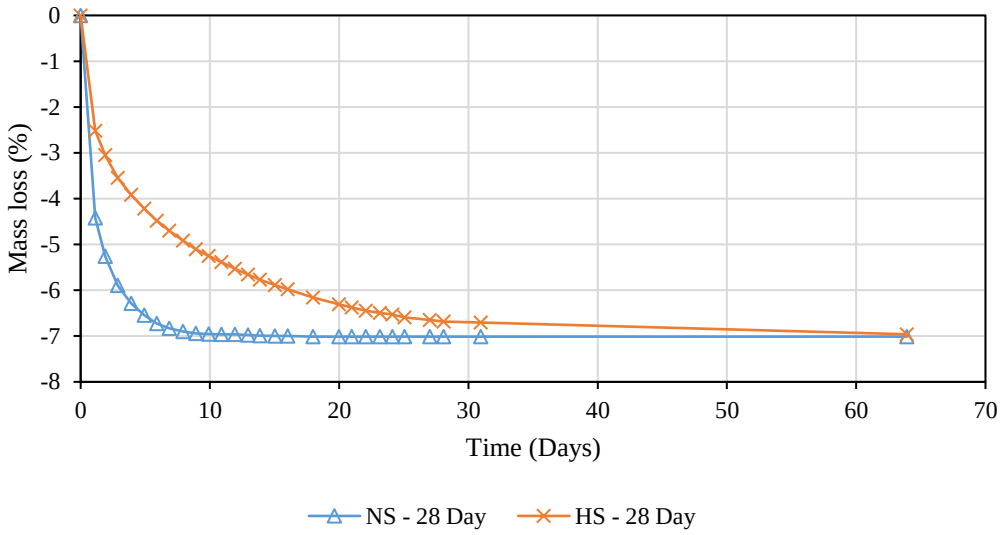

Figure 4.5: Rate of moisture loss in sorptivity samples cored from concrete after 28 days

4.5 SHRINKAGE

Figure 4.6 is the plastic settlement measured of both concretes on sealed Ø100 mm cylinders. The plastic settlement was taken as the deformation that occurred in the concrete up until the point of IST of the concrete. This is due to the IST representing the point where workability and plasticity of the concrete is lost and further compaction of the concrete cannot be achieved without damaging the concrete, therefore it was assumed deformation that takes place after this point would be due to autogenous shrinkage of the concrete. From this figure it is seen that significant settlement is achieved within both concretes but with the most pronounced effects being seen in the NS concrete. This figure indicates that concrete which does not contain SCM experiences more settlement, with the concrete experiencing further compaction after being cast. This is due to the SCM making the concrete more cohesive and stickier therefore affecting the workability of the concrete.

Figure 4.7 depicts the early age shrinkage measured for 11 days that took place after the plastic settlement of the concrete was measured as shown in Figure 4.6. The reason for 11 days was due to a Covid-19 lockdown causing that the samples could not be demoulded after 7 days. From Figure 4.7 it can be seen that the NS concrete experiences far greater early age shrinkage than the HS concrete. This could be due to the HS concrete having a lower w/b ratio to that of the NS concrete therefore resulting in less deformation of the concrete taking place. Visser (2019) found that the addition of either fly ash or silica fume to concrete resulted in less shrinkage of the concrete. The reason for the lower shrinkage being measure could be due to no super-plasticizer being used where super-plasticizer allows for more dispersion of the fly

ash and silica fume particles and thus resulting in a refinement of the pore structure of the concrete to take place (Visser, 2019). Additionally, fly ash has been found to inhibit autogenous shrinkage due to a reduction in the rate at which internal relative humidity decreases with concrete containing fly ash (Malhotra, 2002).

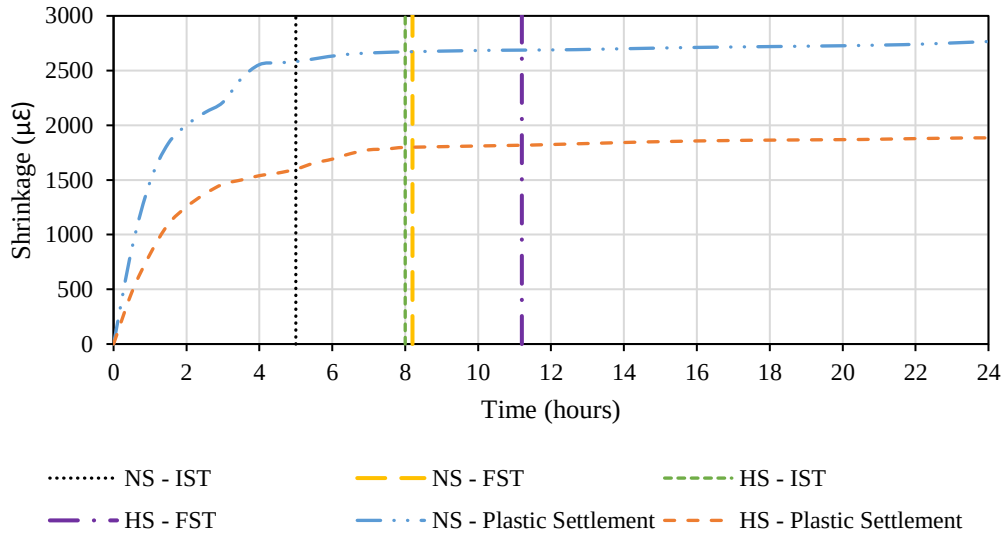

Figure 4.6: Plastic settlement of concrete measure in Ø100 mm × 300 mm cylinders

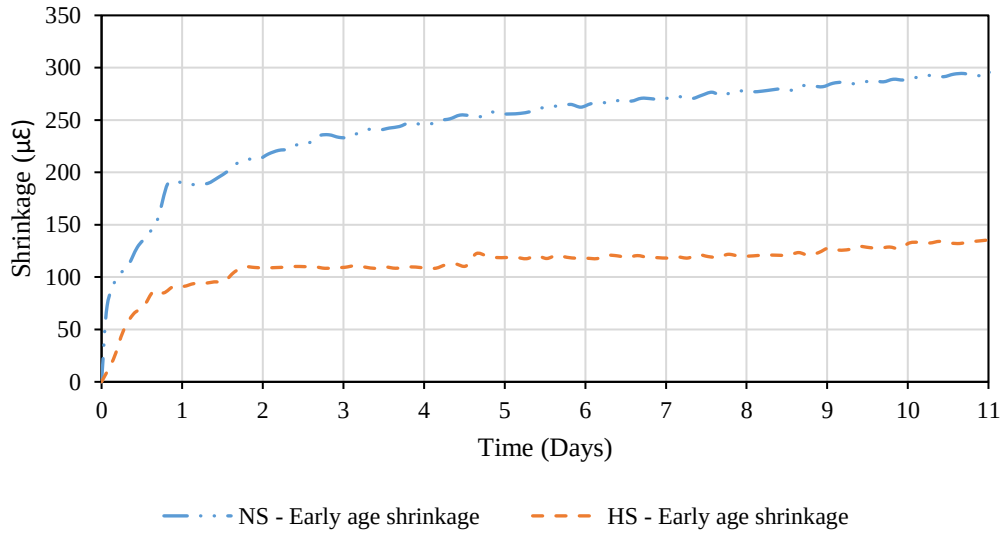

Figure 4.7: The early age shrinkage measured for the first 11 days in Ø100 mm × 300 mm cylinders

The drying shrinkage of the Ø100mm × 300 mm cylinders after removing the outer casing are shown in Figure 4.8. This figure indicates that both concretes experience a similar amount of drying shrinkage. This is due to the w/c ratio of both concretes remaining the same with the same cement content being used between both mixtures of concrete. The total deformation measured using the Ø100mm × 300mm cylinders is shown in Figure 4.9.

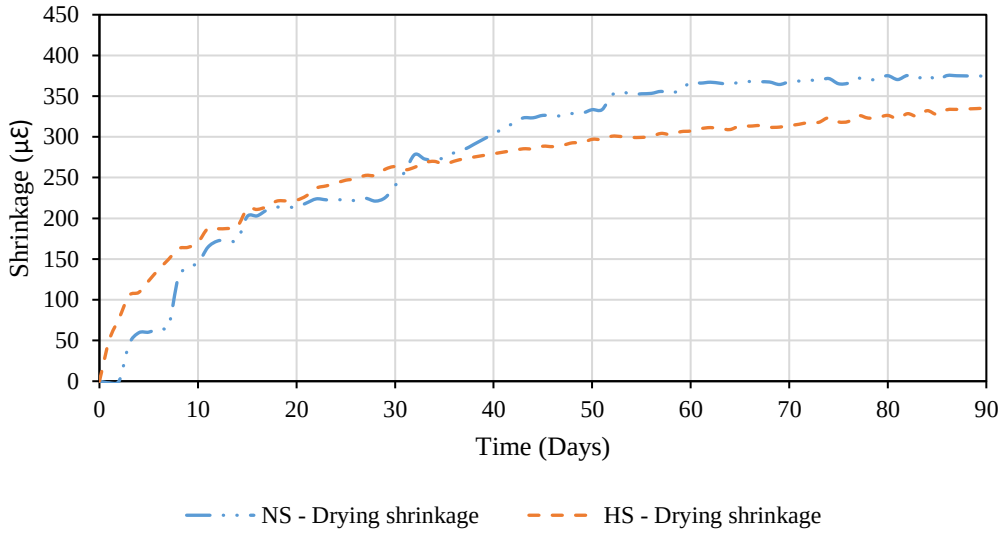

Figure 4.8: Drying shrinkage measured on Ø100 mm × 300 mm cylinders

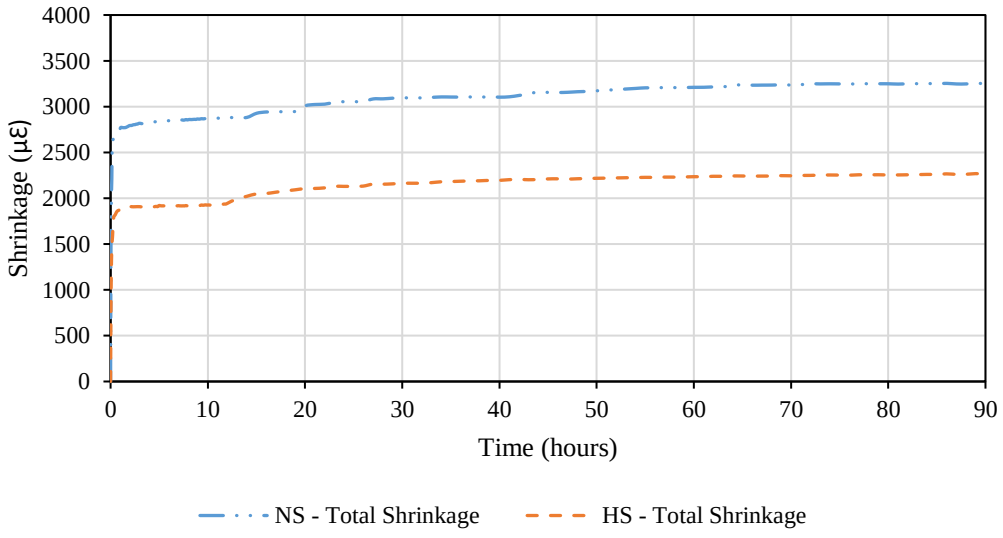

Figure 4.9: The total deformation measured using the Ø100 mm × 300 mm cylinders

The drying shrinkage measured in Figure 4.8 is similar to that of the 50 × 50 × 300 mm drying shrinkage prisms shown in Figure 4.10 with only a difference in the magnitude of drying shrinkage experienced between the different concrete samples. The 50 × 50 × 300 mm drying shrinkage prisms are assumed to be capable of drying out completely due to the relatively small dimensions of these samples. It is also assumed that the effects of a moisture gradient within these samples are negligible due to the samples relatively small dimensions. It is noted that the 50 × 50 × 300 mm prisms dry out faster that the Ø100 mm cylinders, indicating that moisture escapes faster and shrinkage of the concrete stopped sooner when thinner concrete elements are used. There is likely to be a moisture gradient within the Ø100 mm × 300 mm cylinders due to the size of these samples, with the centre of the sample experiencing lower drying shrinkage and higher internal relative humidity and as a result, restraining the drying shrinkage of the outer areas of concrete that experience higher drying shrinkage and lower internal relative humidity.

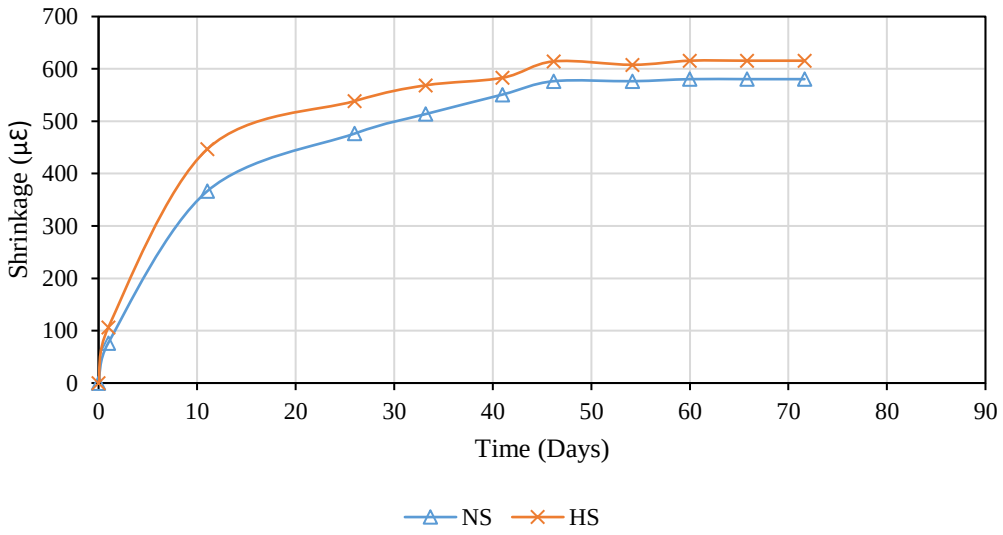

Figure 4.10: Drying shrinkage measured on 50 × 50 × 300 mm prisms

4.6 SHRINKAGE AND MOISTURE LOSS

The relationship between drying shrinkage and internal relative humidity was determined on a 100 × 100 × 300 mm drying shrinkage prism with relative humidity sensors placed at the centre and 10 mm from the specimen's surface. The drying shrinkage of these 100 × 100 × 300 mm prisms are shown in Figure 4.11. From this figure, it is seen that the drying shrinkage of the NS concrete is higher than that of the HS concrete. When looking at Figure 4.12 of the internal relative humidity of the concrete, it is noticed that the NS concrete dried out at a faster rate than

the HS concrete with a steeper slope in the decrease in internal relative humidity of the concrete. Figure 4.4 and Figure 4.5 as discussed earlier also show that the HS concrete retains water a lot longer than the NS concrete, with the NS concrete drying out more rapidly. This result in a higher drying shrinkage being seen in the NS concrete due to the rate and amount of moisture loss within the concrete.

Figure 4.12 also indicates that the HS concrete remains at an internal relative humidity above 80%, which is the level of relative humidity above which hydration of the cement within concrete can takes place, as discussed in Section 2.4. This indicates that the HS concrete continues to gain strength for a longer period of time then the NS concrete due to the lower rate at which the HS concrete loses moisture. This is evident by the graph representing the strength development of the concrete over time in Figure 4.3.

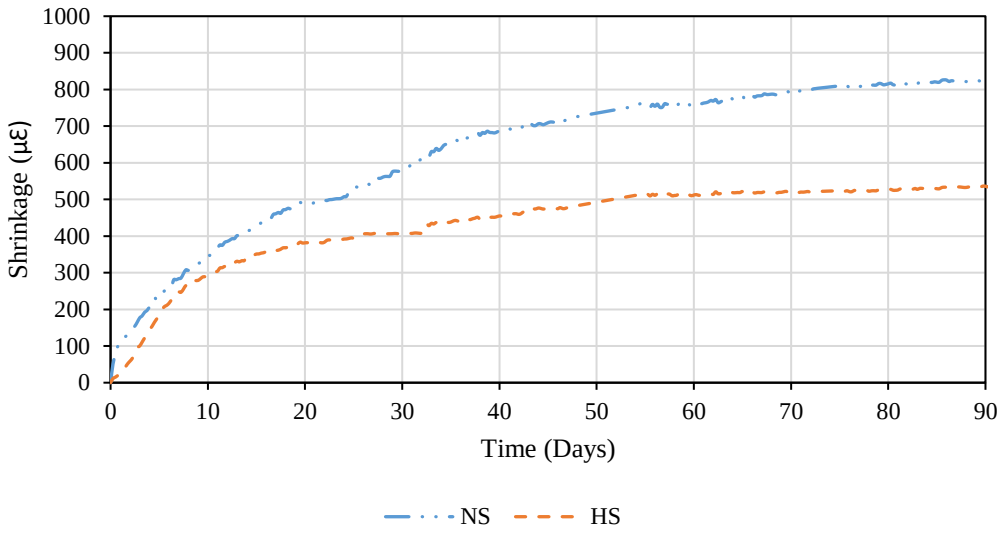

Figure 4.11: Drying shrinkage measured on 100 × 100 × 300 mm prisms

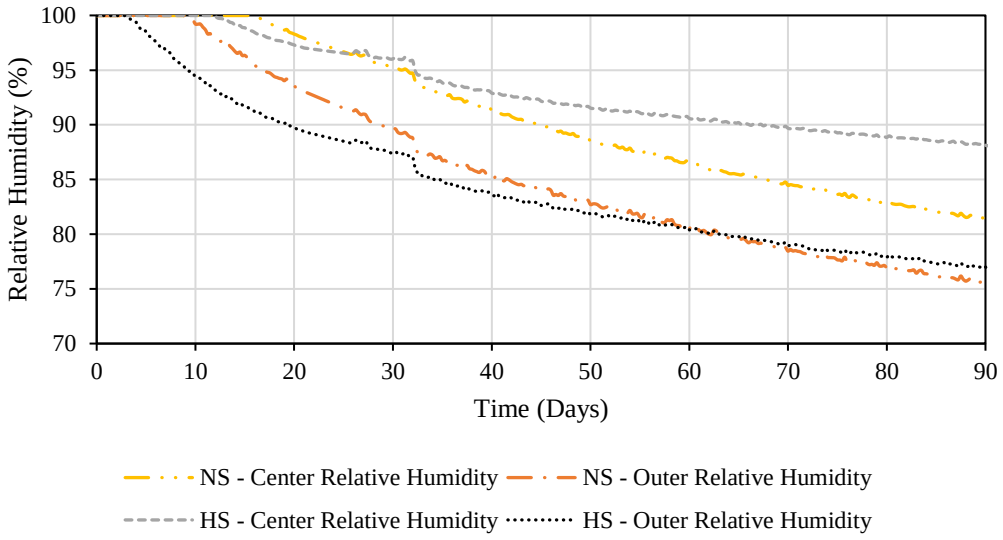

Figure 4.12: Decrease in relative humidity over time at surface and centre of concrete

Figure 4.13 is a plot of the drying shrinkage versus internal relative humidity of the concrete. The relative humidity is taken as a weighted average of the centre and outer internal relative humidity values. The weighted average was determined by assuming that the outer relative humidity sensor represents the moisture content of the outer 25 mm (7500 mm^2) of the concrete and the internal relative humidity sensor represents the moisture content of the internal area of the concrete (2500 mm^2). This creates a 75% and 25% split between the surface and centre relative humidity sensor values and as a result the effect on the drying shrinkage of the concrete. The graph in Figure 4.13 depicts that there was a long period where the NS concrete experienced shrinkage while the concrete remained fully saturated (100% relative humidity) and then the concrete began to dry out, with a linear relationship between the drying shrinkage and internal relative humidity of the concrete. The HS concrete experienced a shorter period where the concrete remained fully saturated and shrinkage of the concrete was measured. After the concrete began to dry out, the relationship between drying shrinkage and internal relative humidity was initially non-linear, followed by a linear relationship between the two.

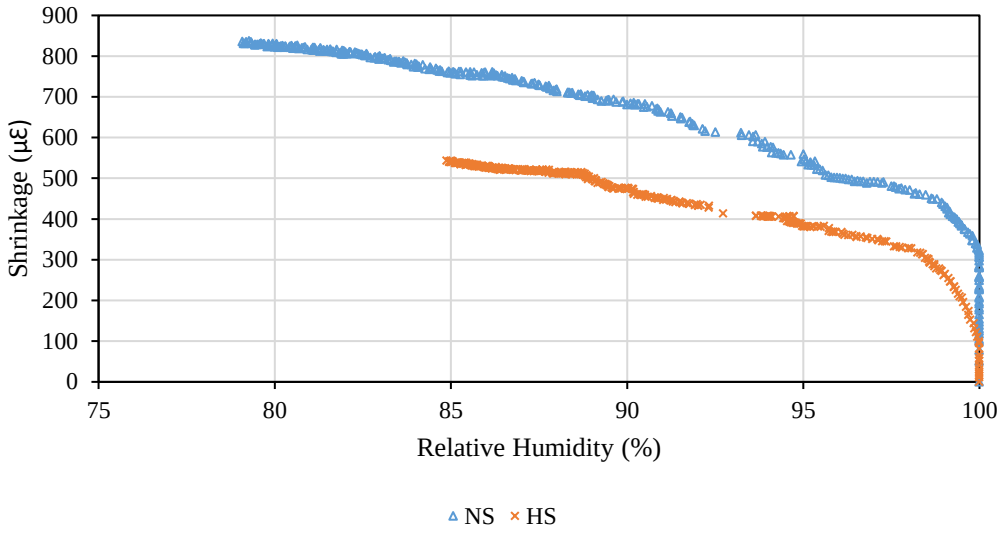

Figure 4.13: Plot of shrinkage strain vs. relative humidity

4.7 SUMMARY

The heat evolution over time due to the heat of hydration of cement in concrete containing SCM experiences a delay in the time when the maximum temperature rise occurs within the concrete. Therefore, concrete cast without the use of SCM to generated concrete of higher strength will experience a more rapid increase in temperature and a will reach IST and FST sooner than concrete containing SCM. This will also result is greater thermal movement stresses and strains developing within concrete that does not contain SCM.

The addition of SCM to the HS concrete resulted in a higher compressive, splitting tensile and MOR strength while keeping the E-value relatively the same between the NS and HS concrete when looking at the characteristic strength values of the concrete. When comparing the mechanical properties of air cured samples to that of the water cured samples, it was seen that the HS concrete containing SCM was more sensitive to the curing conditions that the concrete was exposed to than the NS concrete. The mechanical properties affected include the compressive strength, MOR strength and E-value while the splitting tensile strength was similar to that of the characteristic strength values.

When comparing the moisture movement properties of the NS and HS concrete, it was found that the HS concrete was far less water absorbent that the NS concrete and held on to any moisture a lot stronger than the NS concrete. This means the NS concrete would both absorb more water and release water much faster than the HS concrete indicating that the HS concrete pavements would not experience as much swelling as the NS concrete pavements and would

take longer to dry out than the NS concrete pavements. It was also noted that the addition of SCM to the concrete resulted in the concrete being more cohesive and sticker resulting in a loss of workability.

When looking at the deformation measured on the NS and HS concrete it was seen that the NS concrete experienced more plastic settlement than the HS concrete indicating that the NS concrete experiences more compaction after being cast. This explains why the NS concrete has a lower porosity than the HS concrete, due to more air being trapped within the stickier HS concrete mix and less compaction of the HS mix leading to larger pores within the concrete.

The early age shrinkage measured within the NS concrete was also found to be higher than that of the HS concrete and this was due to the addition of fly ash and silica fume to the concrete which reduces the amount of shrinkage concrete.

The amount of drying shrinkage of the NS and HS concrete was found to be similar when looking at the results from the Ø100 mm × 300 mm cylinders and 50 × 50 × 300 mm prisms. The results from the 100 × 100 × 300 mm drying shrinkage prism with embedded relative humidity sensors indicated that there is a linear relationship between that decrease in relative humidity and drying shrinkage of the concrete. It was also noted that the rate at which the relative humidity decreased within the NS and HS concrete was different with the relative humidity within the NS concrete decreasing more rapidly as seen with the drying out curves.

The relative humidity levels within the HS concrete remained above 80% for longer than the NS concrete. This indicated that the HS concrete experienced more hydration for a longer period of time than the NS concrete due to the lower rate at which moisture is lost within the HS concrete. This caused the HS concrete to continue gaining strength over a longer period of time due to more moisture remaining within the pores of the HS concrete. The addition of SCM contributes to the pozzolanic reactions that take place within the concrete therefore resulting in a long tern gain in strength.

Table 4.6 summarises all the stresses and strains that would develop within a restrained concrete element based on the result determined within this chapter. From this table it can be seen that significant stresses may potentially develop within a restrained concrete pavement due to thermal movement as well as shrinkage.

Table 4.6: Summary of predicted stresses and strain development within restrained concrete elements.

Property	NS - Concrete			HS - Concrete		
Thermal affects						
	Calorimetry	**150 mm cube**	**100 mm cube**	**Calorimetry**	**150 mm cube**	**100 mm cube**
IST	5h00	1h30	1h00	8h00	3h05	3h30
FST	8h20	6h00	4h20	11h20	8h55	7h40
Thermal expansion strain	93.64 με	39.40 με	30.26 με	87.12 με	30.49 με	25.05 με
Thermal expansion stress	2.51 MPa	1.06 MPa	0.81 MPa	2.30 MPa	0.80 MPa	0.66 MPa
Thermal contraction strain	-65.09 με	-0.57 με	1.71 με	-68.61 με	-9.80 με	0.00 με
Thermal contraction stress	-1.75 MPa	-0.02 MPa	0.05 MPa	-1.81 MPa	-0.26 MPa	0.00 MPa
% of 48 hour of compressive strength used	14.12%	5.96%	4.56%	12.04%	4.19%	3.46%
% of 48 hour tensile strength used	69.17%	0.79%	-	60.13%	8.64%	0.00%
Short term behaviour						
14 Day Compressive strength	33.09 MPa			41.44 MPa		
14 Day tensile strength	2.69 MPa			3.19 MPa		
14 Day E-value	26.76 GPa			26.49 GPa		
Plastic settlement	2581.81 με			1798.16 με		
Autogenous shrinkage	300.21 με			144.29 με		
Stress due to autogenous shrinkage	-8.03 MPa			-3.82 MPa		

Long term behaviour		
180 Day compressive strength	35.82 MPa	51.92 MPa
180 Day E-value	26.54 GPa	26.65 GPa
180 Day tensile strength	2.36 MPa	3.18 MPa
Total dry shrinkage 50 mm prisms	580.39 με	615.69 με
Dry shrinkage stress for 50 mm prisms	-15.40 MPa	-16.41 MPa
Total drying shrinkage 100 mm prisms	823.00 με	530.00 με
Dry shrinkage stress for 100 mm prisms	-21.84 MPa	-14.07 MPa

** Stresses calculated using* $\sigma = E\varepsilon$

5 THIN PAVEMENT SECTIONS RESULTS AND DISCUSSION

5.1 INTRODUCTION

The movements seen within a concrete pavement are due to either shrinkage/swelling and/or thermal contraction/expansion as already discussed previously. This movement results in internal stresses that develop within the concrete that could result in cracking of the concrete pavement. The thermal movement of a concrete pavement is dependent on not only the change in average temperature of the pavements but also on the built-in temperature gradient within the pavement while the shrinkage/swelling of the concrete pavement is dependent on the moisture content and moisture gradient of the pavement.

This chapter looks at the behaviour of NS and HS thin concrete pavement sections in response to the ambient environmental conditions that the pavement sections are exposed to. The effect of heat of hydration and early age shrinkage behaviour of the pavement segments are taken into account. The heat of hydration, built-in temperature gradient, linear temperature gradient, surface strain, curvature, stresses and moment development within the NS and HS concrete pavement sections are discussed. The behaviour is drawn back to the environmental conditions the pavement sections were exposed to as well the mechanical and moisture movement properties of the concrete.

5.2 HEAT OF HYDRATION, BUILT-IN TEMPERATURE GRADIENT AND CHANGE IN LENGTH OF PAVEMENTS

Figure 5.1 and Figure 5.2 are the plots of the heat of hydration from the heat that was generated within the concrete pavement sections for the first 24 hours after casting the NS and HS concrete pavement sections respectively. From these figures it can be seen that the maximum temperature reached within each of the pavements increased with pavement thickness and the temperature was higher in the NS concrete than in the HS concrete mix which contained SCM. It is also noted that the NS concrete experienced a rapid increase in temperature while the temperature rise within the HS concrete was more gradual over time. The reason for this has already been discussed in Section 4.2 where it was found that the addition of SCM reduces the peak temperature reached within the concrete due to the prolonged development of the heat of hydration curves. Figure 5.1 and Figure 5.2 also indicate the IST and FST of both the NS and HS concrete. From these figures it is seen that the setting times determined from the heat of hydration of the pavements is similar to the IST and FST determined using the semi-adiabatic calorimetry setup. Indicating that the semi-adiabatic calorimetry setup can be used to determine the setting times of thin concrete pavements through lab testing while the heat evolution

measured within the 100 mm and 150 mm cubes will give an indication of the shape of the heat of hydration cures that would develop within a thin concrete pavement.

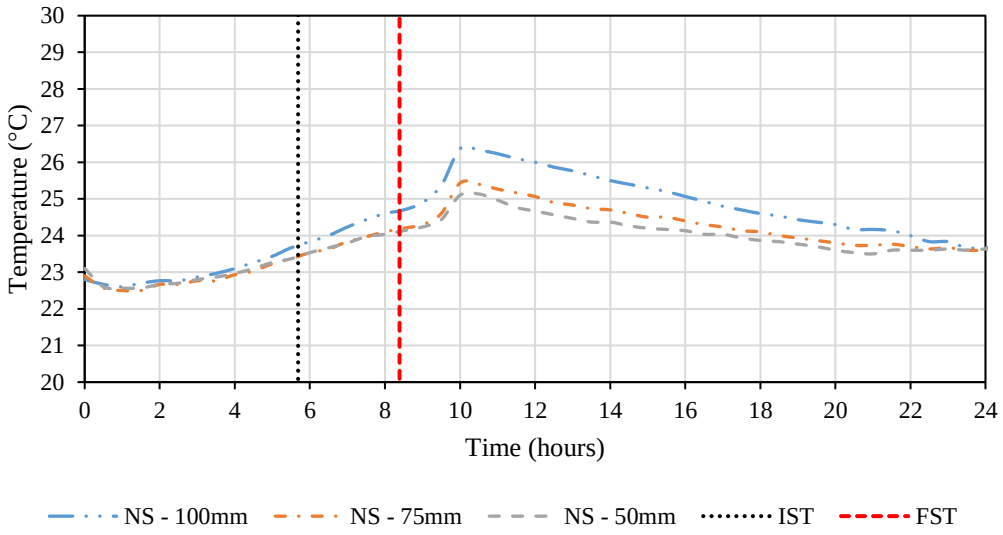

Figure 5.1: NS concrete heat of hydration measured for first the 24 hours

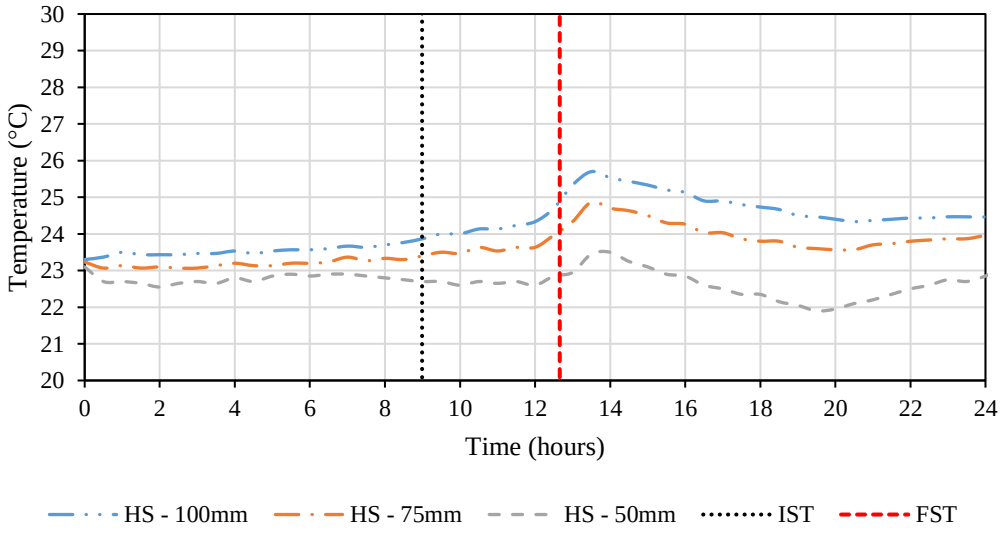

Figure 5.2: HS concrete heat of hydration measured for first the 24 hours

When analysing the data of the temperature distribution within the concrete pavements during the curing period, it was noted that due to how thin the pavement sections were, there was no temperature gradient within the concrete pavement sections due to the heat of hydration taking place within the first 48 hours after casting. The pavement sections are seen to have an almost uniform increase in temperature over the first 48 hours, with the average temperature of the

concrete pavements at the IST and FST shown in Table 5.1 and Table 5.2. The values in Table 5.1 and Table 5.2 represent the built-in temperature of the pavement. If the pavement sections temperature is to increase or decrease above or below this temperature, the pavement would experience a thermal expansion or thermal contraction of the solid concrete. These table also summarise the stresses and strains that would develop within a UTCRCP due to thermal expansion and contraction of the pavement sections. The values in these tables are compared to those determined using the semi-adiabatic calorimetry setup and the 100 mm cubes. These values indicate that the semi-adiabatic calorimetry setup can be used to predict the setting times of the concrete pavement sections while the 100 mm cubes can be used to determine the stresses that would develop within the pavements due to thermal expansion and contraction of the concrete.

Table 5.1: Summary of data from heat evolution of the NS concrete pavements

Pavement thickness	**NS – 100 mm**	**NS – 75 mm**	**NS – 50 mm**	**NS - Calorimetry**	**NS – 100 mm cube**
IST	5h30	5h50	5h40	5h00	1h00
FST	8h20	8h30	8h10	8h20	4h20
IST Temperature (°C)	23.70	23.50	23.40	25.78	23.26
FST temperature (°C)	24.70	24.20	24.10	30.70	24.85
Strain due to thermal expansion (με)	19.22	13.89	12.18	93.64	30.26
Stress due to thermal expansion (MPa)	0.51	0.37	0.33	2.51	0.81
Strain due to thermal contraction (με)	-19.22	-13.89	-12.18	-65.09	1.71
Stress due to thermal contraction (MPa)	-0.51	-0.37	-0.33	-1.75	0.05

Table 5.2: Summary of data from heat evolution of the HS concrete pavements

Pavement Thickness	HS – 100 mm	HS – 75 mm	HS – 50 mm	HS - Calorimetry	HS – 100 mm cube
IST	8h50	8h30	8h40	8h00	3h30
FST	12h00	12h20	12h30	11h20	7h40
IST Temperature (°C)	24.2	23.6	22.7	26.50	23.62
FST temperature (°C)	24.2	23.6	22.7	31.30	25.00
Strain due to thermal expansion (με)	14.70	10.16	2.72	87.12	30.26
Stress due to thermal expansion (MPa)	0.39	0.27	0.07	2.30	0.81
Strain due to thermal contraction (με)	-14.70	-10.16	-2.72	-65.09	0.00
Stress due to thermal contraction (MPa)	-0.39	-0.27	-0.07	-1.75	0.00

Figure 5.3 represents the change in length of the pavements prior to demoulding which took place 7 days after casting. This change in length was normalised over the length of the pavement for comparison purposes and was determined by measuring the gap on either side of the concrete pavement between the pavement and end block using a micrometre. From this figure it is seen that the HS concrete experienced a slightly higher change in length prior to the demoulding of the concrete than the NS concrete pavements. This pattern is similar to the shrinkage seen in the 50 × 50 × 300 mm prisms of Figure 4.10. From Figure 5.3 it is also seen that for both the NS and HS concrete, the change in length of the pavements increased with an increase in pavement thickness.

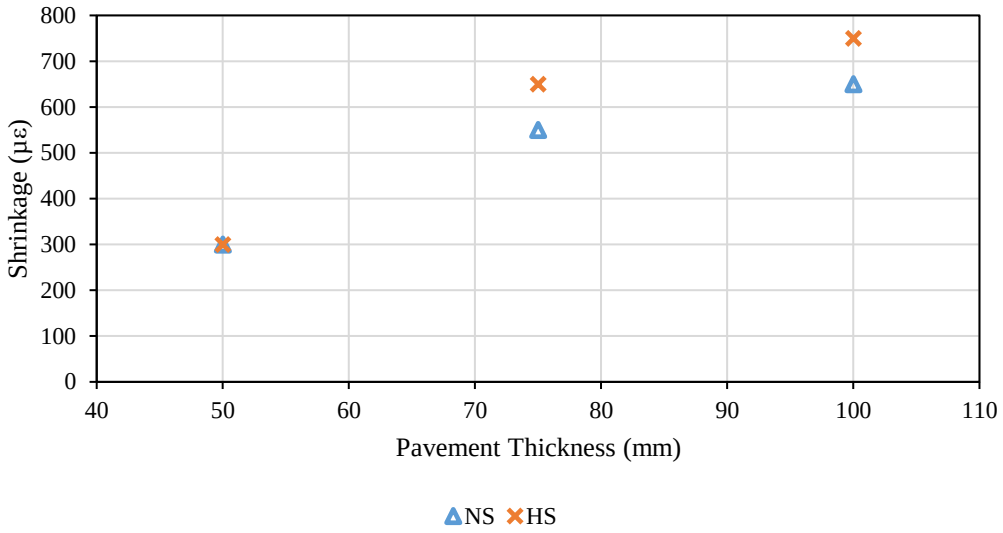

Figure 5.3: Shrinkage of pavements measured after 7 days using a micrometre

5.3 THIN PAVEMENTS RESPONSE TO ENVIROMENTAL EFFECTS

The enviromental conditions of ambient air temperature, relative humidity, wind speed, solar radiation and rain fall that the thin concrete pavements were exposed to over the 125 day analysis period is shown in Figure 5.4. This figure was used to see how the ambient enviromental conditions affected the behaviour of the pavement sections. From this figure it is seen that the ambient air temperature fluctuated by ± 10°C on a daily basis and that the ambient relative humidity fluctuated by ± 20% daily. Figure 5.4 shows that the daily solar radiation peaked at around 1000 W/m^2 with a ±100 W/m^2 deviation in the peak solar radiation, with the biggest dips in the solar radiation occuring due to cloud cover. It should be noted that the days when the pavement experienced rain fall was 1st June 2021 which amounted to 2 mm of precipitation, 30th September 2021 which amounted to 16 mm of precipitation, 1st October 2021 which amounted to 36 mm of precipitation and 2nd October 2021 which amounted to 2 mm of precipitation. The pavement section also experienced a light drizzle on the 24th August 2021, 27th August 2021 and 7th September 2021 which amounted to less than 0.5 mm of precipitation that lasted less than an hour. The times when precipitaion occured is an important fact to keep in mind when analysing the data further in order to understand the effect of precipitation in combination with the other enviromental conditions shown in Figure 5.4 on the pavement sections.

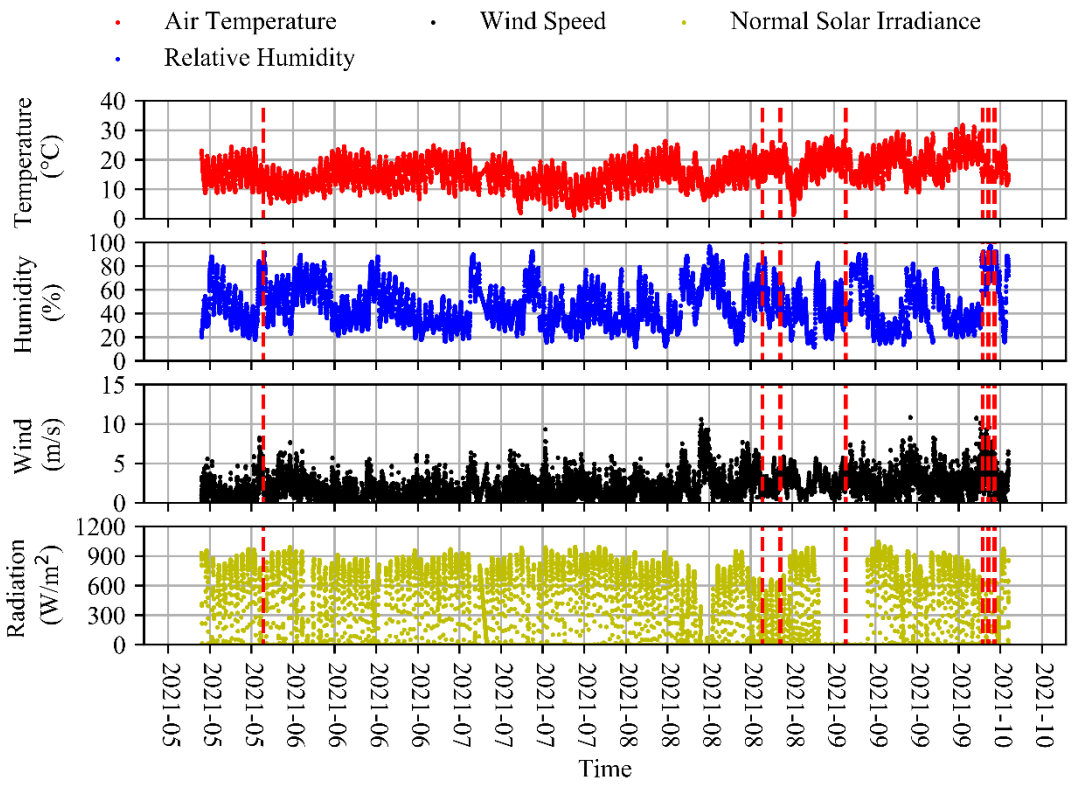

Figure 5.4: Ambient temperature, relative humidity, wind speed and solar radiation

5.3.1 Measure responses to environmental loading

Figure 5.5 depicts the strain that was measured in the top and bottom of the thin NS concrete pavement sections using surface mounted strain gauges. When analysing this figure, it is seen that the fluctuation of strain measured in the top and bottom of the concrete pavements are almost uniform for the period from 23rd May 2021 to 31st May 2021. This was due to the cyclic thermal expansion and contraction of the pavements taking place on a daily basis. After the rainfall that took place on the 1st June 2021, it is noted that all the NS concrete pavement sections showed an instantaneous thermal contraction due to the rapid cooling of the pavements followed by the swelling of the concrete due to the absorption of moisture into the concrete's pores. It is noted that the most swelling occurred in the bottom of the NS concrete pavements and it is interesting to note the shrinkage of the concrete that then took place over time with the drying out of the concrete pavements after moisture was absorbed and then a repeat of the swelling of the pavements due to the rainfall between the 30th September 2021 to 2nd October 2021. From Figure 5.5, it is seen that the 75 mm NS concrete pavement is the pavement that is the worst affected by the ambient environmental conditions due to the most significant variations in strain being seen within this pavement. It is also noted that the 100 mm NS

concrete pavement is the pavement that seems to perform the best with the least amount of variation in strain being measured within this pavement.

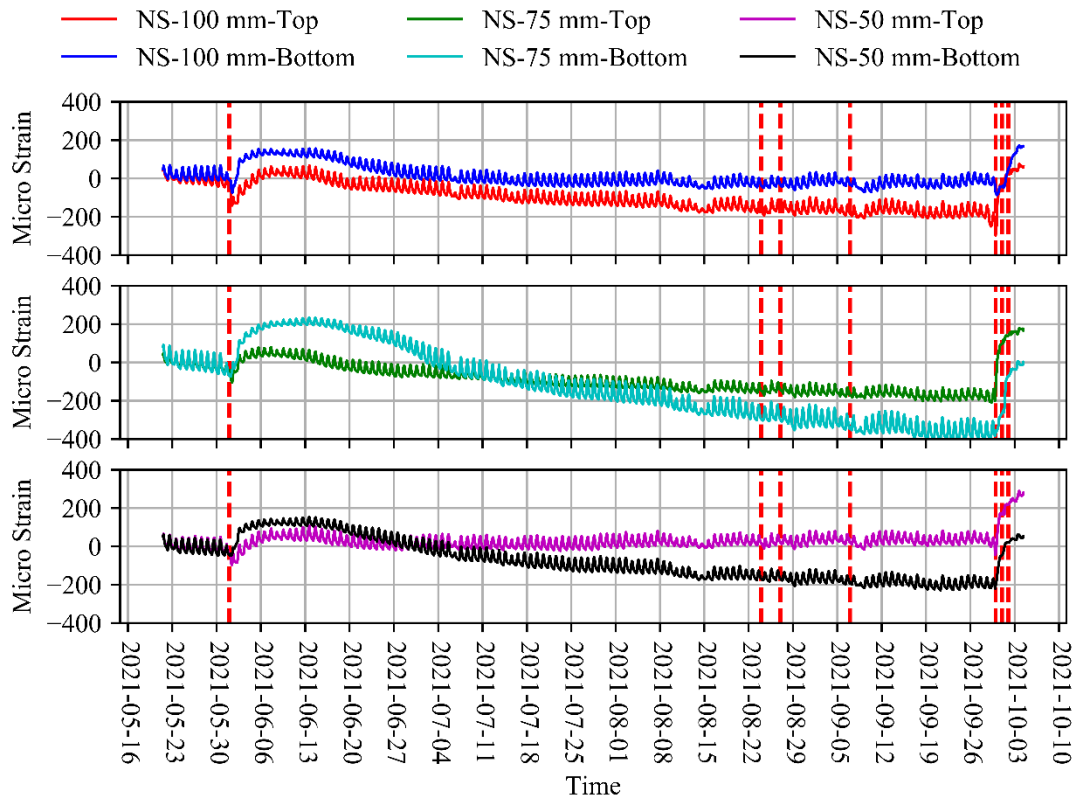

Figure 5.5: Strain measured on the top and bottom of the NS concrete pavements

Figure 5.6 is a plot of the strain measured in the top and bottom of the HS concrete pavements using surface mounted strain gauges. When comparing Figure 5.6 to that of Figure 5.5, it is seen that the HS concrete is not as significantly affected by the precipitation that took place on 1st June 2021 and between the 30th September 2021 and the 2nd of October 2021. Similar to the behaviour of the NS concrete pavements, the HS concrete pavements also experienced a thermal contraction due to the rapid cooling caused by the rainfall, but the HS concrete pavements did not experience the same magnitude of swelling as that of the NS concrete pavements. This comes back to the moisture movement properties defined in Section 4.4 where the HS concrete experiences significantly less sorptivity than that of the NS concrete, therefore less water enters the HS concrete pavements and as a result less swelling of the concrete took place. As a result, the predominant factor affecting the HS concrete pavements was the thermal effects with the effects due to moisture playing a minor role in the strains that develop within the HS concrete pavements. It is also useful to note from Figure 5.6, the predominant swelling

of the concrete occurred in the top of the HS concrete pavements whereas the NS concrete pavements predominantly saw swelling in the bottom of the concrete.

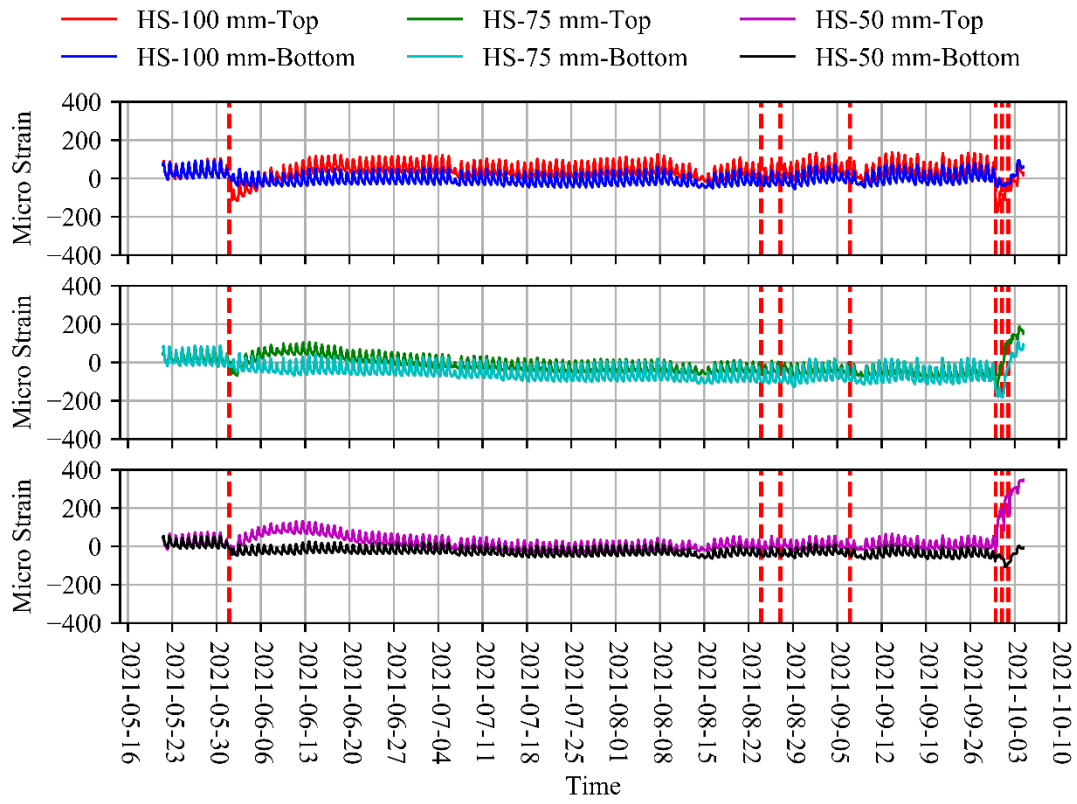

Figure 5.6: Strain measured on the top and bottom surfaces of the HS concrete pavements

Figure 5.7 is a plot of the stresses within the top and bottom of the concrete pavement sections determined using the formula shown in Equation 5.1.

$$\sigma = \frac{F}{A} \pm \frac{M}{z} \qquad \text{(Equation 5.1)}$$

From the plotting of Figure 5.7, it is seen that there is quite the significant contraction that takes place within the NS concrete pavement sections that results in a tensile stress within the concrete that is greater than the tensile strength of the concrete of 2.53 MPa. This is an important factor to consider when casting UTCRCP due to the stresses that could develop within the continuous concrete pavement as a result of thermal contraction and/or shrinkage of the concrete. From both Figure 5.5 and Figure 5.7, it is seen that effects due to the presence of moisture and its intrusion into the pores of the concrete has the most pronounced effect on the NS concrete pavements with a daily fluctuation in strain being seen within the pavements due

to the thermal expansion and contraction of the concrete pavements. From these figures, it can be seen that moisture was the predominant source of distress within the pavements which is worsened by daily thermal effects which could lead to fatigue of the pavement.

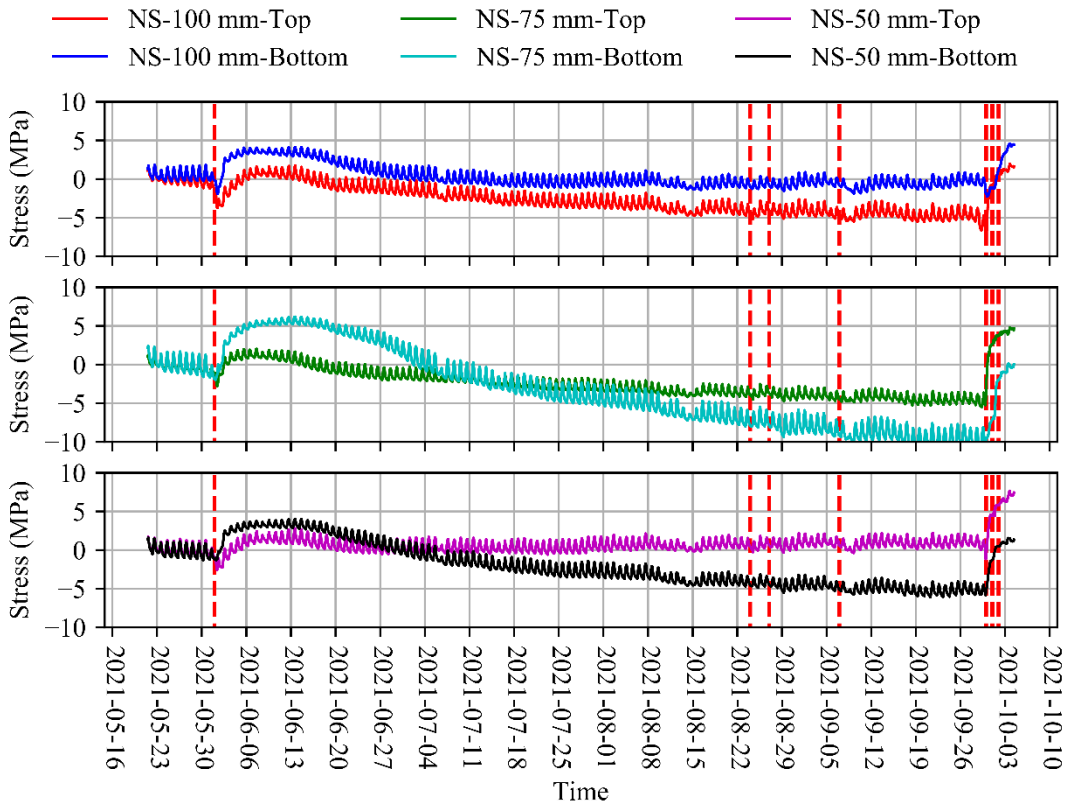

Figure 5.7: Stress calculated in the top and bottom surfaces of the NS concrete pavements

Figure 5.8 is a plot of the stresses calculated using Equation 5.1. Again, when comparing Figure 5.8 to Figure 5.7, it is seen that the HS concrete pavement sections experienced significantly less stresses than that of the NS concrete pavement sections, with only the 75 mm HS concrete pavement experiencing tensile stresses greater than the tensile strength of the concrete of 3.20 MPa indicating that there may be a critical pavement size of 75 mm thickness where the worst effects of environmental conditions are experienced by the pavement.

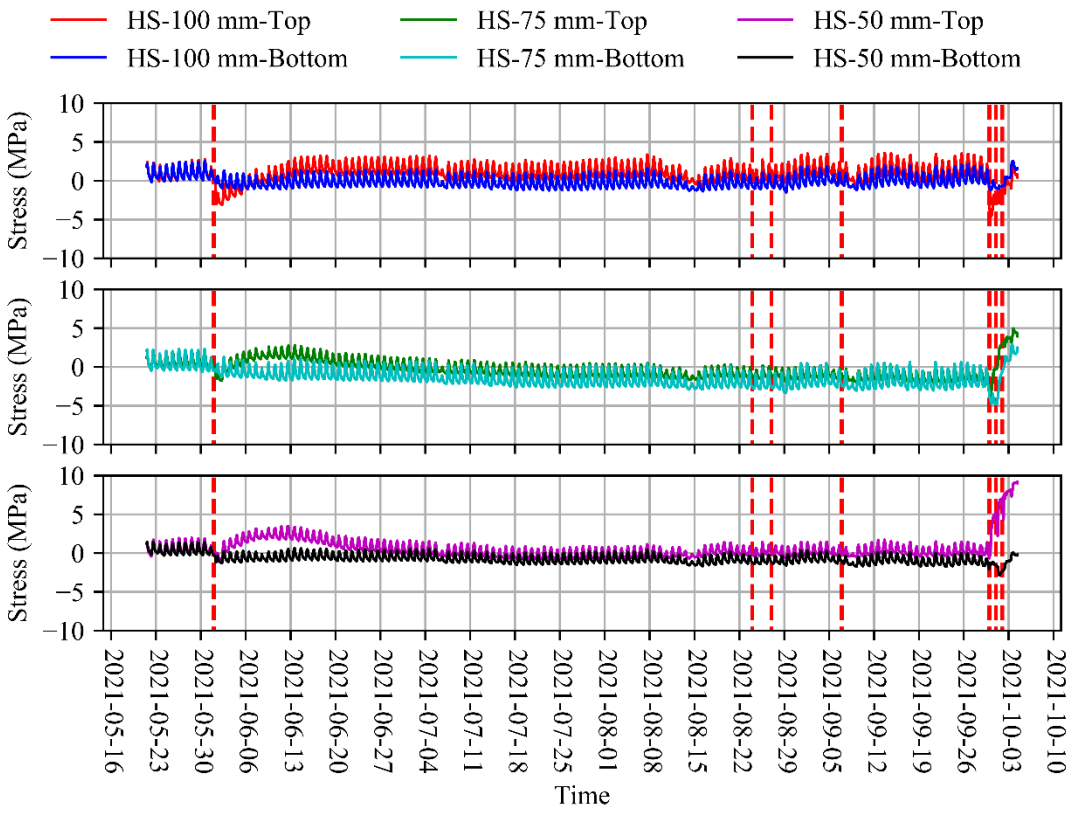

Figure 5.8: Stress calculated in the top and bottom surfaces of the HS concrete pavements

Figure 5.9 is a plot of the average strain within the NS and HS concrete pavement sections. The average strain within the pavement sections is the strain that results in uniform expansion and contraction of the pavement. Figure 5.9 indicates how pronounced the effect of the presence of moisture is on the behaviour of the NS concrete pavement sections. From this figure it can be seen that the NS concrete pavements experienced significant swelling due to the intrusion of moisture into the pores of the concrete. The HS concrete pavement sections, on the other hand, experienced a small amount of swelling due to the presence of moisture. Figure 5.9 also indicated that the pavements experience a daily thermal expansion and contraction due to the heating and cooling of the pavement sections. This movement was within ± 100 με, therefore would result in small stresses developing within the pavement sections if restrained due to the uniform thermal expansion and contraction of the pavements.

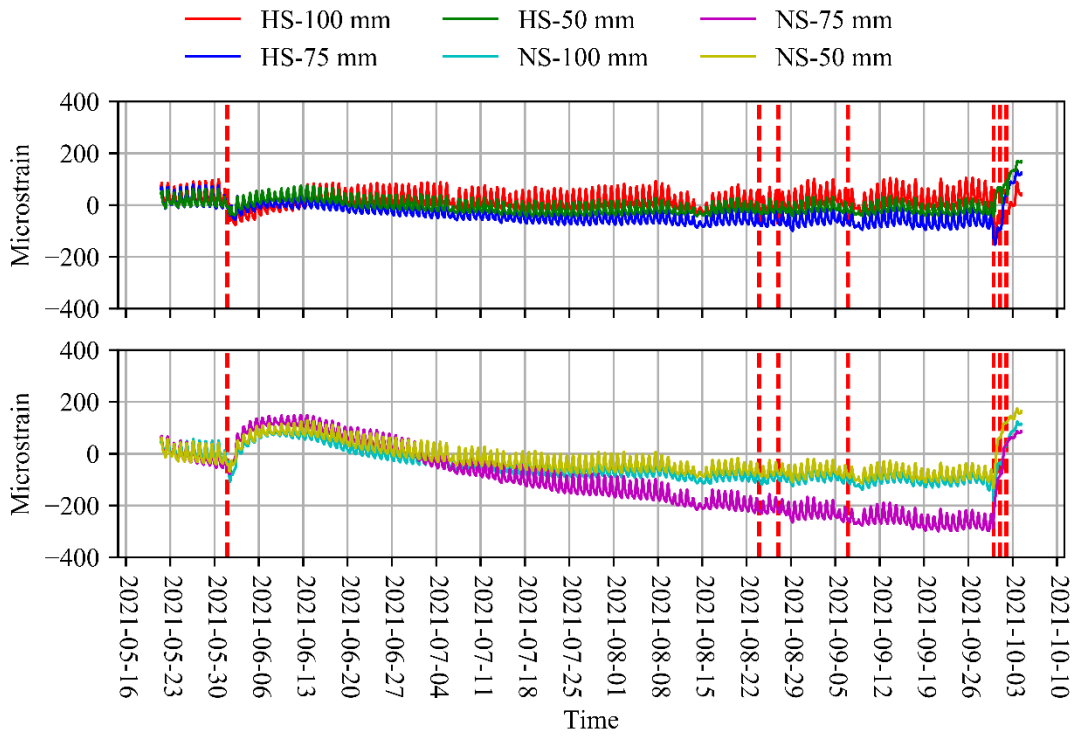

Figure 5.9: Average strain within the pavement sections.

5.3.2 Moisture effects on thin concrete pavements

Figure 5.10 and Figure 5.11 are plots of the strain within the concrete pavement sections that induce curvature of the concrete pavements. The curvature strain was determined using Equation 5.2. When comparing Figure 5.10 and Figure 5.11 it is seen that the NS concrete pavement sections experienced significantly more curvature strain than the HS concrete pavement sections. This indicated that the NS concrete experienced more curling and warping. The reason for more curling and warpling seen in the NS concrete pavement sections was due to the presence of differential shrinkage/swelling within the concrete pavements arising from a moisture gradient existing within the concrete pavements.

$$\varepsilon_k = \varepsilon_{Total} \pm \varepsilon_{Average} \qquad \text{(Equation 5.2)}$$

The most pronounced effects of curvature are seen within the 75 mm thick concrete pavements, indicating that more bending occurred within 75 mm thick pavement sections than within the pavements of 100 mm and 50 mm thickness. This resulted in a higher bending moment within the 75 mm thick concrete pavement as seen in Figure 5.13.

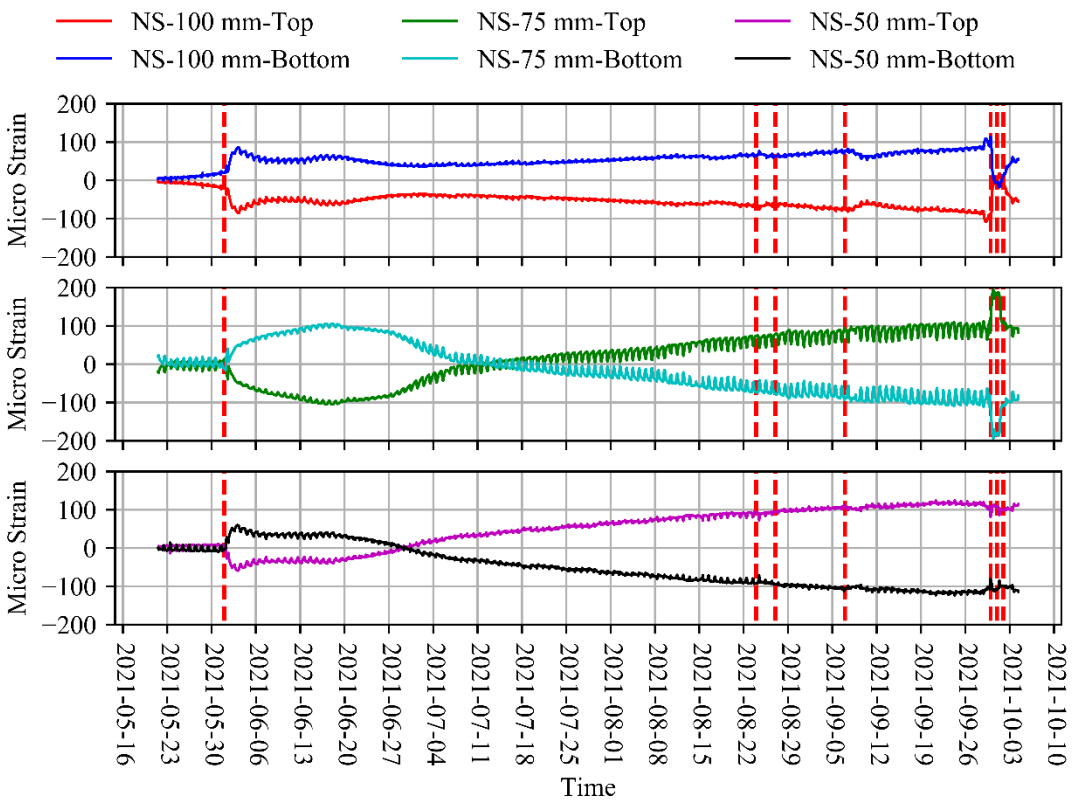

Figure 5.10: Curvature inducing strain within the NS concrete pavement sections

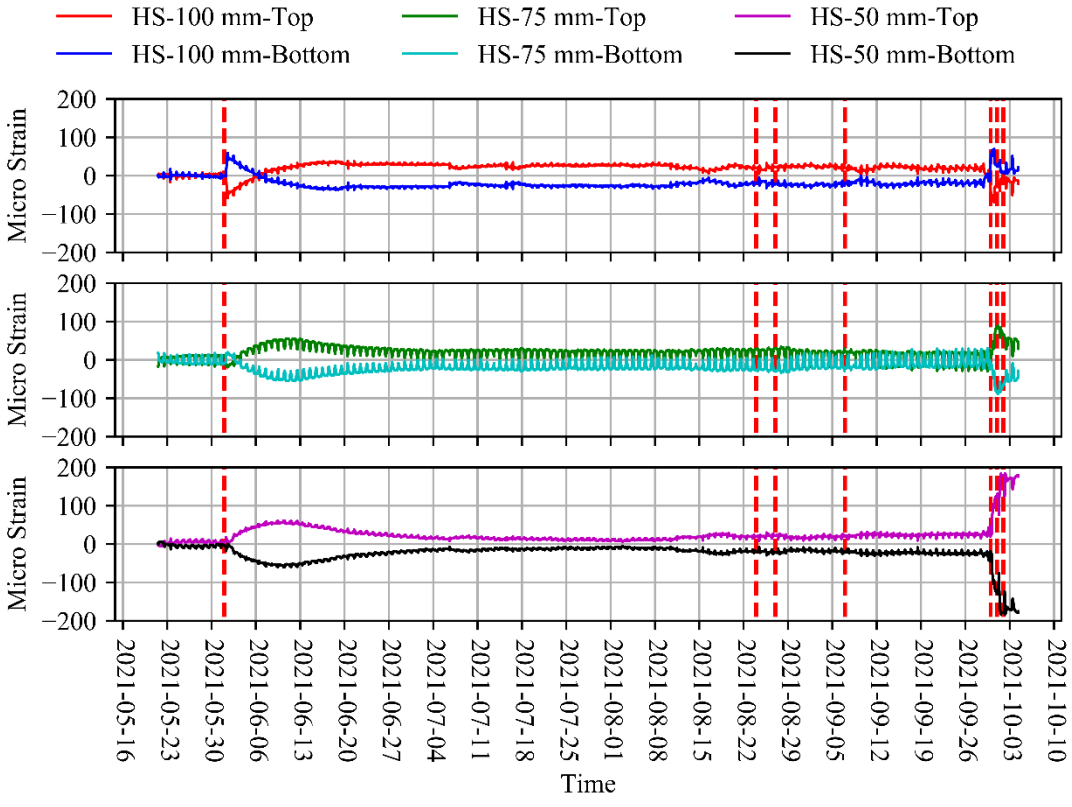

Figure 5.11: Curvature inducing strain within the HS concrete pavement sections

Figure 5.13 is a plot of the bending moment from the curvature in Figure 5.12 within the NS and HS concrete pavements determined using Equation 5.2 which relates the curvature and moment within a material based on its material and sectional properties. From this figure it can be seen that the pavement thickness that performs the best is the 50 mm pavement which experience the smallest internal moment as well as the smallest change in the internal moment. It can also be seen that the moments achieved within each of the pavements are not significantly high, with a spike in the internal moments of the pavements occurring upon wetting of the concrete pavement sections and reduces as the concrete dries out.

$$\kappa = \frac{M}{EI} \qquad \text{(Equation 5.3)}$$

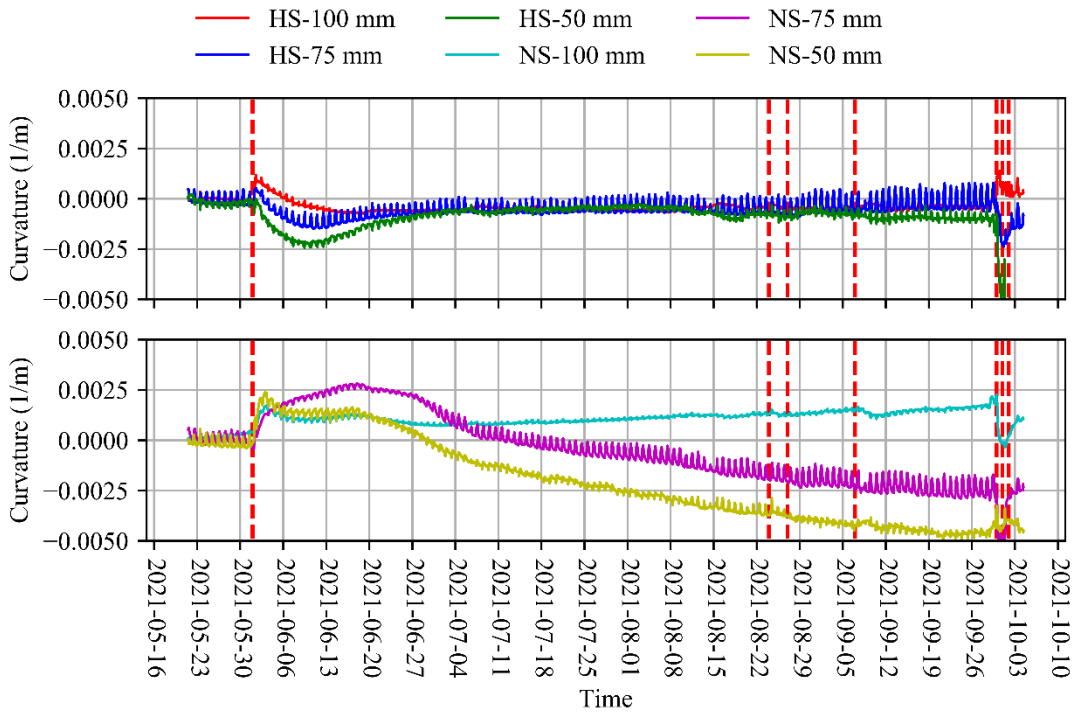

Figure 5.12: Curvature of the concrete pavement sections

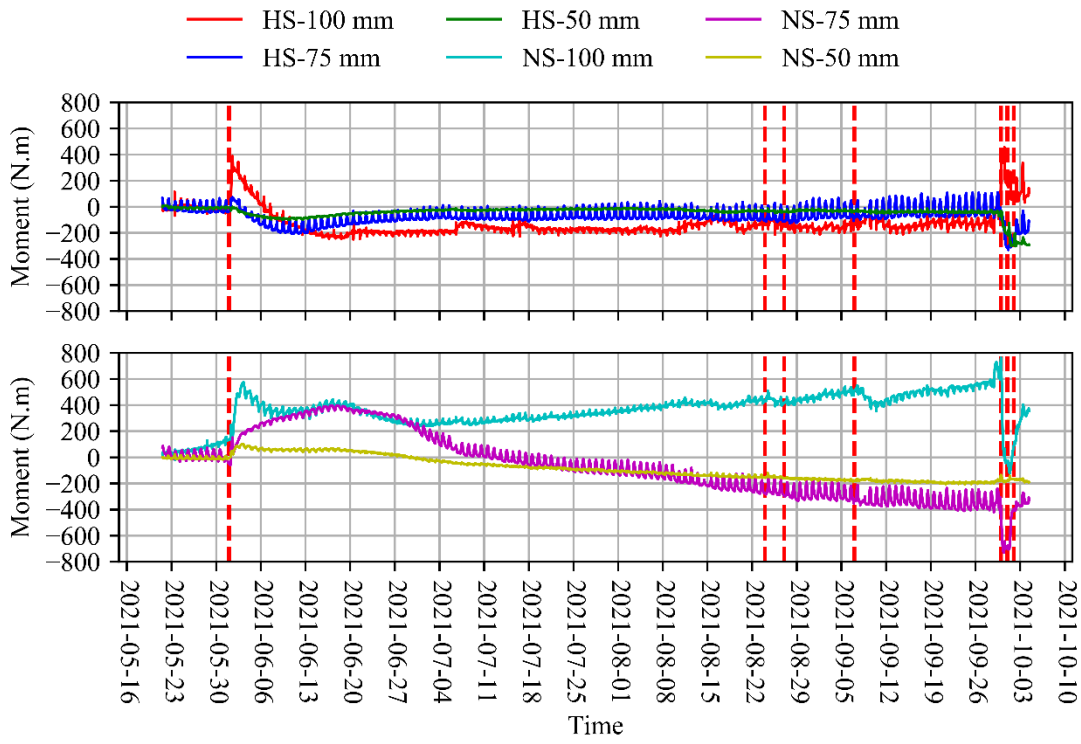

Figure 5.13: Moment in the concrete pavements

5.3.3 Temperatures effect on thin concrete pavements

Figure 5.14 depicts the strain measured as a function of the temperature measured in the top and bottom the NS concrete pavements. The relationship between the change in strain and change in temperature is scattered due to a change in the moisture content of the concrete causing shrinking and swelling of the concrete, therefore masking the linear thermal expansion of the concrete. Figure 5.15 is a plot of the average strain within the concrete pavement sections against the average temperature of the pavements. When comparing Figure 5.14 and Figure 5.15 it is seen there is a reduction in the scatter of the points, indicating that the movement of the NS concrete pavement sections was due to the uniform thermal expansion and contraction of the concrete pavement sections and due to the curling and warping of the pavement caused by a moisture gradient within the pavements.

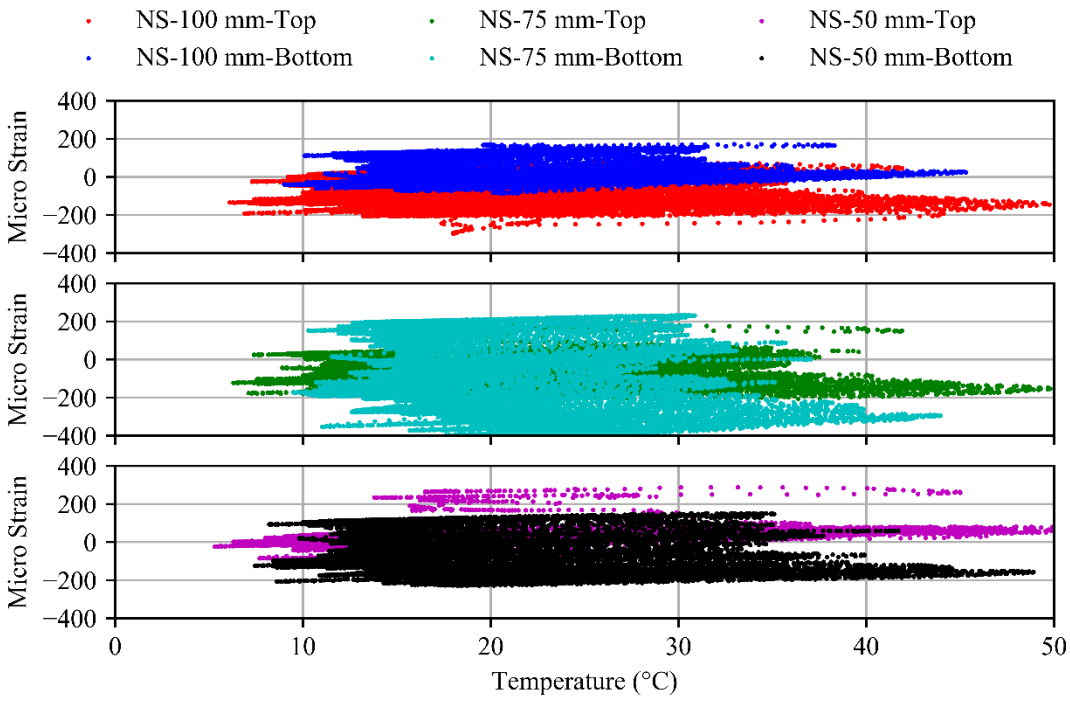

Figure 5.14: Plot of strain vs. temperature in the top and bottom of NS concrete pavements

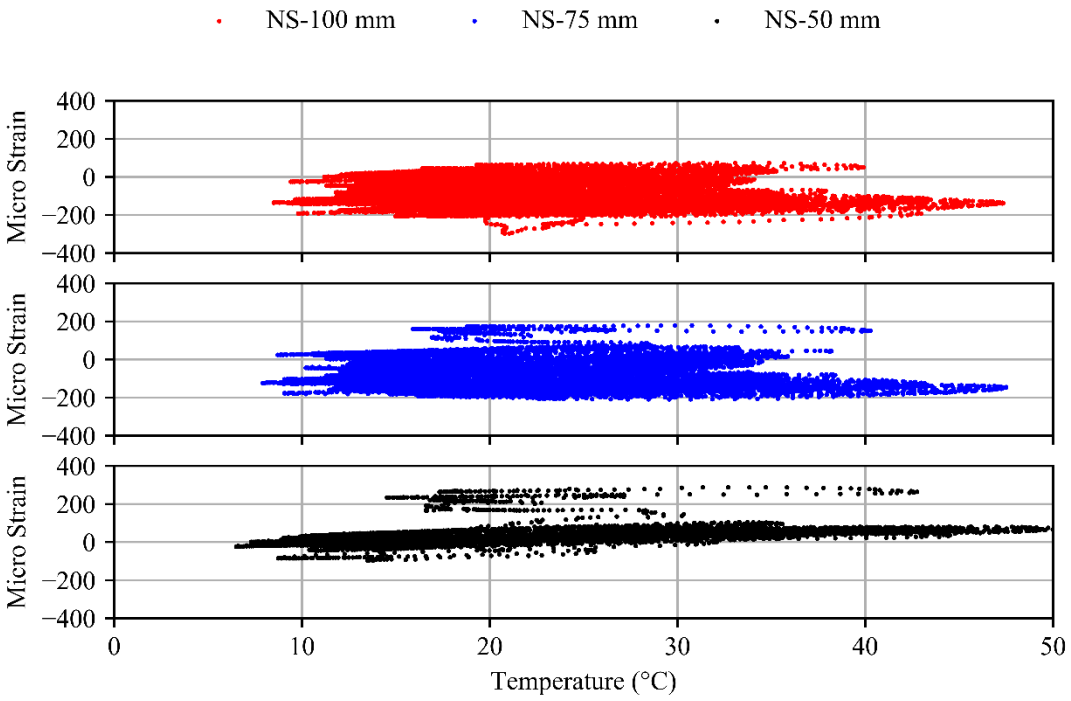

Figure 5.15: Plot of average strain vs. temperature in the NS concrete pavements

Figure 5.16 depicts the strain measured as a function of the temperature measured in the top and bottom the HS concrete pavement sections. When comparing Figure 5.14 and Figure 5.16 it is apparent that the HS concrete pavement sections demonstrate a weak linear relationship between the change in strain due to a change in temperature within the concrete pavements. The comparison of these figures indicates that there was far less scatter of the points than seen in the NS concrete pavements. This was due to less moisture entering the HS concrete pavements resulting in less scatter of the strain readings. This indicates that the predominant cause of the deformation in the HS concrete was due to thermal effects and not due to the curling and warping of the concrete pavement sections. This was supported by the plot of average strain within the pavements against the average pavement temperature shown in Figure 5.17.

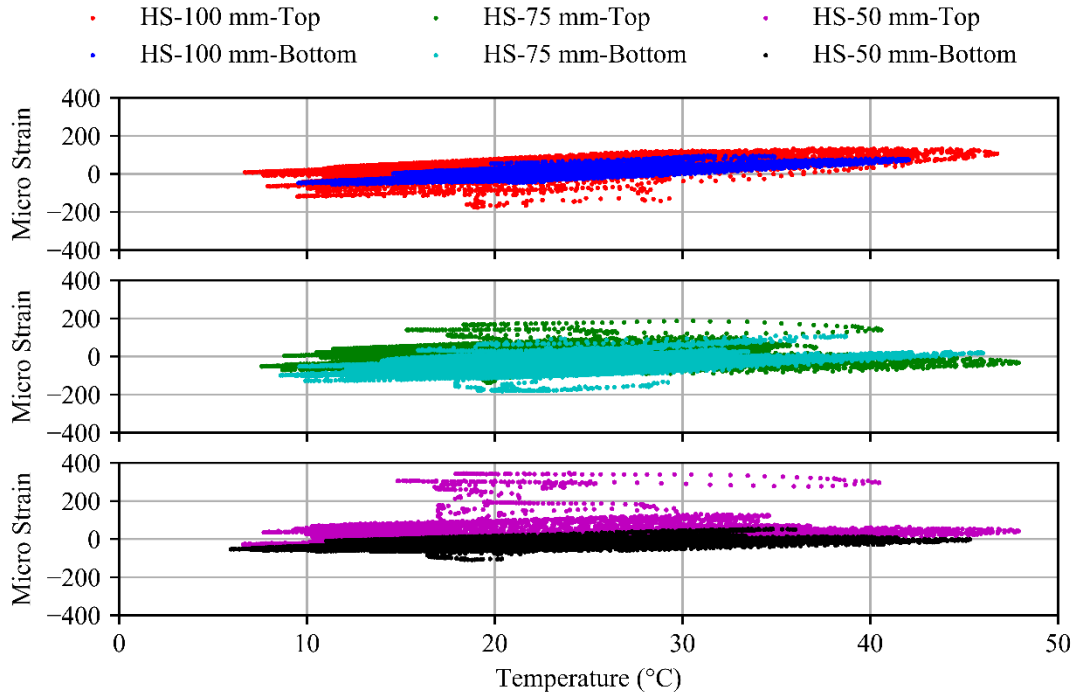

Figure 5.16: Plot of strain vs. temperature in the top and bottom of HS concrete pavements

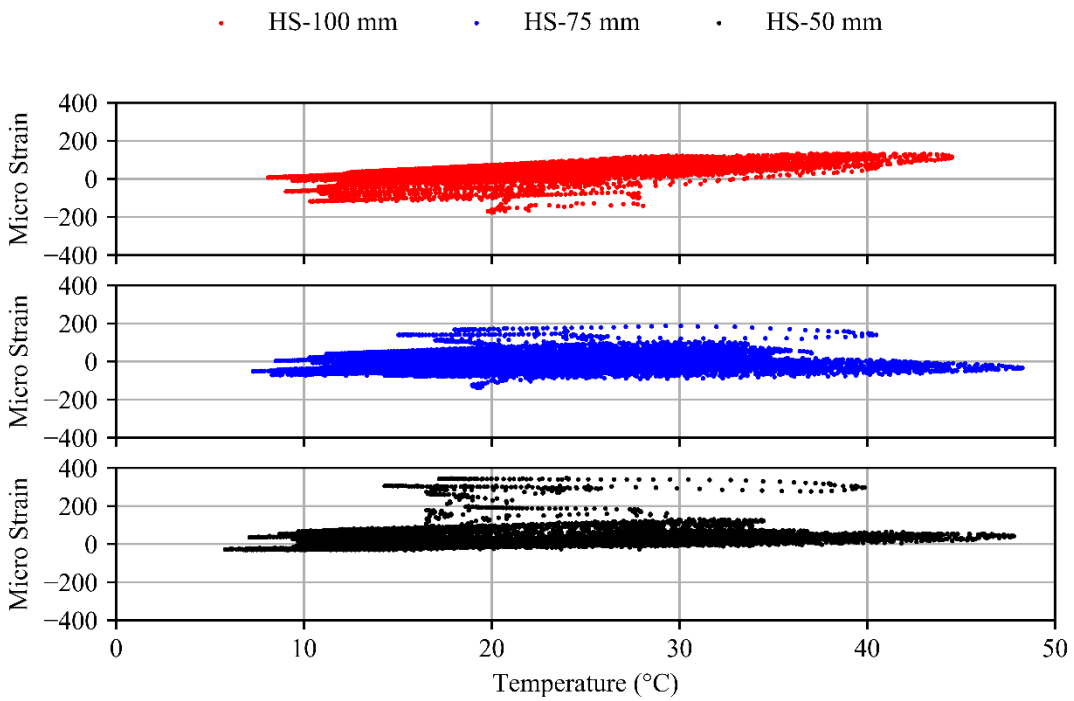

Figure 5.17: Plot of average strain vs. temperature in the HS concrete pavements

Figure 5.18 and Figure 5.19 are plots of the temperature gradients measured within the concrete pavement sections for a rainy day, a cold day and a hot day. These figures indicate that the pavements experienced a uniform increase/decrease in temperature. These figures indicate that there was an insignificant difference in the temperature measured at the surface, centre and base of the pavement sections. When comparing Figure 5.18 and Figure 5.19 to Figure 2.21, there is a noticeable difference in the temperature distribution within an ordinary concrete pavement and a thin concrete pavement, with ordinary concrete pavements experiencing curling and warping due to a temperature gradient within the concrete pavement and thin pavements experiencing uniform expansion and contraction due to the even distribution of temperature within the pavements.

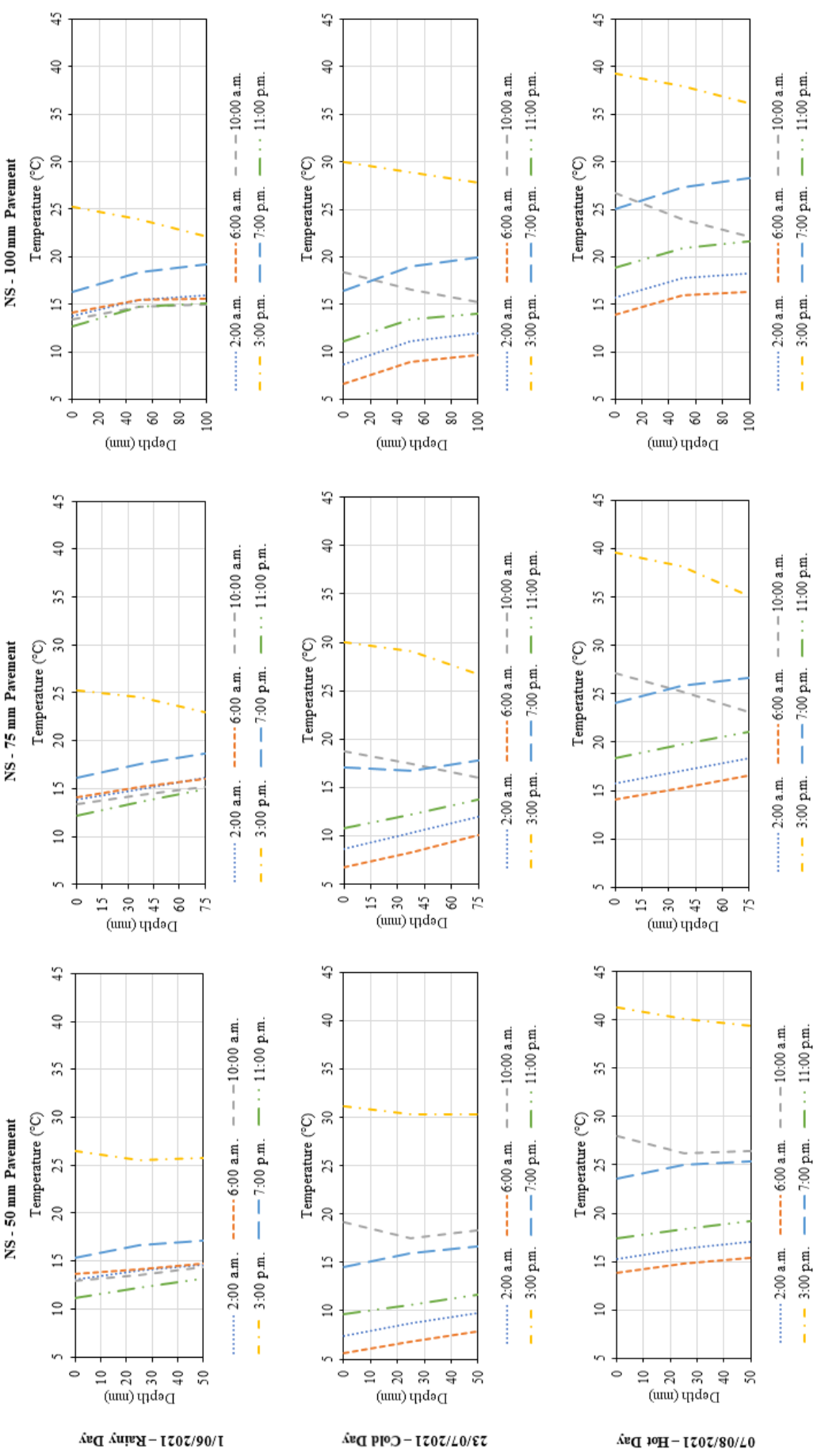

Figure 5.18: Temperature gradients within the NS concrete pavements

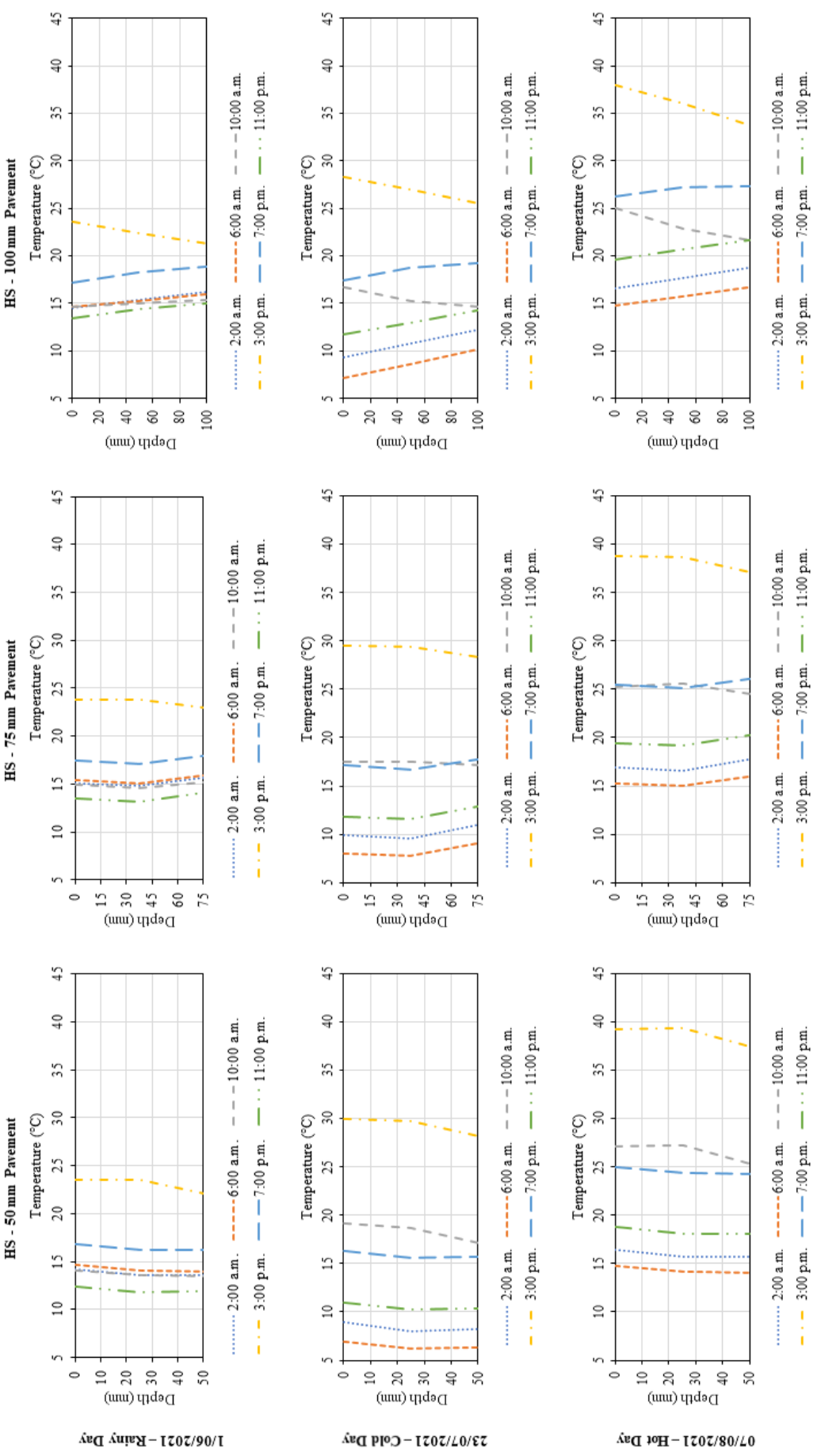

Figure 5.19: Temperature gradient within the HS concrete pavements

5.4 MAXIMUM AND MINIMUM STRAIN AND TEMPERATURE

Table 5.3, Table 5.4, Table 5.5 and Table 5.6 were developed by analysing the data from the strain measured in the top and bottom of the concrete pavements as well as the temperature measured at the top, centre and bottom of the concrete pavements when exposed to the ambient environmental conditions. Table 5.3 and Table 5.4 summarises the time of day that the maximum and minimum strain and temperature occurs at the different measuring points within the pavements while Table 5.5 and Table 5.6 represents the range of maximum and minimum strain and temperature values seen at the different measuring points within the concrete.

Table 5.3 and Table 5.4 both indicate that the time interval when the maximum strain and temperature within the pavements occurs, is during the afternoon hours between 1:00 p.m. to 4:00 p.m. and that the minimum occurs during the early morning between 6:00 a.m. to 8:00 a.m.. This is understandable due to the sunrising at around 6:40 a.m. and setting at around 5:40 p.m. daily over the analysis period (sunrise-and-sunset.com, 2021). The coldest time of day is known to occur just before the sun rises and the hottest time of the day occurs a few hours after 12:00 a.m. in the day due to solar radiation still heating up the surface of the concrete and the surrounding environment until the point that the sun sets.

Table 5.3: Times of maximum and minimum strain and temperature in NS pavements

NS mix						
Property	**Time of Maximum (95% confidence)**			**Time of Minimum (95% confidence)**		
Pavement Thickness	**50 mm**	**75 mm**	**100 mm**	**50 mm**	**75 mm**	**100 mm**
Strain at pavement surface	12:00 to 4:00 p.m.	1:30 to 4:00 p.m.	1:30 to 5:30 p.m.	6:00 to 8:00 a.m.	6:00 to 8:00 a.m.	6:00 to 8:00 a.m.
Strain at pavement base	1:00 to 4:30 p.m.	2:00 to 3:00 p.m.	1:00 to 5:00 p.m.	6:00 to 8:00 a.m.	6:30 to 8:00 a.m.	6:00 to 9:00 a.m.
Surface temperature	1:15 to 2:15 p.m.	1:15 to 2:15 p.m.	1:15 to 2:15 p.m.	6:00 to 8:30 a.m.	5:45 to 7:45 a.m.	6:00 to 8:00 a.m.
Centre temperature	1:30 to 2:30 p.m.	1:30 to 2:30 p.m.	2:00 to 3:00 p.m.	6:00 to 8:30 a.m.	6:00 to 8:00 a.m.	6:00 to 8:00 a.m.
Base temperature	1:30 to 2:30 p.m.	2:00 to 3:00 p.m.	2:30 to 3:30 p.m.	6:00 to 8:30 a.m.	6:00 to 8:00 a.m.	6:00 to 8:00 a.m.

Table 5.4: Times of maximum and minimum strain and temperature in HS pavements

HS mix						
Property	**Time of Maximum (95% confidence)**			**Time of Minimum (95% confidence)**		
Pavement Thickness	**50 mm**	**75 mm**	**100 mm**	**50 mm**	**75 mm**	**100 mm**
Strain at pavement surface	1:00 to 3:00 p.m.	1:30 to 4:30 p.m.	1:30 to 5:30 p.m.	6:00 to 8:00 a.m.	6:00 to 8:00 a.m.	6:00 to 8:00 a.m.
Strain at pavement base	1:00 to 3:00 p.m.	1:30 to 3:00 p.m.	3:00 to 4:00 p.m.	6:00 to 8:00 a.m.	6:30 to 8:00 a.m.	6:00 to 9:00 a.m.
Surface temperature	1:30 to 2:30 p.m.	1:30 to 2:30 p.m.	1:45 to 2:45 p.m.	6:00 to 8:00 a.m.	6:00 to 8:00 a.m.	6:00 to 9:00 a.m.
Centre temperature	1:30 to 2:30 p.m.	1:30 to 2:30 p.m.	2:00 to 3:00 p.m.	6:00 to 8:00 a.m.	6:00 to 8:00 a.m.	6:00 to 8:00 a.m.
Base temperature	1:30 to 2:30 p.m.	1:45 to 2:45 p.m.	2:30 to 3:30 p.m.	6:00 to 8:00 a.m.	6:00 to 8:00 a.m.	6:00 to 8:00 a.m.

When looking at the values shown in Table 5.5, there is a significant deviation in the magnitude of the maximum strain and temperature experienced within the concrete pavements during the time intervals shown in Table 5.3. This is due to factors such as ambient air temperature, wind speed, solar radiation intensity and cloud cover affecting the magnitude of these strains and temperatures seen within the concrete pavements. Another factor that affects the strain seen within the concrete is the moisture content within the pavements and its distribution within the concrete pavements. It is noticed that the largest strains are seen within the 75 mm pavement as already shown in Figure 5.5 and Figure 5.9. Steyn et al. (2005) found that the 75 mm pavement was the pavement that performed the worst when looking at thin concrete pavements of 50 mm, 75 mm, 100 mm and 140 mm thickness subjected to 400 000 equivalent 80 kN axial loads. The data shown in Table 5.4 indicates that the 75 mm pavement sees the most movement due to environmental effects and as a result would see the greatest stresses developing within the pavement if fully restrained. When looking at the range of minimum values found in Table 5.5, it is seen that the range for the strain and temperature within the pavements is far smaller than that of the maximum ranges. This is due to the only factor affecting the pavement in the evening time is the ambient air temperature causing the concrete pavement to cool gradually until it is in equilibrium with the surrounding environment.

Table 5.5: Range of maximum and minimum strain and temperature in NS pavements

NS mix						
Property	**Range of Maximum (95% confidence)**			**Range of Minimum (95% confidence)**		
Pavement Thickness	**50 mm**	**75 mm**	**100 mm**	**50 mm**	**75 mm**	**100 mm**
Strain at pavement surface (με)	35 to 80	-30 to 50	-40 to 45	-35 to 15	-30 to 80	-105 to -15
Strain at pavement base (με)	-5 to 120	10 to 195	35 to 130	-70 to 70	-90 to 5	-30 to 80
Surface temperature (°C)	30 to 40	30 to 35	30 to 35	9 to 12	10 to 13	10 to 13
Centre temperature (°C)	30 to 35	30 to 35	25 to 35	10 to 13	11 to 14	11 to 15
Base temperature (°C)	30 to 35	25 to 30	25 to 30	10 to 14	12 to 15	12 to 15

Table 5.6 indicates that the HS concrete pavements experience a smaller variation in the strain within the pavements when compared to that of Table 5.5 measured within the NS concrete pavements. This has already been seen in Figure 5.5 and Figure 5.6 with the NS concrete pavement experiencing more movement as a result of the moisture that enters the concrete through precipitation. The effect of moisture on the movement of the pavements is made evident by comparing the range of temperature values summarised in both Table 5.5 and Table 5.6. These tables indicate that the range of temperature values in the top, centre and bottom of the concrete pavements are almost identical for the NS and HS concrete pavements. This proves that the difference in the strain values measured is due to the intrusion of moisture into the pores of the concrete and this is dependent on the moisture movement properties of the concrete.

Table 5.6: Range of maximum and minimum strain and temperature in HS pavements

HS mix						
Property	**Range of Maximum (95% confidence)**			**Range of Minimum (95% confidence)**		
Pavement Thickness	**50 mm**	**75 mm**	**100 mm**	**50 mm**	**75 mm**	**100 mm**
Strain at pavement surface (με)	30 to 90	20 to 80	60 to 120	-20 to 40	-20 to 20	-30 to 40
Strain at pavement base (με)	0 to 30	0 to 30	20 to 60	-50 to - 20	-75 to - 25	-45 to - 15
Surface temperature (°C)	25 to 35	30 to 35	25 to 35	9 to 12	11 to 15	10 to 13
Centre temperature (°C)	25 to 35	25 to 35	25 to 30	8 to 11	11 to 14	11 to 14
Base temperature (°C)	25 to 35	30 to 35	25 to 30	9 to 12	11 to 14	12 to 15

5.5 SUMMARY

The heat of hydration within the pavements increases with an increase in pavement thickness and the NS concrete pavements experience a higher and more rapid temperature rise similar to the results seen in Section 4.2. This due to the SCM in the HS concrete reducing and delaying the time of occurrence of the peak temperature rise. The results of the temperature distribution within the concrete pavements indicated that due to the relatively small dimensions of the thin pavement sections, the heat of hydration of the concrete results in a uniform increase in the temperature within the pavement resulting in a uniform built-in temperature instead of a built-in temperature gradient commonly seen in pavements of ordinary thickness. This indicates that when pavements are cast, the thicker the pavement layer there would be a greater heat of hydration within the that pavement layer resulting in a higher built-in temperature.

From the change in length measured on the thin concrete pavements prior to demoulding of the pavements, it was noted that the HS concrete experienced more shrinkage than the NS concrete.

The most predominant environmental factor affecting the behaviour of the thin concrete pavements was due to rainfall, resulting in the concrete rapidly thermally contracting and then swelling due to the moisture absorbed into the pores of the concrete. The effect of rainfall was more predominant in the NS concrete than in the HS concrete pavements due to the HS concrete being less water absorbent than the NS concrete. The moisture affects were accentuated by the daily temperature effects arising from the cyclic thermal expansion and contraction of the

concrete pavements. This indicates that the effect of moisture will be a predominate environmental factor affecting behaviour of thin concrete pavement cast with the majority of stresses developing within thin concrete pavements due to the wetting and drying cycles of the concrete causing shrinking and welling of the pavement, with this movement being in excess of the tensile strength of the concrete resulting in cracking of the concrete pavement.

Due to how thin the concrete pavement sections are, the temperature distribution within the thin concrete pavements results in a uniform increase and decrease in the temperature within the pavements with the heat diffusing into and out of the concrete rapidly to create a uniform temperature distribution within the pavements. This indicates that when thin concrete pavements are cast, the temperature will be evenly distributed throughout the pavement resulting in uniform contraction and expansion of the pavement rather than curling a warping due to a temperature gradient within the pavement.

The pavement worst affected by the environmental effect on the thin concrete pavements was the 75 mm pavements while the best performing thin concrete pavement was the 50 mm concrete pavement. This is based on the magnitude and change in curvature, moment and stresses that develop within the thin concrete pavements with the greatest effects being seen in the 75 mm thick pavements and the least being seen in the 50 mm thick pavements.

6 CONCLUSIONS AND RECOMMENDATIONS

6.1 CONCLUSIONS

The primary objective of this study was to investigate the response of thin concrete pavements to the environmental conditions they are exposed to. A secondary objective of this study was to investigate how a difference in the material properties and the influence of pavement thickness of the concrete affects the haviour of the thin concrete pavements.

When considering the built-in temperature gradient in thin concrete pavements, it was found that due to how thin the tested pavements were, the heat of hydration within the concrete pavements resulted in a uniform increase in the temperature within the pavements. This resulted in:

- A built-in temperature within the pavements rather than a built-in temperature gradient commonly seen in concrete pavements of ordinary thickness (± 300 mm thickness). This means that uniform contraction and expansion of the thin concrete pavement will be seen rather than curling and warping of the pavement due to a temperature gradient within the pavement.

- The built-in temperature of the pavements increased with pavement thickness and was higher in the NS concrete that did not contain any SCM.

Upon studying the effect of environmental conditions on the length change, internal stresses, internal moment and curvature of thin concrete pavements, the environmental factor influencing the change in length, curvature, internal stresses and moment development within the thin concrete pavements the most was the rainfall. The rainfall caused:

- The pavements to rapidly thermally contact and then swell due to moisture entering the pores of the concrete.

- The moisture effects were accentuated by the daily thermal expansion and contraction of the concrete pavement accounting for minor movement in the concrete pavement.

- The effects due to rainfall were noted to be far worse within the NS concrete than in the HS concrete due to the NS concrete being more water absorbent than the HS concrete which contained SCM.

Bearing in mind the effect of daily and seasonal environmental conditions on pavements of different thicknesses, the 75 mm thick pavement was the most effected by the ambient environmental conditions that the pavement was exposed to.

- This pavement saw the highest change in length, curvature and internal stresses and moment development within the concrete indicating the 75 mm pavement is a critical pavement thickness.

- The 50 mm thick pavements on the other hand performed the best with the lowest change in length, curvature and internal stresses and moment development within the concrete.

The material properties were found to play a significant role in the behaviour of the concrete pavements when considering the mechanical, shrinkage and moisture movement properties of the concrete. It was found that:

- The addition of SCM to concrete produced concrete that was less water absorbent than concrete that did not contain SCM.

- It was also found that concrete containing SCM held on to moisture a lot stronger than concrete without SCM. This resulted in less shrinkage and swelling of concrete containing SCM due to less moisture being lost and absorbed by the concrete.

- Concrete containing SCM was more sensitive to the curing conditions that the concrete was exposed to while, by adding SCM to concrete, the pavement was not as sensitive to the environmental conditions the pavements were exposed to with less curvature and internal stresses and moment development within the concrete pavements.

6.2 RECOMMENDATIONS

- Cast thin concrete pavement section of 50, 75 and 100 mm thicknesses using different concretes containing SCM, replacing fine aggregate and/or cement to determine optimum combination.

- Cast thin pavement section in-situ to determine the behaviour of the pavement is cast on BSM layer or asphalt surface.

- Study the amount of reinforcement (steel reinforcement and /or steel fires) which is required to resist a combination of environmental and traffic loading.

- Measure the response of the thin concrete pavements to more drying and wetting cycles.

- When casting relative humidity sensors into concrete, be vigilant and careful when vibrating the concrete so not to damage the delicate electronics of the relative humidity sensors.

6.3 REFLECTION

Reflecting back on the study there were some useful lessons learnt which included:

- The quarter bridge strain gauge setup using logged using a MX1615 HBM™ gives the most accurate reading and is temperature compensated when using the patented 4 wire connection of HBM™ and the wires are to be soldered on as close to the strain gauge as possible.

- The use of relative humidity sensors in a concrete pavement section poses more complications than benefits received from the incorporation of relative humidity sensors in the pavements. It is better to cast relative humidity sensors within test segments to analyse the behaviour under laboratory conditions which give an accurate enough indication of the real life behaviour.

- Focusing more intently on specific behavioural characteristic give a clearer understanding than looking broadly at many properties and characteristic.

By reflecting further on the results obtained from this study, the data indicated that the concrete pavements would crack due to the shrinkage of the concrete. This indicated that concrete pavements should not be cast without including steel reinforcement to strengthen the concrete pavements to tensile forces. Additionally high strength concrete containing SCM performs better than concrete without SCM and results in the concrete hydrating for longer and leads to less shrinkage of the concrete. From the temperature versus strain data, it can be seen that casting thin concrete pavements on a ± 25°C day is optimal due to this being the mean temperature of the pavement over the analysis period. Therefore, resulting in uniform expansion and contraction due to heating and cooling of the pavement.

7 REFERENCES

Abbasnia, R., Shekarchi, M. & Ahmadi, J. 2013. Evaluation of Concrete Drying Shrinkage Related to Moisture Loss. *ACI Materials Journal*, Vol. 110 (3), pp. 269-278.

Akpolat, A., Oktay, H. & Yamrutas, R. 2015. Mechanical and thermophysical properties of light weight aggregate concretes. *Construction and Building Materials*, Vol. 96, pp. 217-225.

Ali, W. & Urgessa, G. 2014. Computational Model for Internal Relative Humidity Distribution in Concrete. *Journal of Computational Engineering*, Vol. 2014, pp. 1-7.

Andolfsson, T. 2013. *Analyses of thermal conductivity from mineral composition and analyses by use of Thermal Conductivity Scanner: A study of thermal properties in Scanian rock types.* Masters Dissertation. Lund University.

Armaghani, J.M., Larsen, T.J. & Smith, L.L. 1987. *Temperature Response of Concrete Pavements.* National Research Council. Transportation Research Record 1121: Effects of Temperature and Water on Pavement Performance. Washington, USA, pp. 23-33.

Armaghani, J.M. & Richardson, J.M. 1987. *Stresses Caused by Temperature Gradient in Portland Cement Concrete Pavements*. National Research Council. Transportation Research Record 1121: Effects of Temperature and Water on Pavement Performance. Washington, USA, pp. 7-13.

Asadi, I., Mahyuddin, N.B. & Shafigh, P. 2018. Concrete as a thermal mass material for building applications – A review. *Journal of Building Engineering*, Vol. 19, pp. 14-24.

Asbahan, R.E. & Vandenbossche, J.M. 2011. Effects of Temperature and Moisture Gradients on Slab Deformation for Jointed Plain Concrete Pavements. *Journal of Transportation Engineering*, Vol. 187 (8), pp. 563-570.

ASTM Committee C09. ASTM Standard C469/C469M-14 – 2014: *Standard Test Method for Static Modulus of Elasticity and Poisson's Ratio of Concrete in Compressio*n.

ASTM Committee C09. ASTM Standard C403/C403M – 2016. *Standard Test Method for Time of Setting of Concrete Mixtures by Penetration Resistance*.

ASTM Committee C09. ASTM Standard C1585-20 – 2020. *Standard Test Method for Measurement of Rate of Absorption of Water by Hydraulic-Cement Concretes.*

Azenha, M., Barros, J., Faria, R. & Quincot, G. 2011. State of the art - Methods to measure moisture in concrete. *Fundação para Ciência e a Tecnologia,* Project Report PTDC/ECM/099250/2008.

Bella, C.D., Wyrzykowski, M. & Lura, P. 2017. Evaluation of the ultimate drying shrinkage of cement-based mortars with poroelastic models. *Material and Structures*, Vol. 50, pp. 1-13.

Benhamou, B., Boukhattem, L., Boumhaout, M., Hamdi, H. & Nouh, F.A. 2017. Moisture content influence on the thermal conductivity of insulating building materials made from date palm fibres mesh. *Construction and Building Materials*, Vol. 148, pp. 881-823.

Bishop, A. 1959. The effective stress principle. *Teknisk Ukeblad*, Vol. 39, pp. 859-863.

Bissonnette, B., Pierre, P. & Pigeon, M. 1999. Influence of key parameters on dry shrinkage of cementitious materials. *Cement and Concrete Research*, Vol. 29, pp. 1655-1662.

Broekman, A., Jordaan, G.J. & Steyn, W.J.vdM. 2020. Digital twinning of asphalt pavements surfacings using Visual Simultaneous Localization Mapping. Contributions to the *2nd International Conference on Advances in Material and Pavement Performance Prediction* (AM3P 2020), San Antonio, Texas, USA, pp. 97-100.

Brooks, J.J. & Neville, A.M. 2010. *Concrete Technology*. 2nd ed. Pearson, UK.

Bredenhann, S., Joubert, P., Strauss, P. & van Heerden, J. 2017. Design of Ultra-Thin Continuously Reinforced Concrete (UTCRC) and Enrobé à Module Èlevé (EME) implemented as alternative remedial actions. *The 10th Internationsl Conference on the Bearing Capacity of Roads, Railways and Airfields (BCRRA 2017)*, 1st ed, Chapter 301, pp. 1-10.

Bredenhann, S., Joubert, P., Strauss, P. & van Heerden, J. 2018. Design and construction of ultra-thin continuously reinforced concrete (UTCRC) on N1 near Hugenote Tunnell. *International Conference on Concrete Repair, Rehabilitation and Retrofitting (ICCRRR 2018)*, MATEC Web Conference, Vol. 199, pp. 1-8.

Bullard, J.W, Garboczi, E.J., Grasley, Z.C. & Zachary, X.L. 2017, Irreversible desiccation shrinkage of cement paste caused by cement grain dissolution and hydrate precipitation, *Materials and Structures*, Vol. 50, pp. 1-14.

Ćećez, M., Markovski, G. & Ŝahinagć-Isović, M. 2012. Shrinkage strain of concrete – causes and types. Građevinar, Vol. 64, pp 727-734.

Çengal, Y.A. & Ghajar, A.J. 2015. *Heat and Mass Transfer: Fundamentals & Applications*, 5th ed. New York: Mc Graw Hill Education.

Chou, C-.P., McCullough, B.F. & Saraf, C. 1987. *Effects of Rainfall on the Performance of Continuously Reinforced Concrete Pavements in Texas.* National Research Council. Transportation Research Record 1121: Effects of Temperature and Water on Pavement Performance. United States of America.

Dempsey, B.J., Hill, H., Thompson, M.R. & Vogel, J. 1987. *Characterizing Temperature Effects for Pavement Analysis and Design.* National Research Council. Transportation Research Record 1121: Effects of Temperature and Water on Pavement Performance. Washington, USA, pp. 14-22.

Du Plessis, L., Kannemeyer, L., Perrie, B.D. & Strauss, P.J. 2007. Ultra-Thin Continuously Reinforced Concrete Pavement Research in South Africa. Proceedings of the 9th International Conference on Concrete Pavements, San Francisco, USA, pp. 1-27.

Du Plessis, L., Kilian, A. & Mngaza, K. 2014. Ultra-thin reinforced concrete pavements (UTRCP): Addressing the design issues. In the *33rd Annual South African Transport Conference*, Pretoria, South Africa, pp. 179-190.

Domone, P.L.J. and Soutsos, M. 2017. *Construction materials: Their nature and behaviour*. 5th ed. CRC Press, USA.

Ebels, L.J., Burger, A.F. & Fontini, D. 2010. Construction of an ultra-thin continuously reinforced concrete pavement. *IMESA (Institute of Municipal Engineering of South Africa) Conference 2010*, East London, South Africa.

Emerson, M. 1973. *The calculation of the distribution of temperature in bridges.* Transport and Road Research Laboratory. TRRL report LR 561. Berkshire, United Kingdom.

Flanagan, P.R. & Hudson, W.R. 1987. *An Examination of Environmental Versus Load Effects on Pavements.* National Research Council. Transportation Research Record 1121: Effects of Temperature and Water on Pavement Performance. Washington, USA, pp. 34-39.

Fwa, T.F. 1987. *Water-Induced Distress in Flexible Pavement in a Wet Tropical Climate.* National Research Council. Transportation Research Record 1121: Effects of Temperature and Water on Pavement Performance. Washington, USA, pp. 57-65.

Gao, X., Liang, S. & Wei, Y. 2016. Numerical Evaluation of Moisture Warping and Stress in Concrete Pavement Slabs with Different Water-to-Cement Ratio and Thickness. *Journal of Engineering Mechanics*, Vol. 143, pp. 1-9.

Grasley, Z.C. 2001. *Internal relative humidity, drying stress gradients and hygrothermal dilation of concrete*. Masters Dissertation. University of Illinois.

Grasley, Z.C., Lange, D.A. & D'Ambrosia, M.D. 2006. Internal relative humidity and drying stress gradients in concrete. *Materials and Structures*, Vol. 39, pp. 901-909.

Groenewald, M. & Van Wijk, I. 2010. Ultra Thin Reinforced Concrete Pavements (UTRCP) – Innovative Technology Which Offers Cost and Socio-economic Benefits for Infrastructure Provision. Proceedings of the 29th Southern African Transportation Conference (SATC 2010), Pretoria, South Africa, pp. 188-200.

Hansen, W. & Mohamed, A.R., 1997. Effects of Nonlinear Temperature Gradient on Curling Stress in Concrete Pavements. *Transportation Research Record 1568*, Transportation Research Board, Washington, DC, pp. 65-71.

Janssen, D.J. 1987. *Moisture in Portland Cement Concrete*. National Research Council. Transportation Research Record 1121: Effects of Temperature and Water on Pavement Performance. Washington, USA, pp. 40-44.

Janssen, D.J. & Snyder, M.B., 2000. Temperature-moment concept for evaluating pavement temperature data. Technical note. *Journal of Infrastructure Engineering*, Vol. 6 (2), pp. 81-83.

Janssen, D.J., Vandenbossche, J.M. & Nassiri, S. 2014. Methodology for identifying Zero-Stress Time for Jointed Plain Concrete Pavements. Transportation Research Record: Journal of the Transportation Research Board No. 2441, Transportation Research Board of the National Academics, Washington, D.C., pp. 62-71.

Joeng, J-.H., Wang, L. & Zollinger, D.G., 2001. A temperature and moisture model for hydrating Portland cement concrete pavements. *Proceedings from the 7th International Conference on Concrete Pavemnts*, Vol. 1, Orlando, Florida, pp. 9-22.

Jeong, J-.H. & Zollinger, D.G. 2005. Environmental effects on the behaviour of jointed plain concrete pavements. Journal of Transportation Engineering, Vol. 131 (2), pp. 140-148.

Kadam, K.N. & Mohod, M.V. 2016. *A Review on Critical Stresses in Concrete Pavement*. National Conference on Advance in Construction Technology and Management. VNIT, Nagpur, pp. 260-266.

Kearsley, E.P., Jacobs, S.W. & Steyn, W.J.VDM. 2014. Centrifuge modelling of Ultra Thin Continuously Reinforced Concrete Pavements (UTCRCP). Proceeding from *the 8th*

International Conference on Physical Modelling in Geotechnics 2014 (ICPMG2014), Perth, Australia, pp. 1-6.

Keste, A.A. & Patil, S.R. 2019. Investigation of concrete solar collector: A review. *ISOR Journal of Mechanical and Civil Engineering* (2nd National Conference on Recent Developments in Mechanical Engineering, Pune, India), pp. 26-29.

Kilian, A., Du Plessis, L. and Mngaza, K. 2014. Ultra-Thin Reinforced Concrete Pavements (UTRCP): Addressing the Design Issues. Proceedings of the 33rd Southern African Transportation Conference (SATC 2014), Pretoria, South Africa, pp. 179-190.

Kodide, U. & Shin A.H.-C. 2012. Thermal conductivity of ternary mixtures for concrete pavements. *Cement and Concrete Composites*, Vol. 34, pp. 575-582.

Krishnaiah, S. & Singh, D.N. 2006. Determination of thermal properties of some supplementary cementing materials used in cement and concrete. *Construction and Building Materials*, Vol. 20, pp. 193-198.

Lange, D.A., D'Ambrosia, M.D. & Grasley, Z.C. 2006. Internal relative humidity and drying stress gradients in concrete. *Materials and Structures*, Vol. 39, pp. 901-909.

Larsson, C. & Svensson, G. 2013. *Realistic Modelling of Thermal Effects in Concrete Bridges*. Masters Dissertation. Lunds University.

Lei, G., Ling, Z., Lixia, G. & Yueming, Z. 2011. Thermal conductivity and heat transfer coefficient of concrete. *Journal of Wuhan University of Technology-Material Science*, Vol. 26, pp. 791-796.

Lim, M., Taylor, P., Wang, K. & Wang, X. 2016. Monitoring of setting time of self-consolidating concrete using ultrasonic wave propagation method and other tools. *Magazine of Concrete Research*, Vol. 68, pp. 151-162.

Lura, P. & Wyrzykowski, M. 2016. Effect of relative humidity decrease due to self-desiccation on the hydration kinetics of cement. *Cement and Concrete Research*, Vol. 85, pp. 75-81.

Malhotra, V.M. 2002. High-Performance High-Volume Fly Ash Concrete. *Concrete international*, Vol. 24, pp. 30-34.

Nassiri, S. 2011. *Establishing Permanent Curl/Warp Temperature Gradient in Jointed Plain Concrete Pavements.* Doctoral Thesis. University of Pittsburgh.

Neville, A.M. 2011. Properties of Concrete. 5th ed. Pearson, UK.

Pérez, L.R. 2013. *Monitoring of the Cement Hydration Behaviour and Determination of Non-Standard Laboratory Indicators of Setting Time*. Masters Dissertation. University of Alicante.

Phillips, B.M., Vandenbossche, J.M. & Wells, S.A. 2006. Quantifying built-in construction gradients and early-age slab deformation caused by environmental loads in a jointed plain concrete pavement. International Journal of Pavement Engineering, Vol. 7 (4), pp. 275-289.

Robertson, E.C. 1988. *Thermal properties of rocks*. United States Department of the Interior Geological Survey. United States Geological Survey Open-File Report 88-441. United States.

Shah, V.R. 1965. *Warping and Curling of Plain Concrete Slabs.* Masters Dissertation. University of Missouri.

Standards South Africa, 2006. SANS 50196-1:2006 Methods of testing concrete: *Part1: Determination of strength.* SABS.

Standards South Africa, 2006. SANS 5864:2006 Concrete Tests – *Flexural strength of hardened concrete.* SABS.

Standards South Africa, 2006. SANS 6253:2006 Concrete Tests – *Tensile splitting strength of concrete.* SABS.

Standards South Africa, 2006. SANS 5862-1:2006: Concrete tests – *Consistence of freshly mixed concrete – Slump test*. SABS.

Steyn, W.J.vdM., Strauss, P.J., Perrie, B.D. & du Plessis, L. 2005. Roodekrans trial sections: The role of structural support under very thin jointed CRC pavements subjected to heavy traffic. *8th International Conference on Concrete Pavements (ICCP)*, pp. 1-16.

Smith, M.S. 2015. *The Effect of Mixture Proportions on the Properties of High Strength Concrete Pavemnts.* Masters Dissertation. University of Pretoria.

Sunrise and sunset, 2021. *Sunrise and sunset* , 4 August 2021, <https://www.sunrise-and-sunset.com/en/sun/south-africa/pretoria/2021/august>.

Texas Department of Transportation, 2011. Tex-428-A: *Determining the coefficient of thermal expansion of concrete.* TxDOT.

Visser, S. 2019. *The Influence of Binder Composition and Content on the Early Age Behaviour of Concrete*. Masters Dissertation. University of Pretoria.

Van Dam, T. 2015. Concrete Pavement Curling and Warping: Observations and Mitigation. Moving Advancements into Practice.

Wang, K., Ge, Z., Grove, J., Ruiz, J.M., Rasmussen, R. & Ted, F. 2007. *Developing a Simple and Rapid Test for Monitoring the Heat Evolution of Concrete Mixtures for Both Laboratory and Field Applications.* Iowa State University. InTrans Project Reports No. 153. United States.

Zhang, J., Dongwei, H. & Wei, S. 2010. Experimental study on the relationship between shrinkage and interior humidity of concrete oat early age. *Magazine of Concrete Research,* Vol. 63(3), pp. 191-199.

APPENDIX A

HEAT OF HYDRATION CURVES

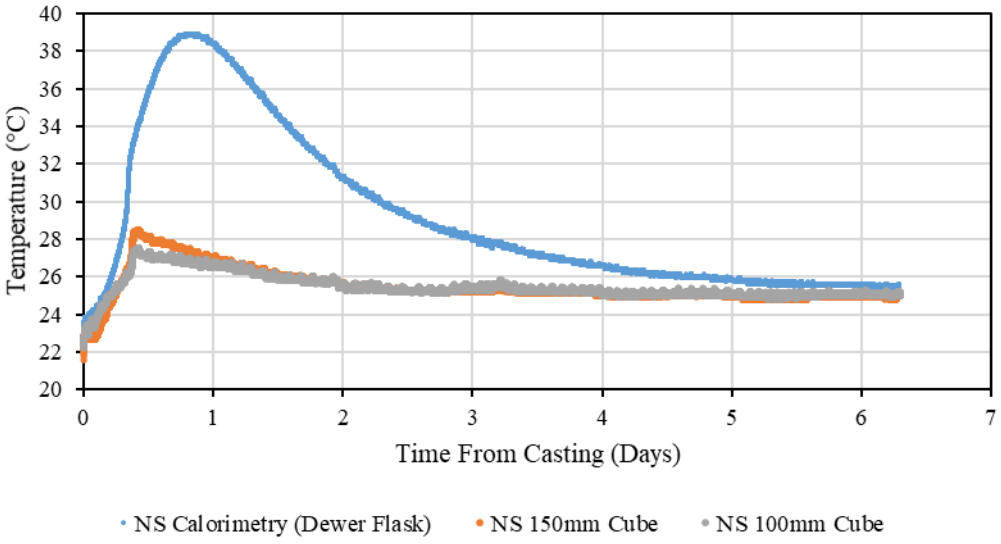

Figure A.1: Heat of hydration curves measured until temperature levels off for NS concrete

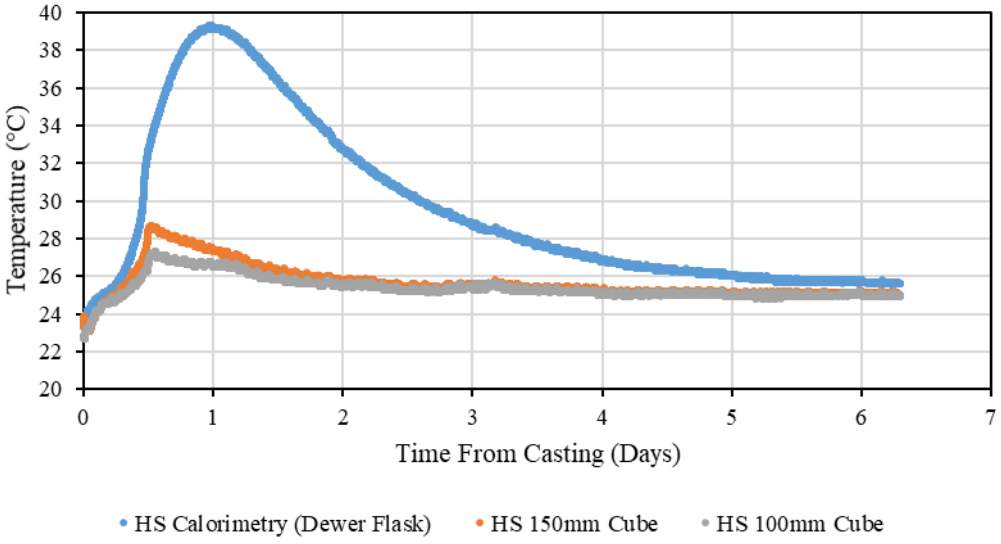

Figure A.2: Heat of hydration curves measured until temperature levels off for HS concrete

APPENDIX B

TEMPERTURE MEASURED WITHIN PAVEMENTS

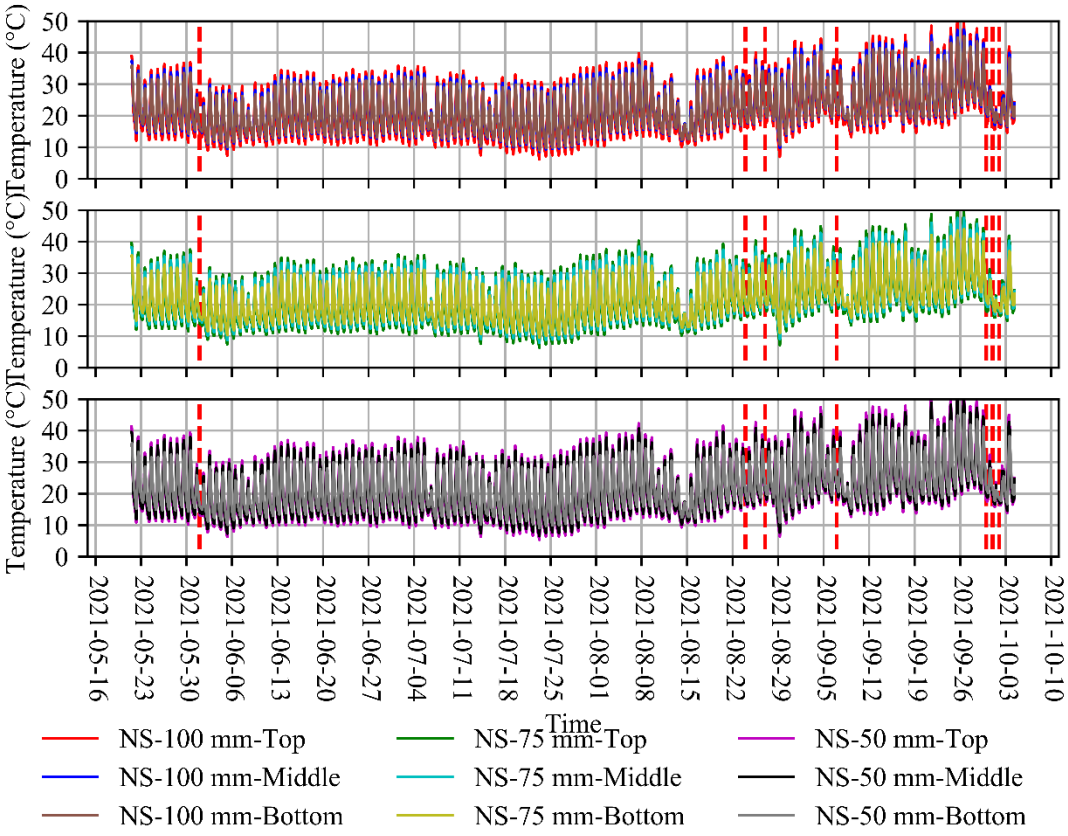

Figure B.1: Temperature measured at the top, centre and bottom of NS concrete pavements

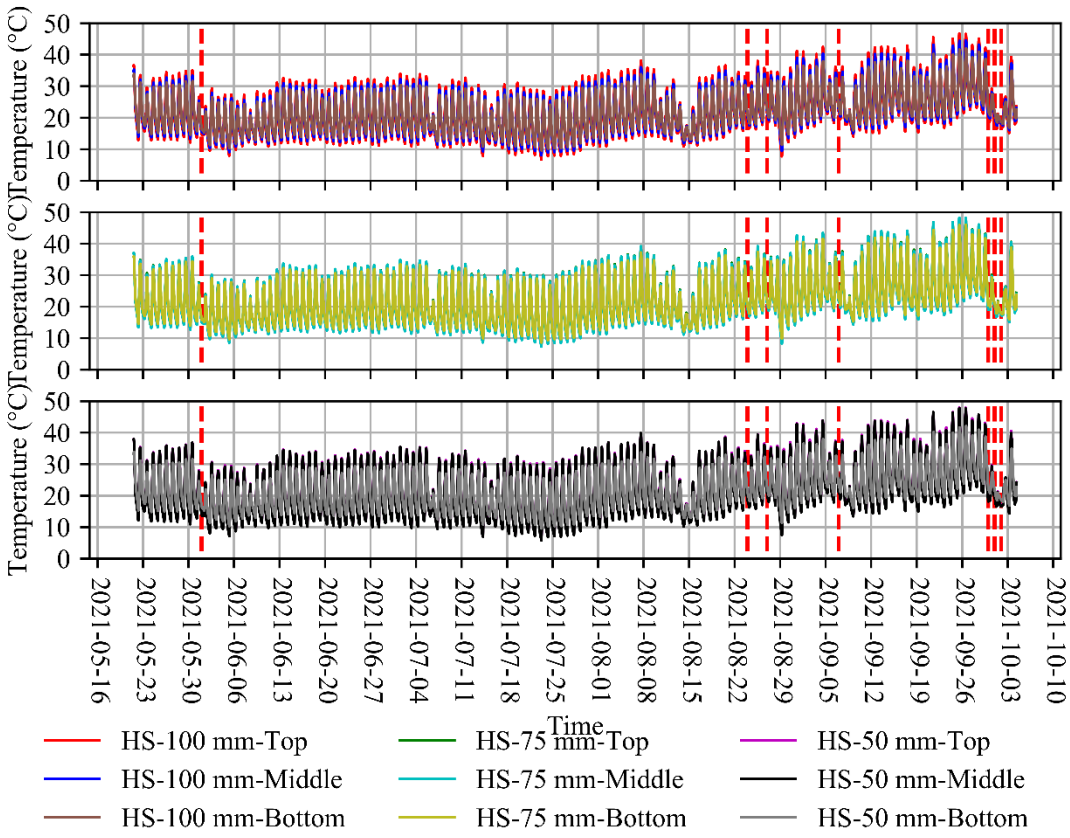

Figure B.2: Temperature measured at the top, centre and bottom of HS concrete pavements

APPENDIX C

RELATIVE HUMIDITY MEASURED WITHIN THE PAVEMENTS

Figure C.1: Relative humidity measured in the top and bottom of the concrete pavements

APPENDIX D

MATERIAL PROPERTIES OF NS AND HS CONCRETE

Table D.1: Summary of the material properties of the concrete

Property	NS Concrete	HS Concrete	Unit
Thermal expansion coefficient	11.42	10.89	με/°C
Workability	35	35	mm
28 Day water cured properties			
Compressive strength	40.60	54.11	MPa
Splitting tensile strength	2.84	3.82	MPa
MOR strength	5.46	7.92	MPa
E-value	33.00	33.25	GPa
Moisture movement properties			
Sorptivity (14 day)	9.50	3.90	$mm/hr^{0.5}$
Sorptivity (28 day)	9.35	4.90	$mm/hr^{0.5}$
Porosity (14 day)	15.6	17.2	Ratio
Porosity (28 day)	15.8	17.4	Ratio
Air cured samples compressive strength			
2 Days	17.78	19.10	MPa
7 Days	28.41	31.42	MPa
14 Days	33.09	41.44	MPa
28 Days	37.01	45.77	MPa
90 Days	38.26	46.76	MPa
180 Days	35.82	51.92	MPa
Air cured samples splitting tensile strength			
7 Days	2.53	3.01	MPa
14 Days	2.69	3.19	MPa
28 Days	2.44	3.19	MPa
180 Days	2.36	3.18	MPa

Air cured samples E-value			
7 Days	26.94	25.98	GPa
14 Days	26.76	26.49	GPa
28 Days	26.74	26.75	GPa
180 Days	26.54	26.65	GPa

APPENDIX E

SUNSET AND SUNRISE DATA OVER ANALYSIS PERIOD

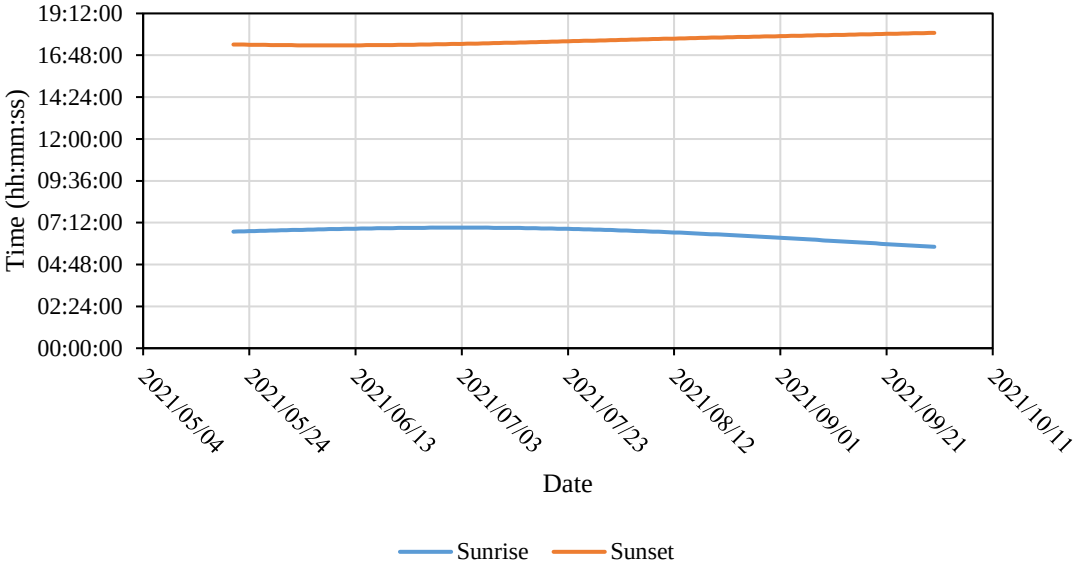

Figure E.1: The times of sunrise and sunset over the analysis period

Table E.1: Date and time of the sunrise and sunset as well as the length of day

Date	Sunrise	Sunset	Length of day
21 May 2021, Friday	06:41:00	17:25:00	10:44
22 May 2021, Saturday	06:42:00	17:25:00	10:43
23 May 2021, Sunday	06:42:00	17:25:00	10:42
24 May 2021, Monday	06:43:00	17:24:00	10:41
25 May 2021, Tuesday	06:43:00	17:24:00	10:40
26 May 2021, Wednesday	06:44:00	17:24:00	10:40
27 May 2021, Thursday	06:44:00	17:24:00	10:39
28 May 2021, Friday	06:45:00	17:23:00	10:38
29 May 2021, Saturday	06:45:00	17:23:00	10:37
30 May 2021, Sunday	06:46:00	17:23:00	10:37
31 May 2021, Monday	06:46:00	17:23:00	10:36
1 June 2021, Tuesday	06:47:00	17:23:00	10:36

2 June 2021, Wednesday	06:47:00	17:22:00	10:35
3 June 2021, Thursday	06:47:00	17:22:00	10:34
4 June 2021, Friday	06:48:00	17:22:00	10:34
5 June 2021, Saturday	06:48:00	17:22:00	10:33
6 June 2021, Sunday	06:49:00	17:22:00	10:33
7 June 2021, Monday	06:49:00	17:22:00	10:33
8 June 2021, Tuesday	06:50:00	17:22:00	10:32
9 June 2021, Wednesday	06:50:00	17:22:00	10:32
10 June 2021, Thursday	06:50:00	17:22:00	10:31
11 June 2021, Friday	06:51:00	17:22:00	10:31
12 June 2021, Saturday	06:51:00	17:22:00	10:31
13 June 2021, Sunday	06:51:00	17:22:00	10:31
14 June 2021, Monday	06:52:00	17:22:00	10:30
15 June 2021, Tuesday	06:52:00	17:23:00	10:30
16 June 2021, Wednesday	06:52:00	17:23:00	10:30
17 June 2021, Thursday	06:53:00	17:23:00	10:30
18 June 2021, Friday	06:53:00	17:23:00	10:30
19 June 2021, Saturday	06:53:00	17:23:00	10:30
20 June 2021, Sunday	06:53:00	17:23:00	10:30
21 June 2021, Monday	06:54:00	17:24:00	10:30
22 June 2021, Tuesday	06:54:00	17:24:00	10:30
23 June 2021, Wednesday	06:54:00	17:24:00	10:30
24 June 2021, Thursday	06:54:00	17:24:00	10:30
25 June 2021, Friday	06:54:00	17:25:00	10:30
26 June 2021, Saturday	06:54:00	17:25:00	10:30
27 June 2021, Sunday	06:55:00	17:25:00	10:30
28 June 2021, Monday	06:55:00	17:26:00	10:30

29 June 2021, Tuesday	06:55:00	17:26:00	10:31
30 June 2021, Wednesday	06:55:00	17:26:00	10:31
1 July 2021, Thursday	06:55:00	17:27:00	10:31
2 July 2021, Friday	06:55:00	17:27:00	10:32
3 July 2021, Saturday	06:55:00	17:27:00	10:32
4 July 2021, Sunday	06:55:00	17:28:00	10:32
5 July 2021, Monday	06:55:00	17:28:00	10:33
6 July 2021, Tuesday	06:55:00	17:28:00	10:33
7 July 2021, Wednesday	06:55:00	17:29:00	10:34
8 July 2021, Thursday	06:55:00	17:29:00	10:34
9 July 2021, Friday	06:54:00	17:30:00	10:35
10 July 2021, Saturday	06:54:00	17:30:00	10:35
11 July 2021, Sunday	06:54:00	17:31:00	10:36
12 July 2021, Monday	06:54:00	17:31:00	10:37
13 July 2021, Tuesday	06:54:00	17:31:00	10:37
14 July 2021, Wednesday	06:54:00	17:32:00	10:38
15 July 2021, Thursday	06:53:00	17:32:00	10:39
16 July 2021, Friday	06:53:00	17:33:00	10:39
17 July 2021, Saturday	06:53:00	17:33:00	10:40
18 July 2021, Sunday	06:52:00	17:34:00	10:41
19 July 2021, Monday	06:52:00	17:34:00	10:42
20 July 2021, Tuesday	06:52:00	17:35:00	10:42
21 July 2021, Wednesday	06:51:00	17:35:00	10:43
22 July 2021, Thursday	06:51:00	17:36:00	10:44
23 July 2021, Friday	06:51:00	17:36:00	10:45
24 July 2021, Saturday	06:50:00	17:37:00	10:46
25 July 2021, Sunday	06:50:00	17:37:00	10:47

26 July 2021, Monday	06:49:00	17:38:00	10:48
27 July 2021, Tuesday	06:49:00	17:38:00	10:49
28 July 2021, Wednesday	06:48:00	17:38:00	10:50
29 July 2021, Thursday	06:48:00	17:39:00	10:51
30 July 2021, Friday	06:47:00	17:39:00	10:52
31 July 2021, Saturday	06:47:00	17:40:00	10:53
1 August 2021, Sunday	06:46:00	17:40:00	10:54
2 August 2021, Monday	06:45:00	17:41:00	10:55
3 August 2021, Tuesday	06:45:00	17:41:00	10:56
4 August 2021, Wednesday	06:44:00	17:42:00	10:57
5 August 2021, Thursday	06:43:00	17:42:00	10:58
6 August 2021, Friday	06:43:00	17:43:00	10:59
7 August 2021, Saturday	06:42:00	17:43:00	11:01
8 August 2021, Sunday	06:41:00	17:44:00	11:02
9 August 2021, Monday	06:41:00	17:44:00	11:03
10 August 2021, Tuesday	06:40:00	17:45:00	11:04
11 August 2021, Wednesday	06:39:00	17:45:00	11:05
12 August 2021, Thursday	06:38:00	17:45:00	11:07
13 August 2021, Friday	06:38:00	17:46:00	11:08
14 August 2021, Saturday	06:37:00	17:46:00	11:09
15 August 2021, Sunday	06:36:00	17:47:00	11:10
16 August 2021, Monday	06:35:00	17:47:00	11:12
17 August 2021, Tuesday	06:34:00	17:48:00	11:13
18 August 2021, Wednesday	06:33:00	17:48:00	11:14
19 August 2021, Thursday	06:32:00	17:49:00	11:16
20 August 2021, Friday	06:32:00	17:49:00	11:17
21 August 2021, Saturday	06:31:00	17:49:00	11:18

22 August 2021, Sunday	06:30:00	17:50:00	11:20
23 August 2021, Monday	06:29:00	17:50:00	11:21
24 August 2021, Tuesday	06:28:00	17:51:00	11:22
25 August 2021, Wednesday	06:27:00	17:51:00	11:24
26 August 2021, Thursday	06:26:00	17:51:00	11:25
27 August 2021, Friday	06:25:00	17:52:00	11:26
28 August 2021, Saturday	06:24:00	17:52:00	11:28
29 August 2021, Sunday	06:23:00	17:53:00	11:29
30 August 2021, Monday	06:22:00	17:53:00	11:31
31 August 2021, Tuesday	06:21:00	17:53:00	11:32
1 September 2021, Wednesday	06:20:00	17:54:00	11:33
2 September 2021, Thursday	06:19:00	17:54:00	11:35
3 September 2021, Friday	06:18:00	17:55:00	11:36
4 September 2021, Saturday	06:17:00	17:55:00	11:38
5 September 2021, Sunday	06:16:00	17:55:00	11:39
6 September 2021, Monday	06:15:00	17:56:00	11:41
7 September 2021, Tuesday	06:14:00	17:56:00	11:42
8 September 2021, Wednesday	06:13:00	17:57:00	11:43
9 September 2021, Thursday	06:11:00	17:57:00	11:45
10 September 2021, Friday	06:10:00	17:57:00	11:46
11 September 2021, Saturday	06:09:00	17:58:00	11:48
12 September 2021, Sunday	06:08:00	17:58:00	11:49
13 September 2021, Monday	06:07:00	17:58:00	11:51
14 September 2021, Tuesday	06:06:00	17:59:00	11:52
15 September 2021, Wednesday	06:05:00	17:59:00	11:54
16 September 2021, Thursday	06:04:00	18:00:00	11:55
17 September 2021, Friday	06:03:00	18:00:00	11:57

18 September 2021, Saturday	06:02:00	18:00:00	11:58
19 September 2021, Sunday	06:01:00	18:01:00	12:00
20 September 2021, Monday	05:59:00	18:01:00	12:01
21 September 2021, Tuesday	05:58:00	18:02:00	12:03
22 September 2021, Wednesday	05:57:00	18:02:00	12:04
23 September 2021, Thursday	05:56:00	18:02:00	12:06
24 September 2021, Friday	05:55:00	18:03:00	12:07
25 September 2021, Saturday	05:54:00	18:03:00	12:09
26 September 2021, Sunday	05:53:00	18:04:00	12:10
27 September 2021, Monday	05:52:00	18:04:00	12:12
28 September 2021, Tuesday	05:51:00	18:04:00	12:13
29 September 2021, Wednesday	05:50:00	18:05:00	12:15
30 September 2021, Thursday	05:49:00	18:05:00	12:16

APPENDIX F

CALIBRATION OF LVDTS AND THERMOCOUPLES

Calibration of the LVDTs was carried out by using a precision stand consisting of a precision scale to accurately measure the change in length, an amplifier to boost the millivolts reading of the LVDT and a logger to display the voltage measured.

The process consisted out of placing a LVDT in the precision scale and rotating a spindle that moves the precision stand up and down to a point that a zero voltage is measured due to this being the centre of the measurement range of the LVDT. The precision scale is then zeroed to mark this as the zero point. Following the zeroing of the precision scale, the spindle is rotated to move the stand up or down in and the displacement as well as the voltage reading is captured to determine the calibration equation of the LVDT relating voltage to displacement measured. Figure F.2 is an example of a calibration curve.

Figure F.1: Calibration of LVDTs using a precision scale

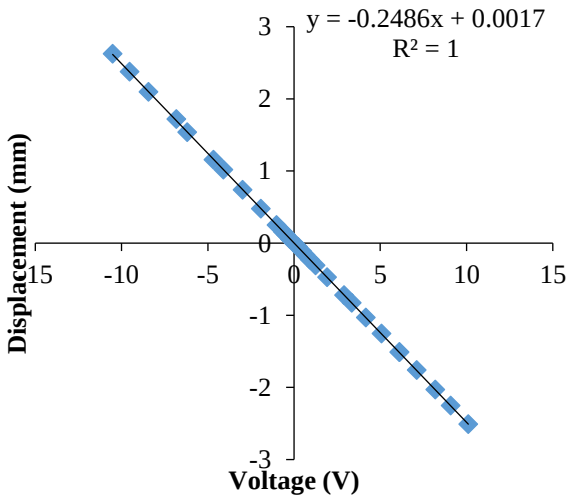

Figure F.2: Calibration curve for a 5mm LVDT

The calibration of the thermocouples used in this study consisted out of placing the thermocouple in a small bath of water containing an accurately defined temperature measuring device as shown in Figure F.3. The deviation in the temperature measurement logged by the GraphTech™ logger and the temperature measurement device is recorded is used to calibrate the thermocouples to the true temperature measured.

Figure F.3: Calibration system used to calibrate thermocouples

Table F.1: Error in temperature readings for thermocouples calibrated

Thermocouple	Error in temperature reading
1	0
2	0.1
3	0.3
4	-0.7
5	0.2
6	0.3
7	0.6
8	1.4
9	0.6

10	0.9
11	0.4
12	0.7
13	0.5
14	0.2
15	0.4
16	0.2
17	0
18	0